The influence of armour layer and core permeability on the wave run-up

An experimental research to give the theoretical research on the 'volume exchange model' a found base

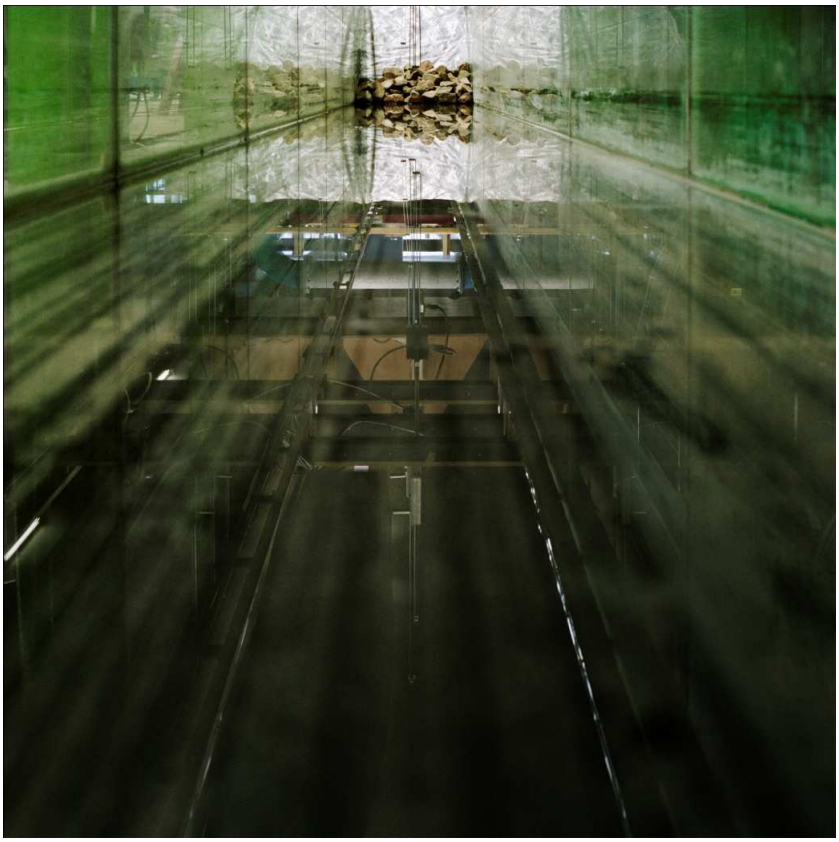

Master of science thesis

P.J.M. van Broekhoven

Delft, April 2011

Delft University of Technology

Dredging, Environmental & Marine Engineering

Title:	Influence of armour layer and core permeability on the wave run-up
Document:	Final report master thesis

Author:	P.J.M. van Broekhoven
Place and date:	Delft, April 2011
University:	Delft University of Technology
Faculty:	Faculty of Civil Engineering and Geosciences
Department:	Hydraulic Engineering

Photo cover: Made by Caren Huygelen

Graduation Committee:

Prof. dr. ir. W.S.J. Uijttewaal	Environmental Fluid Mechanics/ Delft University of Technology
Ir. H.J. Verhagen	Hydraulic Engineering/ Delft University of Technology
Ir. C. den Heijer	Hydraulic Engineering/ Delft University of Technology
Ir. J. Maertens	Dredging, Environmental & Marine Engineering (DEME)

Delft University of Technology

Dredging, Environmental & Marine Engineering

Preface

This study is performed in order to obtain the degree of Master of Science at Delft University of Technology of the Master Hydraulic Engineering. It has been carried out at the Water laboratory of the faculty of Civil Engineering and Geosciences.

In this master thesis a large variety of work was included; from practical work, like constructing a rubble mound breakwater into the flume, to academic work, e.g. by deriving the influence of different processes on the reduction of the wave run-up. It was interesting to see what physically happens when waves run up and flow into an armour layer/core. Apart from that, the tests, not in the least due to the generation of different wave fields, contributed a lot to create an increased insight in waves.

First of all I want to thank my graduation committee for their supervision and guidance during my master thesis. I am grateful for the advices and supervision from Henk Jan Verhagen, Wim Uijttewaal and Kees den Heijer. In general I want to thank the company DEME for their support of my master thesis, especially Jonas Maertens for his advice and support. Furthermore I also want to thank the lab personnel for supporting me during my work at the water laboratory: Sander de Vree for his help with the measuring equipments and wave generator; Hans Tas for helping me with the construction of some slopes, especially for lifting in of all kinds of materials into the wave flume; Arie den Toom for giving me practical advices and last but not least Jaap van Duin for his advice and comical remarks. Lastly, I want to thank my friends who reviewed my thesis and, above all, my family for their unconditional support throughout my entire study.

Patrick van Broekhoven

Delft, April 2011

Summary

In JUMELET [2010] a more physical based approach (so called “Volume Exchange model”) to determine the ‘notional’ permeability coefficient P was developed. The ‘notional’ permeability coefficient was previously introduced in VAN DER MEER [1988] in the stability formula of the armour layer. In this latter study this coefficient was empirically based for three different structures. Due to the limited validity it is difficult to apply a coefficient for different breakwater configurations. The Volume Exchange model determines the permeability coefficient by computing the difference between the surface wave run-up on an impermeable core and a permeable core. The volume of water that flows into the core causes a reduction of the wave run-up. This volume can be determined by using the porous flow equations. The reduction of the run-up due to inflow of water into the core is computed by,

$$R_{u;s;r} = \frac{V_{Ru;s;f} - V_{b;N}}{V_{Ru;s;f}} * R_{u;s;f}$$

In this formula the external volume is given by $V_{ru;s;f}$ and the volume of inflow by $V_{b;N}$. The ratio between the wave run-up reduced by the inflow $R_{u;s;r}$ and wave run-up reduced by surface friction $R_{u;s;f}$ is the run-up reduction factor c_r. However, the Volume Exchange model was still in an early stage of development and needed improvement on a number of points. For example in the VE-model the surface roughness was considered to reduce the run-up with a factor of 0.75. Moreover, the run-up at the core was considered to be 50 % of the run-up at the surface. Both assumptions had no founded basis.
The objective of this study was to improve the insight in the physical process related to the influence of the core permeability on the armour layer stability. Therefore, the difference in wave run-up between an impermeable core and a permeable core was investigated. Next to the main objective, also the separate influences of the slope surface roughness and the permeability of the armour layer on the reduction of the wave run-up were investigated. Lastly the wave run-up at the surface of the core was of interest since this determined the length over which inflow took place.

From a literature study it became clear that data from other studies could not be used to meet the objectives above. It was also not possible to meet the objectives by performing computations. Therefore, physical scale model tests were conducted. The tests were carried out in the wave flume of the water laboratory at Delft University of Technology. On four different configurations (Smooth slopes, Rough impermeable slope, Armour layer on an impermeable core and permeable core) tests were conducted. During the tests the wave run-up was measured by video observations and resistance wires. Apart from these observations also the wave run-up (and inflow) was recorded from the side view with a digital camera.

In the analysis the influences of the surface roughness, energy dissipation in the pores of the armour layer and the reduction of the wave run-up due to inflow into the core were determined. A relation was established for the run-up at the core. However, for an impermeable core the resistance wire gave results that were not very reliable. So, for this configuration the relation found is more an estimation.

It can be concluded that for surging waves the surface roughness of an armour layer has a negligible influence on the wave run-up height. In the transition zone ξ=3.5 -4.0 an influence was visible. However, the transitional zone for a permeable armour layer occurred at lower values of the Iribarren number. So, for a permeable breakwater the reduction of the wave run-up due to the surface roughness was lower. For surging waves the energy dissipation caused by the porous flow led to the reduction of the wave run-up. The results also showed that the Iribarren number is not a proper value to describe the wave run-up height on a structure with an armour layer. Therefore in this study a

relation was derived in which the energy dissipation is related to the Reynolds number and $(\xi*H)/d_{n50}$. The reduction caused by the armour layer can then be related to the stone diameter d_{n50} or to the layer thickness. However, a distinction could not be made in this study, because the layer thickness was dependent on the stone diameter. Hence, in this study a dimensionless wave run-up parameter was chosen including d_{n50}, which led to following relation: $(R_u/H)(d_{n50}/H)^{0.6}$. The value of *'0.6'* was based on the measurements. By using this latter parameter a clearer trend was visible as a function of the Iribarren number. However, the trend found will need more research, in which one must place interest in the influence of the layer thickness and/or the incoming wave volume.

In the Volume Exchange model the reduction factor c_r was based on the reduction of the surface wave run-up due to inflow of water into the core during the run-up period. So, the reduction factor c_r is a ratio between the run-up on an impermeable core and a permeable core. In this study it turned out that the surface wave run-up was not reduced for the cases with permeable core. The infiltration of water into the core had a negligible influence on the reduction of the wave run-up. Most probably the amount of water infiltrated was small enough to have no influence. This latter explanation was supported by observations made with a camera from the side of the flume. During the run-up period the water in the core flowed parallel to the slope, but after maximum run-up the direction of the flow at the surface changed into an inward directed flow. A second phenomenon that could be of influence was the hindrance of the coming wave by the return flow. The return flow on an impermeable core was situated entirely in the armour layer, which caused significant hindrance (or dissipation) on the incoming wave run-up. For cases with a permeable core the return flow occurred via the armour layer and core, causing less hindrance to the coming wave run-up.

Here above, it was mentioned that after maximum run-up the flow is directed into the core. Just after the maximum surface run-up the run-up on an impermeable core will increase. Due to infiltration of water into the core this increase is less (or nil) when the core is permeable. A lower porosity of the core leads to a larger wave run-up at the core. The influence of the core permeability can therefore be given as the ratio between the core run-up on an impermeable core and a permeable core. So, the run-up reduction factor must be redefined by:

$$c_r = \frac{R_{u;c;r}}{R_{u;c;imp}}$$

When regarding the run-up at the core instead to the surface run-up also the inflow period is different as was used in the former VE-model. In the former Volume Exchange model it was expected that the inflow occurred during the run-up period, which is approximately one fourth of the wave period. The inflow period after the maximum run-up however is shorter than one fourth of the wave period. Estimations of the inflow period were made based on the side view recordings, and then varied between one fifth and one eight of the wave period.

The governing loads on the stones for the case of surging waves occurred during the return flow. This was larger when the whole volume of run-up flowed back via the armour layer and/or when the run-up height was higher. For the case of an impermeable core both the run-up was higher and the return volume via the armour layer was larger with respect to a permeable core.

The results of this thesis were implemented in the volume exchange model. In short this resulted in the following adjustments:

- No surface roughness reduction factor was included.
- For the run-up at the core a trend line based on the measurements was used.
- Inflow period was shorter than one fourth of the wave period; for the test results one sixth of the wave period was used.

- The run-up reduction factor was a relation between the run-up on an impermeable core and a permeable core.

Computations were made with this adjusted Volume Exchange model, and compared with the measured values. While computed values were in the range of $c_r \approx 0.95$ the measured values were in the range of $c_r \approx 0.70$. Moreover, the trend of the reduction factor was also different. Most probably this was caused by an overestimation of the external wave run-up volume. The external volume was assumed as a triangular wave run-up wedge. The base of the triangle increases with increasing wave length leading to a larger external volume with increasing Iribarren number. When the inflow volume does not increases proportional with the increase of external volume then the reduction factor will increase with increasing Iribarren number. In reality the wave run-up had a more concave shape with a smaller volume. In here, the relative influence of the inflow of water into the core increased. In this study the wave run-up shape was not investigated. Therefore, a curve fitting was made between the computed values and the measured values. The adjusted Volume Exchange model is used to determine a formula for the permeability coefficient. This has led to the conclusion that the permeability coefficient is dependent on the Iribarren number and the structural configurations and /or properties.

.

Table of contents

List of Figures

List of Tables

Symbols

A	Constant	[-]
	Shape coefficient	[-]
a	Laminar dimensional coefficient of the Forchheimer equation	[s/m]
a_δ	Directional coefficient	[-]
B	Constant	[-]
b_c	With of the core	[m]
b	Turbulent dimensional coefficient of the Forchheimer equation	[s^2/m]
	Width	[m]
b'	Turbulent dimensional coefficient in the fully turbulent flow eqaution	
C	Dimensionless constant	[-]
	Chézy coefficient	[$m^{1/2}$/s]
c	Inertial dimensional coefficient of the Forchheimer equation	[s^2/m]
	Dimensionless coefficient	[-]
c_r	Run-up reduction factor	[-]
$c_{r;\gamma}$	Adjusted run-up reduction factor	[-]
D	Constant	[-]
d	Stone diameter	[m]
	Water depth	
d_w	Distance between resistance wire and slope	[m]
d_{n50}	Median nominal stone diameter	[m]
d_{n15}	Nominal stone diameter exceeded by 85 % of the stones	[m]
d_{n85}	Nominal stone diameter exceeded by 15 % of the stones	[m]
f	Frequency	[s^{-1}]
f_p	Peak frequency	[s^{-1}]
g	Gravity acceleration	[m/s^2]
h	Height	[m]
	Water layer thickness	
H	Wave height, regular waves	[m]
H_{m0}	Spectral significant wave height	[m]
H_s	Significant wave height ($H_s \approx 0.95H_{m0}$)	[m]
k_t	Layer thickness coefficient	[-]
l	Length	[m]
L’	Equivalent wave length inside the breakwater	[m]
L	Wave length	[m]
L_0	Deep water wave length	[m]

L_p	Peak wave length (wave spectrum)	[m]
N	Number of waves	[-]
n	Porosity	[-]
P	(Notional) permeability factor	[-]
p(x)	Pressure height at point x	N/m^2
u	Characteristic pore velocity	[m/s]
u_p	Flow velocity in porous medium	[m/s]
Q	Discharge	$[m^3/s]$
R	Hydraulic radius	[-]
$R_{u,f}$	Wave run-up reduced by the surface roughness	[m]
$R_{u,r}$	Wave run-up reduced by the permeability of the armour layer and core	[m]
R_u	Wave run-up height (regular waves)	[m]
$R_{u2\%}$	Wave run-up height of the two percent largest waves (irregular waves)	[m]
ΔR_u	Error made due to the distance of the resistance wire with the slope	[m]
$R_{u;c}$	Wave run-up at the core	[m]
S	Damage level	[-]
s	Wave steepness	[-]
T	Wave period	[s]
T_p	Peak wave period	[s]
$T_{m-1,0}$	Spectral period	[s]
t_a	(structural) Layer thickness	[m]

Greek symbols

Δ	Relative density	[-]
α	Slope angle	[°]
	Energy scale parameter in the JONSWAP spectrum	[-]
α	Coefficient dependent on the Reynolds number, shape/ roundness of the stones	[-]
α'	Coefficient dependent on the Reynolds number, shape/ roundness of the stones for fully turbulent flow	[-]
β	Coefficient dependent on the Reynolds number, shape/ roundness of the stones.	[-]
	Angle of the wave front with SWL, (=α-5s)	[°]
β'	Coefficient dependent on the Reynolds number, shape/ roundness of the stones for fully turbulent flow	[-]
γ_I	Dimensionless coefficient for added mass phenomena in the inertia term of the Forchheimer equation	[-]

γ_p	Peak enhancement factor in wave spectrum	[-]
$\gamma_{f;c}$	Combined roughness coefficient	[-]
$\gamma_{f;p}$	Roughness coefficient due to energy dissipation in the pores of the armour layer	[-]
$\gamma_{f;r}$	Surface roughness coefficient	[-]
γ_b	Reduction factor for berms	[-]
γ_f	Reduction for the roughness of a slope (combined roughness)	[-]
$\gamma_{f;c}$	Reduction coefficient for the combined roughness	[-]
γ_β	Reduction factor for oblique waves	[-]
γ_{cr}	Reduction factor run-up reduction factor	[-]
δ	Damping coefficient	[-]
ε	Spectral width parameter	[-]
μ	Average values of a sample	Var.
ν	Kinematic viscosity (for water $\nu \approx 1.1*10^{-6}$)	[m^2/s]
ξ_0	Iribarren number based on deep water wave length (regular waves)	[m]
ξ_m	Iribarren number based on H_{m0} and $T_{m-1,0}$	[m]
ξ_p	Iribarren number based on the peak period T_p	[m]
ρ	Specific density	[kg/m^3]
σ	Standard deviation	Var.
σ_a	Peak width factor in the JONSWAP spectrum for $f \leq f_{peak}$	[-]
σ_b	Peak width factor in the JONSWAP spectrum for $f > f_{peak}$	[-]
τ_w	Shear stress	[N/m^2]
ω	Angular frequency ($2\pi/T$)	[s^{-1}]

Abbreviations

GWK	Large wave flume , Hannover, Germany
RW	Resistance wire
SWL	Still Water level
Waterlab	Water laboratory of the faculty Civil Engineering and Geosciences
VE-model	Volume Exchange model
WG	Wave gauge

Chapter 1

Introduction

1.1 General

Coastal regions have often a high concentration of population and a lot of commercial activities take place along the cost. Also, very diverse natural environments can be found in these regions. To protect the coastal regions against flooding, erosion of the shore line, wave hindrance and siltation at unwanted places a great variety of coastal structures can be constructed. In this thesis only one type of coastal structure is considered, namely breakwaters.

Breakwaters are used to protect coastlines from erosion and harbour/ ports. In the case of harbour protection breakwaters minimizes wave intrusion and siltation of the navigation channel. This increases the availability of the port facilities and provides shelter for ships. Within the class of breakwaters a distinction can be made between, monolithic breakwaters, rubble mounds, composite and special types (e.g. floating breakwaters). In this thesis only rubble mound breakwaters are considered. This type of breakwater is build out of rubble material with a trapezium shaped cross section. A rubble mound breakwater withstands the extreme conditions by placing large stones/blocks in the outer layer of the breakwater, the so called armour layer. Most of the times the rubble mound consists of multiple layers, normally the stone size decreases from outer to inner layer. A breakwater that only consists of large armour layer stones (so called homogeneous breakwater) has three disadvantages, large transmission of waves, allows sediment transport through the breakwater, and huge stones are expensive, thus it is not economical. To avoid these problems, the inner layers are composed of smaller stones than the outer layer. Smaller stones are overall less expensive (material cost, transport and placing) and the transmission is less. To prevent washing out of the smaller stones a filter layer is needed. Thus, a breakwater often consists of three main layers. Next, to this also a toe structure, crown walls and filters on the bottom are most of the time necessary, see also Figure 1.1. A downside of smaller stones in the core of a breakwater is that waves cannot penetrate into the structure, due to the lower permeability of the core. Therefore, the loads on the outer layer are larger compared to the situation with a (more) permeable core, which leads to an increase of the required stone diameter in the armour layer.

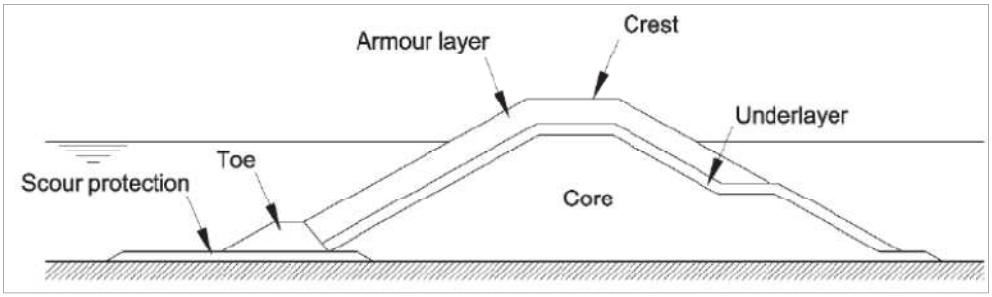

Figure 1.1: General lay-out of a breakwater, CUR/CIRIA [2007]

The armour layer of a rubble mound breakwater can be constructed with a large variation of armour units. The traditional way is placing large rocks as an armour layer, but nowadays various types of concrete armour units are applied such as, cubes, Xbloc, dolos, acropode, tetrapode etc. sometimes also manufactured with a high density. In this study, however, only rock rubble mound breakwaters are considered. The slope angle is generally between 1:1.5 and 1:2.5, the angle of repose of rock material lies around 1:3.3 - 1:1.5, a more gentle slope leads to a larger volume of the breakwater

(CUR/CIRIA [2007]), which is not economically efficient. The toe-structure is a foundation for the armour layer, and can most of the time constructed out of smaller stones than the armour stones.

Common formulas to determine the diameter of the armour stones for rubble mound breakwater are the VAN DER MEER [1988] formulae. In these formulae the permeability of the breakwater is included in the form of the notional permeability coefficient P. In this latter study this P-factor was based on empirical research.. At this moment the P-factor is only determined for three different configurations of breakwaters. Expert judgement is in practice the common method to determine the 'notional permeability factor for other configurations. Because of this, discussions can occur between the client and contractor. In JUMELET [2010] a basis is formed to determine the 'notional' permeability factor with a physically based method, so called Volume exchange model. Eventually the research to a physical based P-factor must lead to a totally abandoning of the current empirical based notional permeability factors. This will make a more economical design of breakwaters possible.

The current study is related to a larger study on the influence of the core permeability on the stability of armour stones. Before, this study a master thesis of JUMELET [2010] and an additional thesis of VILAPLANA [2010] are performed on the same topic. Therefore, these studies need to be discussed and also the origin of the notional permeability factor is briefly introduced in this chapter. The discussions of the previous study will result in the research objectives for this thesis.

1.2 Armour layer stability

A rubble mound breakwater consists almost always of multiple layers, as is shown in Figure 1.1. The armour layer is the critical layer that protects the structure against environmental loads. The environmental conditions are mainly determined by the hydraulic environment. When waves encounter a breakwater the will flow over and in the armour layer and when the waves 'retreat' this flow will be reversed. This phenomenon has led to the first stability formulae (Hudson [1953]) based on the drag force, resisting force of the stones, and influence of the slope angle. The same principle was used as for stability of stones in 'normal' flow conditions. This approach has its shortcoming, such as permeability, types of breaking and more processes not accounting for. In the formula of Hudson (reference SCHIERECK [2000]) the shortcomings were included in the formula by implementing a so called 'dustbin' factor.

The way waves break on slopes is important for the stability concept and can be categorized by the Iribarren number, as determined by BATTJES [1974] (reference SCHIERECK 2000). The types of breakers are shown in Figure 1.2. Were the different types are categorised in the breaker parameter:

$$\xi_p = \frac{\tan\alpha}{\sqrt{H/L_0}} \qquad \text{eq. 1.1}$$

Where H is the local wave height, L_0 the deep water wave length and α the slope angle.

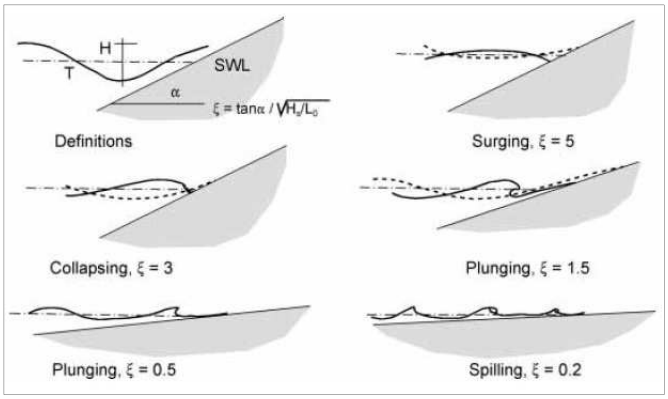

Figure 1.2: Breaker types, SCHIERECK [2000]

In Figure 1.2 it can be seen that the above approach of basing the stability of the stones if they were situated in 'normal' flow conditions is only applicable for the case of surging waves.
Over the course of time more research was done to the stability of the armour stones. Currently. The most widely applied formulae are those derived by VAN DER MEER [1988]. In this latter study, formulae were derived based on small and large scale physical model tests of three different geometries. In Figure 1.3 the principle of the geometries are shown. The design formulae after curve fitting are shown below,

$$\frac{H_s}{\Delta d_{n50}} = c_{pl} P^{0.18} \left(\frac{S}{\sqrt{N}} \right)^{0.2} \xi_m^{-0.5} \qquad \text{Plunging breakers, } \xi \le 3 \qquad \text{eq. 1.2}$$

$$\frac{H_s}{\Delta d_{n50}} = c_s P^{-0.13} \left(\frac{S}{\sqrt{N}} \right)^{0.2} \sqrt{\cot \alpha} \xi_m^{P} \qquad \text{Surging breakers } \xi > 3.5 \qquad \text{eq. 1.3}$$

Between the plunging and surging breaker type a transitional zone occurs, in this zone the breaker type is of the collapsing type. The transition depends on the permeability and slope angle. The transition point is also determined by VAN DER MEER [1988] and, lies between ξ_m=2.2 to 4. In formula:

$$\xi_m = \left(6.2 P^{0.31} \sqrt{\tan \alpha} \right)^{1/(p+0.5)} \qquad \text{eq. 1.4}$$

Parameter	Definition	Unit
H_s	Significant wave height	[m]
D_{n50}	Median stone diameter	[m]
Δ	Relative mass density	[-]
c_{pl}	Coefficient for plunging waves (= 6.2)	[-]
c_s	Coefficient for surging waves (=1.0)	[-]
P	Notional permeability	[-]
S	Damage level	[-]
N	Number of waves	[-]
α	Slope angle	[º]
ξ_m	Iribarren number	[-]

Table 1.1: Parameters formulae VAN DER MEER [1988]

The left term in eq. 1.2 is the dimensionless wave height parameter, which for static stabile breakwater lies between 1 and 4. The term with *S* and N is a value of which amount of damage is allowed or

occurs. The 'notional' permeability is implemented to take the permeability of the breakwater into account. This factor describes the ratio between the grain sizes in the subsequent layers.
The permeability of the structure can be divided into two different areas. These are the permeability of the armour layer and the permeability of the core/ filter layer. A larger permeability of the armour layer leads to a reducing flow at the surface of the armour layer, because a part of the wave volume flows in the armour layer. As a consequence, with increasing permeability of the armour layer an increase in energy dissipation (JUMELET [2010]) will occur. An increase of the permeability of the core leads to more inflow of the wave volume into the core, which results in a volume reduction of the rush down volume. Thus, reduce of flow velocity in the armour layer.

In BURCHARTH [1993] and BURCHARTH et al. [1998] (reference JUMELET [2010]) it is stated that for slopes with an impermeable core the flow is concentrated in the armour layer, causing large forces during run-down. In the case of an impermeable core long waves are more damaging, than short waves due to the difference in water volume. For a slope with a permeable core the water infiltrates into the core and the flow become less violent. In the case of long waves more water can flow into the core, which reduces the forces on the armour units. In coarse core materials the amount of water that penetrates into the core is dependent on the wave period. A long wave has more time to flow into the structure than short waves. So, more reduction of the forces on the armour units in the case of long waves then in the case of short waves, when comparing the situations with an impermeable core and permeable core. However, a long wave is almost always a more severe condition than short waves due to the amount of water volume. The above holds only for surging wave for plunging wave the mechanism is different.

1.2.1 The notional permeability coefficient

The notional permeability is based on curve fitting of the test result of VAN DER MEER [1988]. Therefore, the 'notional' permeability has no physical base. For the three tested geometries a different value of *P* could be fitted, impermeable structure with P=0.1, permeable geometries P=0.5 and for homogeneous structures P=0.6. No tests are conducted with structures between $0.1 < P < 0.4$. Although these structure configurations are common in daily practice. The value P=0.4 is an assumed value.

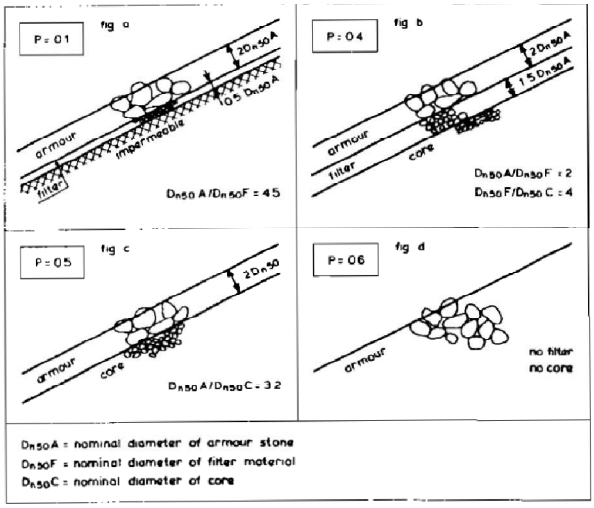

Figure 1.3: Notional permeability factor with the tested structures, VAN DER MEER [1988]

1.3 Volume exchange model

In the master thesis of JUMELET [2010] a literature study is performed to improve the insight in the physical process related to the core permeability. The ultimate objective is to substitute the 'notional' permeability in the formulae of VAN DER MEER [1988] with a physical based permeability coefficient. With a physical description of the permeability the notional permeability factors between 0.1 and 0.4 can be determined. However, in the current phase of this research this is not yet possible. In this section a summary of the thesis of JUMELET [2010] is given, explaining the main principle of the Volume Exchange model and the 'critical' assumptions.

In the formulae of VAN DER MEER [1988] a division is made between plunging and surging waves. The load mechanism of plunging waves differs from surging waves. Plunging waves dissipate most of their energy when the wave first hits the armour layer. Therefore, the permeability of the core is not as important as in the case of surging waves. This can also be seen in the formulas of VAN DER MEER [1988]. The loads that are governing for surging waves is rush down of the waves along the slope. Therefore, JUMELET [2010] formulated a volume-exchange model (VE-model) based on the principle that the change of external volume is equal to the change of the internal volume. This model is only applicable for surging waves, ξ> 3.3. The inflow (change of internal volume) is larger in the case of a permeable core, thus the rush down volume is reduced in case of a more permeable core. This can also be explained as, a reduction in the run-up height compared to the run-up in the case of an impermeable core, due to inflow of water into the core. Therefore, the rush down velocity is lower as this is related to run-up height and the wave period. For the run-up period a sinusoidal wave run-up is considered with a time span of one quarter of the period according to results of MUTTRAY [2000] (JUMELET [2010]).

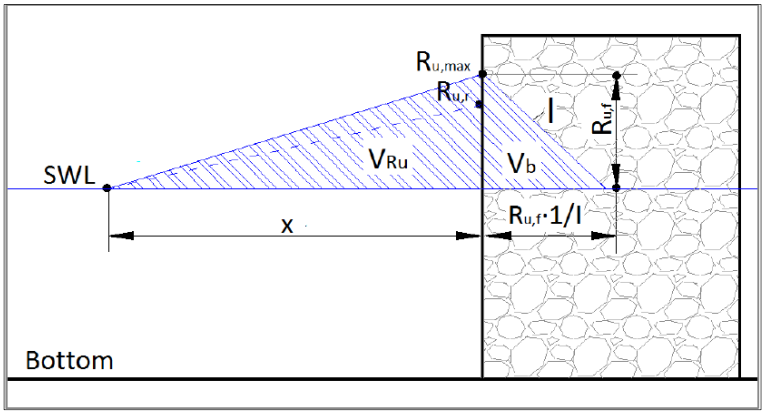

Figure 1.4: Principle of the volume exchange model with vertical transition, JUMELET [2010]

According to the above theories a run-up reduction factor c_r can be derived. The reduction coefficient for the permeability of the structure is defined as the reduced surface run-up $R_{u;s;r}$ (reduced, due to friction and inflow) divided by the surface run-up reduced by friction $R_{u;s;f}$:

$$c_r = \frac{R_{u;s,r}}{R_{u;s,f}} \qquad \text{eq. 1.5}$$

The VE-model is divided into two areas, the external water motion, outside the core of the breakwater, including the armour layer. Secondly, the internal water motion within the core and filter layers of the breakwater. The external volume is determined by the incoming wave. The maximum run-up and shape of the wave on the slope is modelled according to the theory of HUGHES [2004], see Figure 1.5.

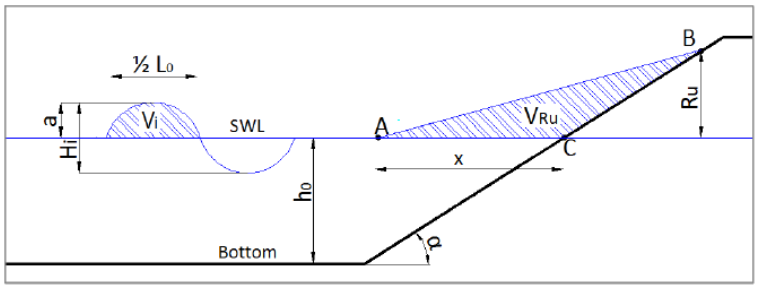

Figure 1.5: Triangular run-up wedge on a smooth impermeable slope, JUMELET [2010]

On an impermeable smooth slope the wave run-up volume is equal to the volume of the incoming wave (V_i=V_{ru}). Also, it holds that on a smooth slope no energy dissipation will take place. The incoming wave energy is transferred to potential energy at maximum run-up. At maximum run-up the run-up tongue has no velocity. This leads to a wave run-up volume as given by eq. 1.6. The derivation from JUMELET 2010 is given in appendix H.

$$V_{ru} = \frac{2}{3}\frac{L_0}{\pi^2}R_u \qquad \text{eq. 1.6}$$

$$R_u = \frac{3}{4}\pi H \qquad \text{eq. 1.7}$$

The above equations are valid for run-up on a smooth slope. For run-up on a rough slope a reduction occurs. For the VE-model the reduction of only the rough surface was of interest. For the reduction coefficient a value of γ_f= 0.75 was roughly assumed. This assumption was not based on found statements. No information is available of the possible value of the slope surface roughness, therefore extra research is needed. The run-up height R_u in eq. 1.6 will be replaced by the run-up height reduced by the slope roughness $R_{u,f}$.

However, for the inflow of water into the core the run-up height at the core is of interest. This is not equal to the run-up height at the surface. Therefore, a rough assumption is made for the run-up at the core. The wave run-up at the core is assumed to be 50% of the wave run-up at the surface of the armour layer, according to JUMELET [2010]. This assumption is based on Figure 1.6. The value of the run-up reduced by the slope surface roughness $R_{u;s;f}$ will be multiplied by 0.5 when using this value in eq. 1.11, eq. 1.12 and eq. 1.14. More research on this topic is needed.

$$R_{u;c} = 0.5 * R_{u;s;f} \qquad \text{eq. 1.8}$$

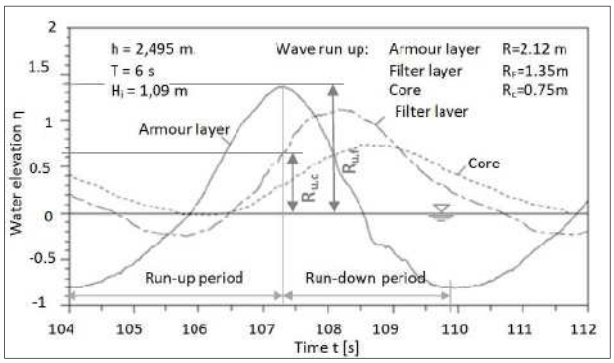

Figure 1.6: Ratio water elevation armour layer and core, MUTTRAY [2000]

The total internal water volume can be assumed as an triangular shape and can be defined as in eq. 1.9, see also Figure 1.4.

$$V_{b,1} = \frac{1}{2} n \left(\frac{1}{I}\right) R_{u;c}^2 \qquad \text{eq. 1.9}$$

Where, *n* is the porosity of the core and *I* is the internal water gradient. For the internal water gradient inside the core the Forchheimer equation is used, but only the turbulent term is taken into account. This leads to a difference of 10 %, when also the laminar and inertial terms are considered. For sloped transition a maximum gradient is assumed, see VAN GENT [1994].

$$I = b u_p^2 \le 1$$
$$b = \beta \frac{1-n}{n^3} \frac{1}{gD} \qquad \text{eq. 1.10}$$

Where *I* is the internal water gradient, and u_p the flow velocity in the porous medium. The β-coefficient is chosen constant at 3.6 in the thesis of JUMELET, but this is not a fixed value.

In the VE-model the period of inflow is assumed to be one quarter of the wave period. The volume of inflow is dependent on the flow into the core (pore velocity) and the period of inflow. With a sinusoidal wave motion the volume of inflow is:

$$V_{b,2} = \frac{1}{\omega} \sqrt{I/b} * \frac{R_{u;c}}{\sin\alpha} \left(1 - \cos\left(\omega * \frac{T_0}{4}\right)\right) \qquad \text{eq. 1.11}$$

The water level gradient inside the core is dependent on the total internal water volume and the volume flowed into the core, $V_{b,1}=V_{b,2}$:

$$\frac{1}{2} n \left(\frac{1}{I}\right) R_{u;s;f}^2 = \frac{1}{\omega} \sqrt{I/b} * \frac{R_{u;c}}{\sin\alpha} \left(1 - \cos\left(\omega * \frac{T_0}{4}\right)\right) \qquad \text{eq. 1.12}$$

If the gradient exceeds the maximum predefined gradient then the maximum value must be used. When the gradient is iteratively determined than the inflow volume can be computed. This reduces the volume of the run-up, and this leads to more iterations with the 'new' run-up height. Because, a smaller run-up height leads to a shorter inflow length, and therefore also inflow volume changes. When determining the influence of the inflow of the permeable core, the volume of the surface run-up reduced by the slope roughness $V_{ru;f}$ is used as the reference value.

$$V_{Ru;f} = \frac{2}{3} \frac{L_0}{\pi^2} R_{u;s;f} \qquad \text{eq. 1.13}$$

The volume that is flowed into the core is determined with the gradient. This gradient is determined after *N* iterations with eq. 1.12.

$$V_{b;N} = \frac{1}{\omega} \sqrt{I_N/b} * \frac{R_{u;c(N-1)}}{\sin\alpha} \left(1 - \cos\left(\omega * \frac{T_0}{4}\right)\right) \qquad \text{eq. 1.14}$$

The reduced surface run-up at the core due to the inflow at the core is determined by:

$$V_{Ru;s;r} = V_{Ru;s;f} - V_{b;N} \qquad \text{eq. 1.15}$$

$$R_{u;s;r} = \frac{V_{Ru;s;r}}{V_{Ru;s;f}} * R_{u;s;f} \qquad \text{eq. 1.16}$$

This can be rewritten to the run-up reduction factor as given in eq. 1.5. With the results obtained in JUMELET [2010] an equation for the notional permeability based on curve fitting with the experimental results of VAN DER MEER [1988] is derived:

$$P = 3.1 s^{-0.3} (1 - c_r)^{0.8} \qquad \text{eq. 1.17}$$

It can be seen that according to JUMELET [2010] the notional permeability is not dependent on the slope angle, which is questionable. In the additional thesis of Vilaplana the influence of the slope angle is investigated.

1.3.1 Parameters of influence and assumptions

Below some parameters that have an influence on the reduction factor are considered. However, more factors may be of influence, but these aren't investigated. Previously, It was mentioned that one quarter of the wave period is the up-rush period (from SWL till maximum wave run-up height). In reality this period is longer as a result of a difference between wave run-up period and the wave run-down period.

The trend that is visible is that with a larger wave period an increase in rush down velocity occurs, due to the fact that a larger increase in external volume than the increase of the internal volume (due to more inflow) will happen. A larger wave period (lower wave steepness) implies also a larger volume of the wave, and the increase of the amount of water that flows into the core (due to larger period) is lower than the increase of the wave volume. With respect to wave height it can be said that a larger wave height gives a relative larger reduction (only with respect to the reduction factor).

The wave steepness is of influence according to the following remarks as stated in/by JUMELET [2010]

- *"The influence of the wave steepness increases when the permeability of the structure increases. Physically this can be explained as follows: when the steepness is small, the wave period is long with respect to the wave height. Therefore, more time is available for the external water volume to flow into the structure. The rate of volume inflow is limited due to the flow resistance in the pores. The associated limited pore velocity is higher in case of a larger permeability. Consequently, the influence of the wave steepness is higher in case of increasing permeability, because in that case the internal flow can easier follow the external flow."*
- *"The run-up reduction increases for increasing wave steepness. Physically this can be explained by the fact that for a long wave (low steepness) the incoming wave crest volume is more significant than in case of a short wave."*

The parameters that have an influence on the inflow of water with respect to the internal volume are the porosity and stone sizes (d_{n50}). These parameters can differ per layer. With increasing porosity and grain size an increase in the run-up reduction is expected. In the thesis of JUMELET [2010] the method is restricted too structures with only two layers in the case of a sloped transition.

The following assumptions are made in order to overcome difficulties that were not relevant at that stage of the research, and to fulfil the demand of a practical formula for the permeability. The assumptions most of interest for this study are above mentioned.

External volume

The wave run-up is modelled as a triangle with a length of distance *x* and a height of $R_{u,f}$. In reality this is a more concave shape. Also, the run-up period is assumed at one quarter of the wave period, according to MUTTRAY [2000]. The model and the reduction factor (and eq. 1.17) are based only on regular waves. The roughness factor of the stones is kept constant at γ_f= 0.75, no physical basis for this assumptions was given.

Internal volume
The following assumptions were made regarding the internal volume:

- Internal water set-up is not taken into account
- Laminar and inertial term in the Forchheimer equation not included
- Constant value for the turbulent term
- Water flow below SWL is not included
- Maximum internal water level gradient for a sloped transition is set as one
- Imposed core run-up is 50 % of the maximum run-up

1.4 Additional thesis Vilaplana

In the additional thesis of VILAPLANA [2010] some aspects of the thesis of JUMELET [2010] are evaluated. Computations are made with the volume exchange model and compared (curve fitted) with the experimental results of VAN DER MEER [1988]. In the first part of this thesis a generalization of the permeability coefficient formula is derived, based on JUMELET [2010] and analyzing the influence of hydraulic parameters and structural properties. In the second part, some assumptions made in the thesis of JUMELET [2010] are varied with the result that the influence of these values can be noticed. In the third part, a damage analysis is done to validate the volume exchange model with the VAN DER MEER test results.

For the generalization of the permeability formula, wave period, wave height, rock size (d_{n50}) and the slope are independently varied. The influence of varying slope is also considered, as it was not considered in JUMELET [2010]. In general it can be said that the run-up reduction coefficient decreases as the angle of the slope increases. However, this trend is also dependent on the combination slope angle and the wave steepness. Except, for the wave height every variable had an influence on the permeability. Therefore, a formula is derived for *P*, related to the three remaining parameters. After curve fitting of the formula in different steps the following formula is the result,

$$P = 1.38(\cot\alpha)^{-0.9} s^{-0.66} (1 - c_r)^{1.44} (2.5 \frac{d_{n50a}}{t_a})^{8.44} \qquad \text{eq. 1.18}$$

In which, α is the slope angle, s the wave steepness, c_r the run-up reduction factor and t_a layer thickness. In the second part the influence of the β- coefficient in the turbulent term of the Forchheimer equation is varied. Also, the roughness reduction coefficient and the reduced core run-up coefficient (γ_{fu}) are varied. The trend is that an increase of the β-value leads to a slight increase of the reduction factor. With respect to the reduced core run-up coefficient the results are questionable. Related to the values of VAN DER MEER [1988] In the case of a homogeneous structure the best fit value is 0.42, for permeable structure the best fit value is 0.48 and for an impermeable structure 0.3. Thus, no linear trend visible between a lower permeability and a smaller reduction is visible.
In the final part of the thesis a validation of the volume exchange model is done. A damage analysis which consists of a comparison of the test results of VAN DER MEER [1988] for surging waves with the volume exchange model, and the generalized formula of the permeability coefficient. The result is that for low damage values the correlation between the tested and estimated values is good. However, the generalized formula for *P* is curve fitted according to the same test results.

1.5 Review of previous work

In the previous sections short summaries are given of two theses. The thesis of JUMELET [2010] is the basis for the further research that will be done in this thesis. The additional thesis is a helpful document to determine the following step in this research. However, some comments can be given on the previous theses.

JUMELET [2010]

In this thesis in an initial stage a vertical transition is considered for the volume exchange model. In order to model the run-up height correctly a roughness reduction was introduced. This reduction factor was chosen such that it only mimicked the effect of roughness. In the situation of a sloped transition this reduction factor returns together with the reduction of the reduced core run-up, γ_{Ru}. This reduced run-up factor is determined according to test results of MUTTRAY [2000]. This factor includes roughness and energy dissipation (dependent to d_{n50}) therefore an extra roughness reduction seems not to be necessary.

The reduced core run-up is taken at the same moment as the maximum run-up at the surface of the amour layer. Due to phase difference the maximum run-up height at the surface of the filter layer is a few seconds later, and is larger than 50% of the wave run-up. Thus, in reality the run-up at the core (in the case of a two layered structure) is higher. Moreover, the run-up height at the surface of the filter is already influenced by the inflow of the wave in the core, see Figure 1.6. In general, it can be said that this assumption is not based on conclusive arguments and further research to this topic is advisable.

Also, the period of run-up is taken a quarter of the wave period. In various researches this was also dependent on the Iribarren number. In BATTJES [1974] the period till maximum run-up was a function of this Iribarren number. For this relation only Iribarren numbers between 0.5 – 1.9 were considered. However, it seems likely that this also varies for surging waves.

VILAPLANA [2010]

In the first part of this thesis different parameters are varied. The wave period shows the same trend as in the thesis of JUMELET [2010]. The wave height, however, has practically no effect for a geometry with a notional permeability of P≤ 0.5, this is in contrast with the findings of JUMELET. For P= 0.6 the trends are the same.

In VILAPLANA [2010] it is stated that the run-up reduction coefficient is larger in the case of a larger d_{n50} in the armour layer. The effect of varying the armour stones results in a different run-up height at the core/filter. Probably with increasing stone diameter there is a decreasing run-height. In the geometries used by VAN DER MEER [1988] the diameter of the stones in the core dependent on the stone size in the armour layer. In reality, the slope roughness, stone diameter and porosity of the armour layer have an influence on the imposed run-up height at the filter/ core. However, the volume exchange model only takes the influence of the core permeability into account. Thus, the only changing factor that has influence on the VE-model is the filter/ core stone properties. In the case of smaller armour stones the filter/ core stones are also smaller. With a constant grading the inflow into core cannot be larger for smaller stones in the core. This is only possible when the imposed core run-up is also varied, however, nothing is mentioned about the variation of this factor. In eq. 1.18 the influence of the slope angle can be noticed, also the wave steepness is of influence. This combination could be changed by placing the Iribarren number in the equation instead of the two different variables.

In the second part of this thesis some assumptions made are varied to determine their influence. The roughness reduction coefficient is also treated, but the same holds here as for the comment on the thesis of JUMELET [2010]. This reduction coefficient must be left out of consideration as this is also taken into account in the 50% reduction of the wave run-up.

The reduced core run-up coefficient (γ_{ru}) shows a remarkable result. The homogeneous structure (p=0.6) has a lower 'fit' coefficient than the permeable structure but a higher coefficient than the impermeable structure. This is not in line with the properties of the structure, as is also mentioned by VILAPLANA.

The reduced core run-up coefficient gives the influence of the roughness and porosity of the armour layer on the run-up at the filter/core surface, see JUMELET [2010]. This depends on the size of stones, which is for the VAN DER MEER tested geometries the same. Also, this reduction depends on the porosity (grading) of the armour layer. The grading of the tested geometries by VAN DER MEER is 1.25, and in the case of an impermeable core the grading is 2.25. The reduced core run-up in the case of the same grading, slope angle and stone diameter should be the same disregarding the permeability of the core. Because, in the VE-model the influence of the core and armour layer is seen separately. The inflow will be computed on basis of the run-up at the core. Nevertheless, the results show that this coefficient (γ_{ru}) has a considerable influence. The influence of a varying imposed core run-up has an influence of 7 – 9 % on the reduction coefficient. This latter is based on computations with the VE-model.

With respect to the damage analysis it can be remarked that the deviation of the damage level using the estimated P-values is not smaller than when using the fixed P-values, as can be seen in Figure 1.7.

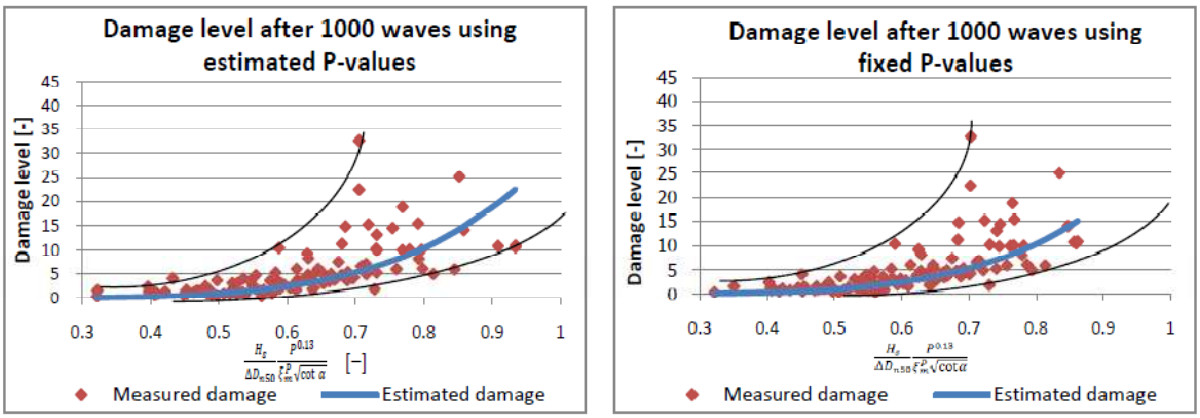

Figure 1.7: Comparison of damage level after 1000 waves, VILAPLANA [2010]

Overall, the volume exchange model is a practical method that is in line with the practical simplicity of the Van der Meer formulae; however, some assumptions were made in order to derive an analytical solution. Some of the assumptions need extra research to improve or validate the assumptions. A lack of knowledge about the slope roughness factor of an armour layer and wave run-up in the armour layer at the surface of the core is. Next, to these also the internal water gradient, internal water set-up and flow below still water level (SWL) are one of the factors that need more investigation, see also section 1.3. More research on many aspects and validation of the method is needed. Moreover, no test results are available that focus only on the permeability of the structure. However, this study will not focus on all the assumptions made in JUMELET [2010]. In the following sections the research objectives of this thesis are given.

1.6 Problem definition

As mentioned before, this thesis is a follow up off the thesis of JUMELET [2010]. Therefore the main problem definition is the same as stated in JUMELET [2010]. The sub-problem that is given is the main topic of this thesis. In section 1.7 the objectives of this thesis are given.

Main problem definition

The influence of the core permeability on armour layer stability is not completely described in literature. In the widely used stability formulas of VAN DER MEER [1988] the influence of the core permeability is described by a coefficient (notional permeability coefficient P) that has no physical

basis. Since the permeability has large influence on the stability relation a more precise description of the core permeability influence is important

In the current situation a method is derived to determine the influence of the permeability. However, still some problems exists that require more research. First, a lot of assumptions are made. Secondly, a lack of knowledge on the behaviour of water in the structure and the run-up in the armour layer. Last, no test results are available where only the permeability of the structure was changed.

Sub-problem definitions
The reduction of the run-up height by the armour layer is not well described in JUMELET [2010]. Also in other literature this is hardly described. This reduction has a relative large influence on the reduction factor c_r. The armour layer reduces the run-up height at the core due to energy dissipation. The dissipation is caused by several factors; roughness and porosity of the armour layer are one of these factors.

The above mentioned problems do not cover every problem that is related to the ultimate goal of deriving a formula for permeability factor based on the physical processes. More problems are to be overcome before such a formula is applicable. Above, only the relevant problems for this thesis are mentioned.

1.7 Research objectives

Main objective
Improving the insight in the physical process related to the core permeability influence on the armour layer stability. Particularly focusing on the research of concretization of the 'notional' permeability coefficient P in the formulae of VAN DER MEER [1988]. Aim is to investigate whether more physical basis can be given to the 'notional' permeability coefficient, which ultimately should lead to more adequate guidance for breakwater practice.

Sub-objective
Improve the knowledge of the physical process(es) that cause(s) the reduction of the wave run-up in the armour layer. This should improve the determination of the notional permeability factor. Therefore, the imposed core run-up at the core for the structures tested by VAN DER MEER [1988] must be determined. During this study a separation between the slope roughness and permeability of the armour layer on the reduction of the run-up should be made. This should lead to a smaller spreading of the results in the damage analysis compared to the results when using the notional permeability factors as derived by VAN DER MEER [1988].

1.8 Report outline

In chapter two a more detailed theoretical background of wave structure interaction will be given. Also, the parameters of influence are listed, this is interesting regarding the experimental program. In chapter three the experimental program is elaborated. The four geometries which are used in the experiments are considered. Comparison between the two measurements method and underestimation by the resistance wire are discussed in chapter four. Chapter five is all about the analysis of the wave run-up results obtained by the experiments. The main conclusions originate from this chapter. With the acquired knowledge of chapter five the Volume Exchange model can be adjusted, which is considered in chapter six. In chapter seven the conclusions and recommendations of this study are presented.

Chapter 2

Wave structure interaction

2.1 Introduction

In the previous chapter the research objectives are stated. In order to meet these objectives it is important that the wave structure interaction is known. Especially, the processes regarding wave run-up are important for this thesis. In this chapter the interaction between waves and breakwaters is considered. Keeping the theory in mind, the influences of different hydraulic and structural parameters on the wave run-up and flow into the breakwater can be determined. Prior research will give better insight in the processes regarding the objectives, and the aim of this thesis is to improve the knowledge about these topics.

2.2 Wave structure interaction

Breakwaters are constructed to limit wave hindrance behind the breakwater. When waves encounter a breakwater different phenomena can occur. During the encounter of the wave with the slope the wave will run-up on the slope. A retreating wave (trough of the wave) will cause run-down, which often induces a lower water level then SWL. During the wave run-up and run down period water inflow and outflow takes place, the amount of inflow depends on the permeability of the breakwater, see chapter 1. Wave run-up is the consequence of a body of water that has enough energy to run-up on the slope. The actual run-up height depends on the wave height, Iribarren number and dissipation of energy and water on and in the slope. When the crest height R_c of a breakwater (or other coastal structure) is not high enough wave overtopping occurs. The permeability of the breakwater influences also the wave transmission. This latter is the phenomenon that the incoming wave energy passes through (or over) the breakwater, which results in a (reduced) wave on the inner side of the breakwater. The wave energy on the lee-side of the breakwater is the result of wave transmission and wave overtopping.
Also, when waves encounter a slope reflection of the wave occurs, With a vertical slope this can be a total reflection, in the case of breakwaters wave reflection is limited due to dissipation.

According to the linear wave theory an incoming waves has an energy that is proportional to the squared wave height ($E \sim H^2$). After the wave has encountered a slope the energy of the incoming wave is transferred to wave overtopping, transmission, wave reflection and part of the energy is dissipated. In formula this yields:

$$E_i = E_t + E_r + E_d + E_o \qquad \text{eq. 2.1}$$

Where E_i is energy of the incoming wave, E_t energy of the transmitted wave, E_r reflected wave, E_d dissipated wave energy and E_o energy of overtopping wave. In this thesis wave overtopping is not considered. From eq. 2.1 it follows, that the dissipated energy can be determined by measuring the incoming, reflected and transmitted wave, in case of no overtopping. The energy of the incoming wave can be determined by the sum of potential and kinetic energy, see eq. 2.2,

$$E_i = E_p + E_k = \frac{1}{2}\rho g a^2 \qquad \text{eq. 2.2}$$

The dissipation of energy can have its origin in the armour layer, filter layer and core. In this thesis the main interest is in measuring the run-up height. The run-up is reduced by dissipation due to roughness, porous flow and water volume flowing in the core of the breakwater.

The run-up height R_u is defined as the vertical distance between maximum wave run-up and still water level (SWL), see Figure 2.1. A requirement is that in prototype situations the run-up has at least a layer thickness of two centimetres, see PULLEN et al. When waves run-up on a breakwater with an impermeable core the waves will penetrate into the armour layer reducing the flow velocities along the surface slope. If also the core of the breakwater is permeable then also flow into the core occurs, this may reduces the run-up height at the surface and in the armour layer. In chapter two is discussed that a lower run-up is favourable with respect to stability of the armour stones.

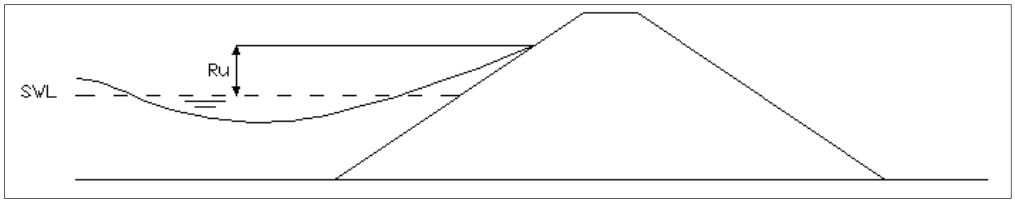

Figure 2.1: Sketch definition wave run-up height

The wave run-up is influenced by the slope surface, flow in the armour layer and flow into the core. The flow along and into the breakwater is highly turbulent, and can be described as a Forchheimer or a fully turbulent flow. Several studies investigated the layer thickness of the run-up, and concluded that eq. 2.3 is a good representation of the layer thickness *h* on smooth slopes. The value of c_h varies for each study, here only the value of SCHÜTTRUMPF [2001] is used as this value showed good correspondence with TAUTENHEIN [1991].

$$h = c_h * (R_u - z); \qquad \text{eq. 2.3}$$
$$c_h = c * n = 0.284 \ (\textit{Schüttrumpf}\ [2001])$$

The velocity of the wave run-up follows by,

$$u = c_u * \sqrt{g * (R_u - z)} \qquad \text{eq. 2.4}$$
$$c_u = 0.94 \ (\textit{Schüttrumpf}\ [2001])$$

The run-up height is influenced by the type of breaking, structural parameters and geometrical configuration. In this study the emphasize lays on surging waves (ξ> 3.3), according to the applicability of the Volume Exchange model, see JUMELET [2010]. The energy dissipation in the armour layer is much larger for plunging waves than for surging waves; therefore the influence of the core is of minor importance when regarding plunging waves.

A lot of research is done to derive the height of the run-up, which resulted in the following general approach. The run-up on a smooth slope is considered, without oblique waves, high values of Reynolds number and Weber number, no fore shore and incompressible water. The run-up height off regular waves on a smooth slope is only dependent on the Iribarren number, see eq. 2.5. This holds, in the case of no oblique waves, high Reynolds and Weber numbers, no foreshore and incompressible water.

$$\frac{R_u}{H} = f(\xi) \qquad \text{eq. 2.5}$$

The run-up height is proportional with the wave height. Therefore, wave run-up is often given as a dimensionless number, so called relative wave run-up.

Many studies have investigated wave run-up on dikes, and basically all of the results have the shape as in eq. 2.6. For regular waves valid till ξ≤ 2.3 and A=1 this equation is known as the formula of Hunt.

$$\frac{R_{u,(2\%)}}{H_{(s)}} = A\xi \qquad \text{eq. 2.6}$$

Where $R_{u2\%}$ is used in the case of an irregular wave field with significant wave height H_s. $R_{u,2\%}$ is the wave run-up height, which is exceeded by 2% of the incoming waves. For wave run-up on dykes or revetments (impermeable structures), PULLEN et al. suggests the following relation:

$$\frac{R_{u2\%}}{H_{m0}} = 1.65 * \gamma_b \gamma_f \gamma_\beta * \xi_{m-1,0} \qquad \text{for } \xi_m < 1.8 \qquad \text{eq. 2.7}$$

$$\frac{R_{u2\%}}{H_{m0}} = \gamma_b \gamma_f \gamma_\beta (4.0 - 1.5/\sqrt{\xi_{m-1,0}}) \qquad \text{for } \xi_m \geq 1.8 \qquad \text{eq. 2.8}$$

In eq. 2.7 three reduction factors can be found, γ_b for the reduction due to berms, γ_f for slope roughness and γ_β oblique waves. The slope roughness γ_f also includes the permeability of the armour layer and also it includes the influence of a permeable core, when relevant. With increasing Iribarren number (ξ) (from ξ=1.8 till 10) the value of γ_f increases linearly till a value of γ_f= 1. In these cases of different geometrical/ structural parameter a single factor is suggested in the literature, disregarding the effect of the two different causes for the roughness (or energy dissipation), namely slope (surface) roughness and permeability (energy dissipation due to permeability of the armour layer). In the remaining part of this thesis this latter is called the combined roughness coefficient, $\gamma_{f;c}$.

The roughness coefficient of rubble mound breakwater differs with varying structural and hydraulic parameters. With increasing breaker parameter a rough slope acts increasingly as a smooth slope, see Figure 2.2. However, Figure 2.3 shows that this holds only for impermeable slopes. A permeable structure influences the run-up by water inflow in the core and inertia of the water inside the structure. In VAN DE WALLE [2003] a curve fitted formula was suggested for a rubble mound breakwater,

$$\frac{R_{u2\%}}{H_{m0}} = A + B\varepsilon + CH_{m0} + DT_{m-1,0} \qquad \text{eq. 2.9}$$

Where, *A*, *B, C and D* are dimensionless coefficients, based on curve fitting. The parameter ***ε*** is the spectral width parameter. VAN DE WALLE [2003] concluded on the basis of this test results that with increasing spectral width also the relative run-up increases. Further, the run-up depends on the significant wave height and wave period. The slope angle is not included, but this is the result of a limited varying slope angle in this study.

The combined roughness for rock slopes is not a constant value, but is dependent on the slope angle, structural parameters and wave conditions. In BRUCE ET AL. [2006] is stated that the combined roughness, $\gamma_{f;c,}$ varies with the slope angle. In LOSADA AND GIMÉNEZ-CURTO [1981] it is stated that the reduction due to roughness varies with the Iribarren number. Thus, a single reduction factor for rock of armour layers does not correspond well with the range of slope angles, permeability and material properties.

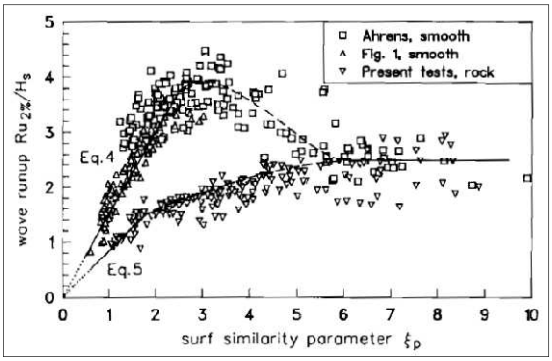

Figure 2.2: Relative wave run-up on rock and smooth slopes, VAN DER MEER and STAM [1992]

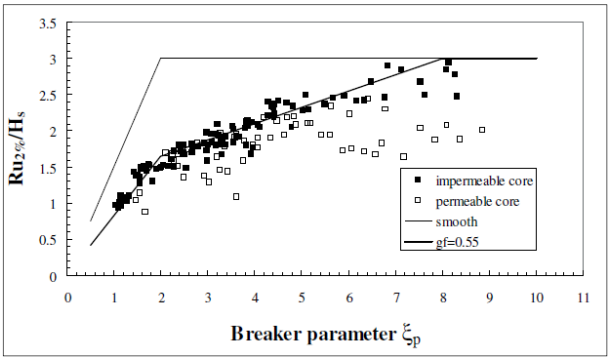

Figure 2.3: Relative run-up smooth slopes and (im)permeable breakwaters, BRUCE ET AL. [2006]

Also, in BRUCE ET AL. [2006] and DE WAAL ET AL. [1992] test results showed a slight difference in the combined roughness of rock sizes of different diameters, and difference in a one or two layered rock slope. In VAN DE WALLE [2003] no difference in run-up could be detected between different armour stone diameters. In this research a high density armour stone of d_{n50}= 0.184 m and a normal density armour stone of d_{n50}= 0.225 m was used. Because the ratio d_{n50}/H varied slightly no difference found. A larger spreading of the ratio d_{n50}/H is needed to show the influence of this factor. Currently no separate reduction factor for the roughness of rock slopes and the permeability of the top layer are derived.

In eq. 2.5 are general expression is given to approach the surface run-up height. This formula does not give the run-up height at the surface of the filter or the core. This is interesting regarding the volume exchange model. However, the run-up at the surface of the armour layer determines over which distance water can flow into the armour layer. Next to this, the imposed core run-up depends also on the permeability (or friction) of the armour layer. In general, The permeability of the armour layer has also a reducing effect on the run-up at the surface, and a more permeable layer allows a higher run-up at the core. Below, a general description of the friction of a porous medium will be given.

2.2.1 Flow in a porous structure

The permeability of a breakwater can be divided into two areas. First, the permeability of the armour layer and second the permeability of the core/filter. The division is based on the difference in stone size and flow properties. During run-up waves or water flow into the armour layer and in the core. The gradient (or flow properties) of the water in the breakwater depends on the layer properties and (external) hydraulic properties.

In DYBBS AND EDWARDS [1984] (reference TROCH [2000]) a distinction is made between different flow regimes in porous media, as shown Table 2.1. The flow between Reynolds number 150 – 300 is a transitional flow, in reality, however, the boundaries are not as clear as stated below. The Reynolds number in a porous medium is related to the size of the pores,

$$\mathrm{Re} = \frac{ud}{\nu} \qquad \text{eq. 2.10}$$

with

$\nu = 1.1 * 10^{-6} [m^2/s]$

$d =$ (charateristic) grain diameter

u= pore velocity

Flow Regime	Re boundaries	Flow equation
Darcy flow	Re< 1-10	I= a''U
Laminar Forchheimer flow	1-10<Re< 150	$I= aU + bU^2$
Fully Turbulent flow	300< Re	$I= a'U + b'U^2$

Table 2.1: Classification of flow types in coarse grained materials

The flow in a breakwater due to waves is non-stationary. For this type of flow the extended Forchheimer equation can be used, VAN GENT[1993]. Below the values of *a* and *b* are supposed to be equal in case of stationary and non-stationary flow.

$$I = au + bu|u| + c\frac{du}{dt}$$ Forchheimer equation: eq. 2.11

$$a = \alpha\frac{(1-n)^2}{n^3}\frac{\nu}{gd^2}$$ Laminar term: eq. 2.12

$$b = \beta\frac{1-n}{n^3}\frac{1}{gd}$$ Turbulent term: eq. 2.13

$$c = \frac{1+\gamma_I\frac{1-n}{n}}{ng}$$ Inertial term: eq. 2.14

In which *u* is the characteristic velocity. Values off the different shape coefficients *α* and *β* can be found in appendix G. For these terms different relations have been found, but above the most common are shown. In non-stationary flows *α* and *β* are not constant. Above, can be seen that the gradient is dependent on the porosity *n* and the stone diameter *d*. Figure 2.4 gives a representation of the influence of the different terms for the different layers in a rubble mound breakwater.

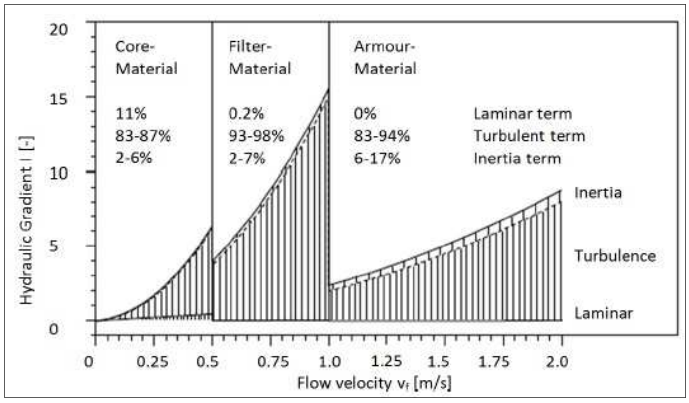

Figure 2.4: Contribution of the friction terms per layer, MUTTRAY [2000]

For oscillating flow in large grained armour layers and filter layers, the inertia term and turbulent term are generally large, as suggested in VAN GENT [1993]. In non-stationary flow the stationary flow coefficient β has an extra contribution β'. With experimental research the turbulent-term and inertia term for oscillatory flow could be derived,

$$b_{non} = \beta_c(1+\frac{7.5}{KC})\frac{1-n}{n^3}\frac{1}{gD_{n50}} \quad where\ KC = \frac{\hat{u}T}{nD_{n50}}$$ eq. 2.15

$$c = \frac{1+\frac{1-n}{n}\gamma}{ng} \quad with \quad \gamma_I = 0.85 - \frac{0.015}{Ac}\ and\ Ac = \frac{\hat{u}}{ngT} > \frac{0.015}{\frac{n}{n-1}+0.85}$$ eq. 2.16

The Keulegan Carpenter number *KC* represents the relative influence between the convective and local accelerations (or ratio between the influence of turbulence and inertia). The influence of the KC-number on the turbulent term is strong, but for the inertial term the acceleration parameter Ac was found to be important instead of the KC number. Boundary layers and eddies will be 'destroyed' if the flow changes direction. On the whole the influence of the turbulence term is dominant, therefore the complex notation for γ_I can be simplified by using a constant value of γ_I= 0.34.

According to BURCHARTH and CHRISTENSEN [1991] (reference TROCH [2000]), the flow in a breakwater is a fully turbulent flow. In these situations laminar flow can be neglected. This resulted in the following equation valid for stone diameter larger than 0.03 m.

$$I = I_c + b'(u - u_c)$$

where I_c and u_c are negligible

$$I = b'u \qquad \text{eq. 2.17}$$

With,

$$b' = \beta' \frac{1-n}{n^3} \frac{1}{gd} \qquad \text{eq. 2.18}$$

For armour layers in scale models this formula is also valid, but when looking to core material this formula may not be applicable, which give influences of scale effects. In the case of non-stationary flow the inertia term must be included. In case of fully turbulent flow the factor *b'* is more sensitive for changes in the porosity and less sensitive for varying d_{n50} and shape factor β as is derived by TROCH [2000] with a sensitivity analysis.

2.2.1.1 Porous flow related effects

The permeability or friction in the porous medium leads to some phenomena that have an influence on the run-up over and in the slope of the layers. During the run-up or run-down of waves some phenomena like disconnection, maximum gradient or reduction to the inertia of the water inside the breakwater can occur. Below a short description of these phenomena is given.

Inertia can be linked to the permeability of the structure. Next to the influence of water inflow in a permeable core a second influence exists. The water that is present inside the structure, will reduce the run-up of waves as a result of the inertia of the body of water in the core. This phenomenon is more likely to be of importance in the case of surging waves. These waves have relative large periods and therefore more interaction between the flow outside and inside of the structure occurs.

Disconnection of the internal and external phreatic surface

Friction in the porous medium limits the internal velocities much more than the external velocities . As the water surface cannot move quicker than the water, also the motion of the internal phreatic surface is more limited than the motion of the external surface. Thus, the friction causes a limited upward speed of the internal phreatic surface during up-rush and during down-rush. This yields the phenomenon of "disconnection" of the water surface. This can occur with small core grain sizes and plunging waves.

Maximum internal water gradient

The waterline in the armour layer is always directed towards the water motion on the outer surface. In run-up the water line will have an upward direction. The maximum downward velocity of the phreatic surface is caused by the friction and gravity forces. The maximum velocity occurs due to only gravity forces. Inside a breakwater the downward water velocity will never be vertical (due outward flow). Therefore, a downward velocity factor smaller than 1.0 is found, see HÖLSCHER et al. [1988]. The upward velocity is influence by the hydraulic parameters, friction and inertia forces. When

disconnection of the phreatic and outside layer occurs, the velocity factor in upward direction can be larger than one, due to inflow of water above the phreatic surface, as also stated in the latter study. In VAN GENT [1994] for a boundary condition of a model he stated that the pressure gradient in vertical direction is smaller or equal than one, see eq. 2.19. For the maximum flow velocity in the Volume exchange model this could also be applicable (as derived in JUMELET [2010]), since between the run-up at the core and phreatic surface in the core no large difference is expected. However, if disconnection occurs a upper value of one is not a correct boundary.

$$I_v = au + bu|u| \leq 1 \qquad \text{eq. 2.19}$$

2.2.2 Combined roughness

As mentioned above, the combined roughness $\gamma_{f;c}$ represents the combined influence of slope roughness and permeability of the armour layer on the wave run-up at the surface. Both components are described below.

2.2.2.1 Slope roughness

The slope roughness is related to the stone diameter in the armour layer. The rougher the slope, the more turbulent the flow over the slope. This gives more energy dissipation, which leads consequently to a reduction in the run-up. In VAN DER MEER and STAM [1992] a relative roughness, d_{n50}/H, was introduced to describe the roughness of the slope..

2.2.2.2 Permeability of the armour layer

Waves flow over and in a permeable armour layer, the flow in this layer is turbulent. The turbulent term is the main contributor to energy dissipation in the porous layer. The permeability of the armour layer depends on the porosity and stone diameter of the armour layer. The porosity depends on the grading, stone shape, and on the method of placing. In general can be said, when the pores are large than more space is available for the dissipation of energy due to turbulence. By increasing the stone diameter the size of the pores also increases (with the same grading), this may result in more energy dissipation inside the pores, and if so this will lead to less run-up at the surface. The latter holds only if the pores are filled with air.

When regarding the effect of permeability on the imposed core run-up a more permeable armour layer leads to a higher run-up at the core. A more permeable layer has less friction, thus the inside water surface can follow the outside water surface more easily. The wave period (or wave steepness) is also of influence on the inflow of water and consequently on the imposed core run-up. It is possible that with a permeable armour layer and long waves the ratio between surface and core run-up is 1:1. So, the imposed core run-up is influenced by the permeability in two different ways, by reducing the surface run-up (which limits the inflow length) and by the amount of friction in the layer. The hydraulic gradient in the porous medium determines the core run-up. In section 2.2.1 porous flow in porous material is considered.

2.2.2.3 Previous work about roughness

When waves run-up a rough slope the roughness of the slope induces energy dissipation, and if the layer is permeable also energy dissipation in the layer takes place. The dissipation of a rough slope has its origin in the shear stress over the slope/bottom. The shear stress is dependent on the velocity over the bed and in turbulent flow the following relation holds for the drag stress

$$\tau_b = c_f \rho u^2 \qquad \text{eq. 2.20}$$

The stress on the stones leads to energy loss. In most situations the drag force is the dominant force. The influence of the roughness of bed material is already investigated in uniform flow conditions and under waves. In uniform flow often the Chézy equation is used to determine flow velocities, where the velocity is given as the average over depth and time. In this equation the coefficient *C* is used as a smoothness coefficient. The value of *C* can be determined by the empirical relation,

$$\bar{u} = C\sqrt{RI} \qquad \text{eq. 2.21}$$

$$C = 18\log\frac{12R}{k_r} \qquad \text{eq. 2.22}$$

Where, *R* is the hydraulic radius and k_r is several times the grain/ stone diameter. In deeper water the influence of the roughness decreases. So, the ratio between water depth and stone diameter influences the energy dissipation in uniform flow.

Above, a relation was given for uniform flow where the boundary layer was fully developed. In not fully developed boundary layers the shear stresses are larger due to accelerations. Also, under short waves not a fully developed boundary layer is present, the layer only exist for half a wave period. In normal water depth of channels/river the wave equation can be used, because the thin boundary layer is small compared to the total water depth. Under short waves the shear stress can be computed by the following relation based on findings of JONSSON [1966] (reference SCHIERECK [2000]),

$$\tau_w = \frac{1}{2}\rho c_f u_b^2 \qquad \text{eq. 2.23}$$

$$u_b^2 = \omega a_b = \frac{\omega a}{\sinh(kd)} \qquad \text{eq. 2.24}$$

Where a_b is the amplitude of the wave motion at the bottom and *d* is the water depth. The factor c_f is the empirical dimensionless roughness coefficient, given by the following relation.

$$c_f = \exp[-6.0 + 5.2\,(\frac{a_b}{k_r})^{-0.19}] \qquad \text{eq. 2.25}$$

In the relations above the amplitude of the wave, water depth over the layer and the size of the grain/stones are of influence on the shear stress on the bed. If wave run-up is seen as a wave motion then the influence of the boundary layer is not negligible, since the water layer above the slope is not large enough, however, the above relations give insight in the processes.

In river flow the roughness of the bed decreases with increasing water depth (Chézy). Also, the forces on bed protection under waves is lower with a larger water depth and /or longer waves, see eq. 2.23. In Figure 2.5 sketches are made of different run-up height based on the idea the run-up can be regarded as a reshaped orbital wave motion of one period and that the layer thickness depends on the run-up, see eq. 2.4. The influence of the stones on the water motion is less when the water layer is thicker. This occurs for larger wave heights and/or Iribarren number. The amount of turbulence in a small layer water over the stones is larger than in the case of a thicker layer.

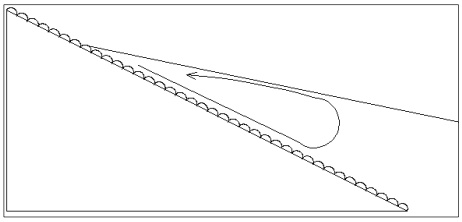

Figure 2.5: Sketch “orbital” motion large wave run-up

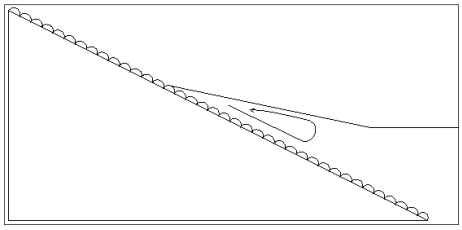

Figure 2.6: Sketch “orbital” motion small wave run-up

Above, the phenomena are described using previous study and qualitative reasoning/ The forces on the stone on a rough slope can be determined by the Morison equation. With this equations forces of an object in flow can be determined.

$$F(t) = \frac{1}{2}\rho_w d C_d u|u| + \rho_w A_d C_I \frac{du}{dt} \qquad \text{eq. 2.26}$$

The drag force term has the same shape as the turbulent term in the Forchheimer equation. The velocity of the run-up is often theoretical determined as,

$$u_{max} = k\sqrt{2gR_u} \qquad \text{eq. 2.27}$$

Where, k is a roughness factor. In SCHÜTTRUMPF [2001] a similar relation was found based on empirical research, see eq. 2.4. When substituting the velocity in the Morison equation the force is a functions as follows,

$$F = f\left(t, d_{n50}, g, R_u, \rho_w, C_d, C_I, \frac{du}{dt}\right)$$
$$C_d = f(\mathrm{Re}) \qquad \text{eq. 2.28}$$

For wave run-up the drag force term is more important, in porous flow the turbulent term is the dominant term. So, eq. 2.28 reduces to eq. 2.29.

$$F = f\left(d_{n50}, g, R_u, \rho_w, \nu\right) \qquad \text{eq. 2.29}$$

The force can be transferred into energy dissipation by regarding the force over the distance. Thus, by regarding it over the run-period and multiply with the velocity.

$$\Delta E = f(t, R_u, g, d_{n50}, \rho, \nu) \qquad \text{eq. 2.30}$$

In ALGERA [2006] it is stated that ΔE can be made dimensionless by reasoning, see eq. 2.31

$$\frac{\Delta E}{\rho g R_u^3 * d_{n50}} = f\left(\frac{\sqrt{gR_u}\, d_{n50}}{\nu}, \frac{R_u}{d_{n50}}\right) \qquad \text{eq. 2.31}$$

The dissipation is dependent on the Reynolds numbers and the run-up divided by the stone diameter. However, the run-up is not an independent variable, but is dependent on the wave height and the Iribarren number.

2.2.3 Energy dissipation and pressures inside breakwaters

The VE-model is based on the inflow of water into the core. The gradients inside the core can be described by the porous flow equations given in 2.2.1. For a proper understanding of the processes and trends regarding damping/ dissipation in breakwaters experimental studies are helpful. In the

following section studies of OUMERACI ET AL. [2010] and TROCH [2000] are considered concerning flow on and in breakwaters.

In BRUUN AND GÜNBAK [1977] tests were conducted with a rubble-mound breakwater of 1:1.5 slope. Two different kinds of core material were tested, d_{50}= 10 mm and 4 mm. Between the core and armour layer a filter material with d_{50}= 20 mm was placed. In the breakwater four pressure transducers were placed in the core. In the experiments it was measured that for fine core material (d_{50}= 4 mm) was a build up of pressures. This led to forces on the filter and armour layer, because the large gradients in the core were located close to the filter. With a more permeable core the pressure gradients were smaller. This is another approach to the influence of the core permeability core on the stability of the armour layer.

In OUMERACI ET AL. [2010] scale model tests are performed in the large wave flume in Hannover (GWK). In these experiments Elastocoast revetments are tested, where pressure cells measured the pressures on and inside the revetment. Elastocoast is capable of sticking rock material together without loss of permeability. The tests were done on Elastocoast revetment of crushed limestone or granite with a layer thickness of 0.15 m and sizes respectively of 20/40 mm or 16/36 mm. Below the Elastocoast part a filter layer of 0.10 m or 0.20 m thick is constructed and the core consists of sand (d_{n50}= 0.34 mm). The core can be seen as an impermeable layer, and this structure has more the characteristics to a (sea)dyke than of breakwaters. Pressure cells were placed on and in the layers. The pressure variations inside the core are not of interest due to the different flow type in rubble mound breakwaters.

The general form of pressure on the revetment can be divided in plunging waves and surging waves. In the case of plunging waves a distinctive peak (below SWL) on impact and a quasi static part are visible. For surging waves a cyclic pressure variation related to the wave motion is visible. In this study is found that in the case of plunging waves 40% damping of the peak pressures on/in the outer layer occurs. For surging waves this is only 10 %. Also no time shift between pressures on and just beneath the Elastocoast layer is visible. The damping is so small that for design purposes the same formula for the pressure is proposed for pressure on and beneath the layer. In the filter layer the more damping, although, the same material as the outer layer only without Elastocoast binding.

In BÜRGER ET AL. [1988], OUMERACI AND PARTENSCKY [1990] [(reference TROCH [2000]) conclusions are made based on large scale model tests done in the GWK. The scale model existed of a tetrapod armour layer, filter layer of 0.5 – 5.0 kg and a core with d_{50} = 0.040 m, see Figure 2.7. Some conclusions are, energy dissipation increases with increasing wave steepness (or reducing breaker parameter); a phreatic surface set-up of 10 % - 20% is present in the core due to incoming waves; and maximum pore pressures decrease rapidly in the direction of wave propagation. TROCH [2000] gives a more detailed analysis of the results of OUMERACI AND PARTENSCKY [1990], review of the conclusion made in the latter study and compares the conclusions with measurements done at the Zeebrugge breakwater.

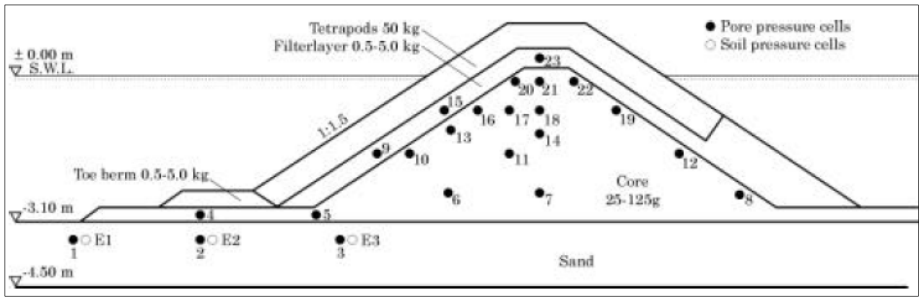

Figure 2.7: Cross-section of the scale model in GWK, OUMERACI [1991].

Based on a more thorough analysis of the scale model results of OUMERACI [1991], TROCH [2000] stated the following trends with respect to the damping coefficient δ,

- *"For a constant wave height H_s and a constant wave period, δ decreases with increasing depth y' below the SWL."*
- *"For a constant depth y' and a constant wave period T_p, δ decreases with increasing wave height."*
- *"For a constant wave height and constant depth y', δ increases with increasing wave period."*

Based on experiments performed by TROCH [2000], it is stated that the first statement has only marginal influence and that the second statement is not valid. For increasing wave height the damping coefficient increases as was found based on the latter experiments. The third statement is verified by TROCH [2000].

Next to this, the incoming wave height H_s is related with the significant pore pressures, in order to get insight in the energy dissipation in the armour and filter layer, see Figure 2.8. This figure shows that more dissipation takes place in the armour/ filter with increasing wave steepness. y' gives the vertical distance between SWL and the pressure cells in the core.

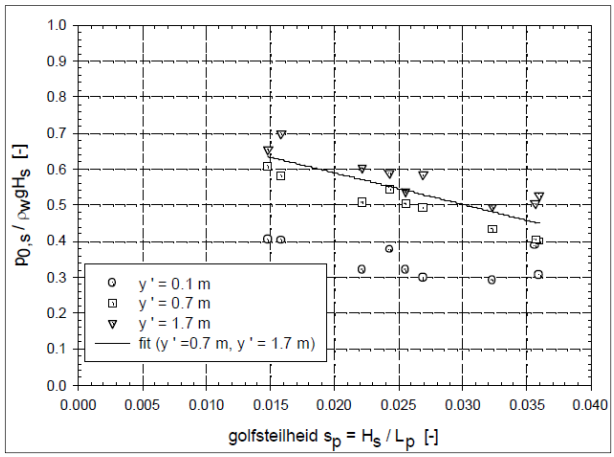

Figure 2.8: Wave steepness related to the pressure height at the surface of the core, TROCH [2000]

In this study a relation of the damping coefficient as a function of H_s, T_p, y' and *n* is made. The findings are in accordance with BURCHARTH ET AL. [1999]. The pressure inside the breakwater can be given by,

$$p(x) = p_0 \exp(-\delta \frac{2\pi}{L'} x)$$

$$\delta = a_\delta \frac{n^{1/2} L_p^2}{H_s b}$$

eq. 2.32

$a_\delta = 0.0141$ Burcharth et al. [1999[

$a_\delta = 0.0145$ Troch [2000] (first result)

In TROCH [2000] also measurements done at the Zeebrugge breakwater are presented. The measurements have the focus on pressures and internal set-up in the core. Several conclusions are drawn from these measurements. With respect to internal set-up can be concluded that, the approach of BÜRGER et al. gives the best set-up predictions, $0.10 < su_{max}/ H_s < 0.20$. These measurements also validate or support the general relation of the damping coefficient, see eq. 2.32. In Figure 2.9 the same trend can be seen as in Figure 2.8. The fitted line is the line that belongs to all measuring points,

the fit is different when regarding the two data sets separately. From this fit the following relations follows,

$$\frac{p_{0,s}}{\rho_w g} = 0.55 H_s \qquad \text{eq. 2.33}$$

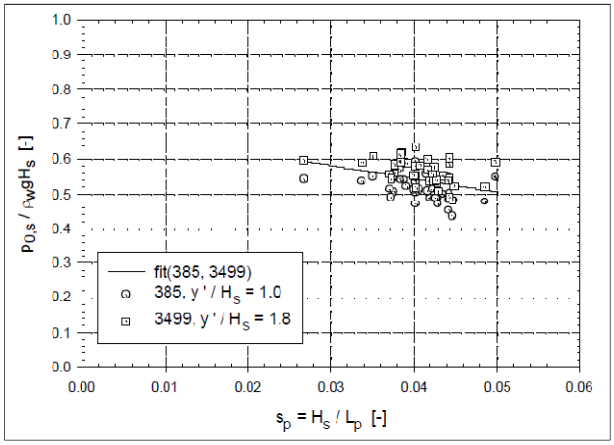

Figure 2.9: Relation wave steepness and pressure height at the surface of the core in the Zeebrugge breakwater, TROCH [2000]

The prototype measurements leads to a damping coefficient a_δ= 0.0123. The model of eq. 2.32 shows that the pressure height reduces exponentially in the core. In comparison to the Forchheimer model, this model does not include a non-linear turbulence term.

2.3 Method to meet the objectives

In short the objectives of this study are stated:

- Describing the surface roughness separate from the permeable influences of the armour layer.
- Improve the knowledge about the relation, hydraulic parameters and imposed core run-up.
- Gain knowledge about the influence of the stone diameter on the surface and core run-up.
- Be able to determine the influence of the core permeability on the run-up.

At this moment no information about the influence of the surface roughness of rock material is available, no relation between the surface run-up and imposed core run-up is present and the influence of the core grading on the run-up needs to be investigated (in more detail). Both the permeability and slope roughness of an armour layer have an influence on the wave run-up. Both phenomena are never separately described for their contribution on the combined roughness. Moreover, a multiple layered armour layer has a larger combined roughness than a single armour layer. It is not yet possible to compute the influences of the above mentioned factors. Therefore, an experimental program will be used to solve these problems. In this experimental program the influence of a permeable core on the wave run-up must be investigated, and also the previously mentioned topics. In the following section the parameters of influence are discussed, leading to a number of parameters that are varied in the experimental program.

2.4 Variables of influence

In the previous section the run-up processes and the flow in porous media were considered. Based on this theory the influential parameters are determined. It is concluded that experiments are needed to be able to meet the objectives of this thesis. In this section the parameters which have an influence on the stated research questions are elaborated. A sub-division can be made into the structural parameters, hydraulic and geometrical parameters.

2.4.1 Structural parameters

2.4.1.1 Shape/Roundness

The roughness of the stones is influenced by the roundness of the stones and the surface texture. A more randomly shaped rock is rougher than a rock that is rounded by e.g. handling or erosion by water. The surface texture depends on the type of material, the way of mining and erosion. The shape/ roundness has an influence on the resistance of the water flow in the layer and stability of the layer. In appendix G the shape coefficients are given, and with the Forchheimer equation this leads to the conclusion that with a more round rock the gradient is less steep (smaller β-values). Also, in VAN GENT [1995] a more round shape showed a smaller hydraulic gradient over the test layer.

The results of VAN GENT [1993] showed that more resistance in the case of rougher rock material than round(ed) material and the resistance increases with decreasing d_{n50}. A classification of shape/ roundness of stone can be made by the length/ thickness ratio, blockiness, cubicity and Fourier asperity roughness (CUR/CIRIA [2007]). In this study no difference in roundness of the stones is considered.

2.4.1.2 Porosity

The porosity of the layers is one of the important factors that determine the permeability of the layers. The porosity depends on the grading of the material in the layer, shape of the stones and on the method of placing. In this study the shape and method of placing will not differ per experiment. So, only the grading is of importance in this study with respect to the porosity.

The grading of the armour layer is defined as the d_{85}/d_{15} ratio of the stones. In a narrow graded layer the variation in stone sizes is small. Therefore, the volume of pores is larger, because no smaller stone that fill up the pores are present. Thus, the grading of the layer influences the porosity *n*.

In VAN DER MEER and STAM [1992] is stated that grading of the armour layer has no influence on the wave run-up at the surface of the armour layer. Two grading were tested, d_{85}/d_{15}= 1.25 (uniform) and d_{85}/d_{15}= 2.25 (rip-rap). Both test were performed with an armour layer on an impermeable core. The wave run-up showed no differences in run-up height between the tests with different grading. The grading range which is normally used for armour layers (grading armour layer is mostly less than 1.5), is to narrow to have significant influence. Off course, for a very wide grading this has an influence, because the permeability is less.

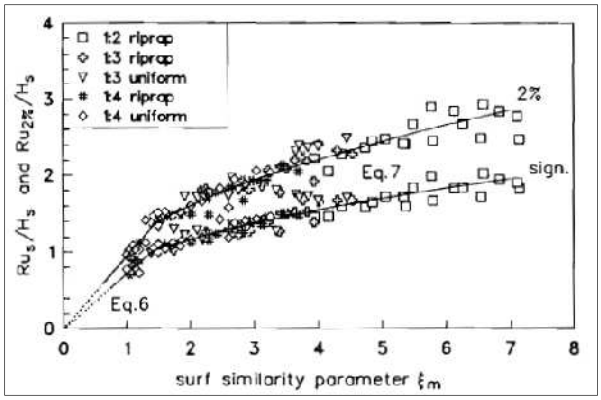

Figure 2.10: Wave run-up on impermeable rock slope with two different grading, VAN DER MEER and STAM [1992]

Also, for the slope (surface) roughness the grading (or porosity) has (almost) no influence on the reduction of the run-up, due to the same reason as above mentioned. For the surface run-up grading has no influence, but for the imposed core run-up the grading has an influence. The grading influences the porosity, thus the gradient in the layer. More inflow is expected in narrow graded material, the resistance in a narrow graded layer is less than in a wide graded layer. However, for the grading range of the typical armour layer this effect is marginal. The influence of the grading of the armour layer is marginal when considering the grading used in practice. Therefore, the grading is not varied in this research.

With respect to the core the porosity is of importance. In BURCHARTH ET AL. [1999] it is stated that the damping of the wave in the core can be given with the damping coefficient δ,

$$\delta = 0.0141 \frac{n^{1/2} L_p^2}{H_s b} \qquad \text{eq. 2.32}$$

Where *b* is the width of the core at a certain level, and *L* the wave length in front of the structure. This is supported with the findings of a sensitivity analysis done by TROCH [2000] on the influence of the *b'* term in the fully turbulent flow equation, see also section 2.2.1.

2.4.1.3 Stone diameter

The stone diameter is often presented as the median nominal diameter, d_{n50}. In section 2.2.1 & 2.2.2 the influence of the stone diameter on the slope roughness and on the permeability of the armour layer is mentioned. The stone diameter can be presented as a relative roughness in the case of the surface roughness and is related flow properties in the layer. The stone diameter should be varied in the experiments when regarding the slope roughness and a permeable armour layer.

With respect to the core, the stone diameter is of less importance as can be concluded from eq. 2.32. The research to the damping coefficient has led to a formula without the parameter d_{n50}. The properties of core material can be a factor in this, core material is usually wide graded, this relatively reduces the influence of d_{n50} (or other stone classification) on the hydraulic gradient ("permeability") in the layer, see also the Forchheimer equation. Thus, the influence of the stone diameter has only a slight influence. Therefore, only the core grading is varied and not the stone diameter.

2.4.1.4 Placing pattern

The configuration of the stones on the slope influences the run-up locally, and generally. If blocks are nicely placed the combined roughness is lower than if they are dumped. Also, the run-up should be measured at multiple places to avoid too large influences of the local configuration of the stones.

2.4.2 Hydraulic parameters

The Iribarren number, ξ, is the common parameter to describe the run-up at the surface of the armour layer.

$$\xi_p = \frac{\tan\alpha}{\sqrt{H/L_0}} \qquad \text{eq. 1.1}$$

In eq. 1.1 can be seen that this the surf similarity parameter depends on the wave steepness and the slope angle. Research on surface run-up has resulted in the conclusion that for long waves on steep slopes (large breaker parameter) the waves are less influenced by the combined roughness, and therefore the run-up is the same as were it on a smooth slope, as stated in BRUCE ET AL. [2006]. This latter only holds if the core is impermeable. The Iribarren number is important for the surface run-up and hence also important for the run-up in the armour layer, since the latter depends highly on the surface run-up.

2.4.2.1 Wave steepness

The influence of the wave steepness is described in the Iribarren number. Above, the influence of the breaker parameter on the wave dissipation is considered. It follows, that for long waves (low steepness) relative less dissipation occurs than in the case of steep waves, see TROCH [2000]. This holds for the dissipation in the armour layer as well as in the core. Also, in the research of JUMELET [2010] the wave steepness is one of the factors that determines the reduction factor, with increasing steepness the factor *P* increases, see eq. 1.17. The wave steepness is determined by the wave height and wave length, where the wave length is determined by the wave period. For deep water waves it holds,

$$s_{deep} = \frac{2\pi H_s}{gT_p^2} = \frac{H_s}{1.56T_p^2} \quad or \quad \frac{H_s}{L_0} \qquad \text{eq. 2.34}$$

An increase in wave height is proportional to an increase in wave run-up. However, the dissipation and the inflow of water into the breakwater are not only related to the wave height, but also to the wave period. The steepness is varied in the experiments by making use of different wave height and periods.

2.4.2.2 Water depth

The water depth can have an influence on the wave properties. When this is the case then it has also an influence on the wave run-up. In the situation were different wave heights and lengths are regarded, the influence (negligible influence) of the water depth should be the same in every test. In the Shore protection manual [1984] (reference VAN DE WALLE [2003]) is stated that the water depth *d* has no influence if d/H > 3. In this study the water depth is always kept larger than three times the wave height.

2.4.2.3 Density of water

The density of water has an influence on the pressures in the breakwater and on the relative density. Mostly breakwaters are placed in salty waters. The experiments will be done in fresh water, $\rho_w \approx 1000$ kg/m^3. This will not influence the mutual results as every experiment is done with the same water density.

2.4.2.4 Shape of the spectrum

When regarding irregular waves the shape and type of the spectrum have influence on the relative wave run-up. In VAN DE WALLE [2003] is concluded that the spectral width parameter ε and peak enhancement factor γ_p has influence on the relative run-up. In this study the peak enhancement factor γ_p and peak width parameter σ of the spectrum are remained constant during the experiments. The

average values for a JONSWAP spectrum are used, σ_a= 0.07, σ_b= 0.09 (σ_a is used if f ≤ f_p and σ_b is used if f > f_{peak}) and γ_p= 3.3, see also HOLTHUIJSEN [2007]

$$E_{JONSWAP}(f) = \alpha g^2 (2\pi)^{-4} f^{-5} \exp\left[-\frac{5}{4}\left(\frac{f}{f_{peak}}\right)^{-4}\right] \gamma_p^{\exp\left[-\frac{1}{2}\left(\frac{f/f_{peak}-1}{\sigma}\right)^2\right]} \qquad \text{eq. 2.35}$$

2.4.3 Geometrical parameters

2.4.3.1 Slope angle

As mentioned before, the Iribarren number is of influence for the run-up at the surface and in the armour layer. For the separation of the slope roughness and the permeability of the armour layer the slope angle is also of importance. A smaller slope angle leads to more contact of the slope with the waves. On the other hand, the inflow of water is 'more' horizontal which can influence the imposed core run-up. In BRUCE ET AL. [2006] it is stated that the $\gamma_{f;c}$ varied with the slope angle for breakwaters with a permeable core. It could also be an influence of the slope angle on the surface roughness and imposed core run-up.

2.4.3.2 Layer thickness

In case of a thicker layer more energy dissipation is possible in the armour layer. The thickness of armour layer is most of the time determined by $2k_tD_{n50}$, smaller (single layer) is not preferred with respect to stability of the (under) layer and a thicker layer is not economical. The layer thickness is not an independent variable, but depends on the stone diameter. The thickness of the armour layer is therefore not varied separately but vary with the stone diameter.

2.4.4 Governing variables

In short the following variables are of influence and are considered in the experimental program,

- Iribarren number; which consist of the wave steepness and slope angle
- The stone diameter in the armour layer
- The grading of the core

The following parameters are kept constant in the experiments

- Stone density
- Water density
- Water depth (at least d > 3H)
- Shape of the wave spectra
- Shape/Roundness of the stones

2.5 Wave conditions

The test series can be done with irregular or regular waves. The advantage of regular waves is that this requires less waves per test and analysing of the results is simpler. Moreover, the hydraulic processes are the same for regular and irregular waves. Therefore, most of the experiments will be done with regular waves. The goal of the experiments is to find a relation between the roughness and the energy dissipation in the armour layer under different hydraulic conditions. This relation can be made visible with regular waves. With respect to the objective to improve the Volume Exchange model this poses also no problem, because at this moment the Volume Exchange model is also derived for regular waves.

Regular waves do not correspond with waves in a real situation (storm). A JONSWAP spectrum gives a good description of waves in reality. Off course, the relative wave run-up differs with regular waves

and irregular waves, as also stated in DE WAAL et al. [1992]. This latter is no problem when regarding impermeable experiment set-ups. The internal water set-up and flow in side of the core differs whit irregular waves in the case of a permeable geometry. Therefore also irregular waves are performed during the experiments. However, the amount of experiments with irregular waves is much less, because it is used for a comparison with the results obtained from the regular wave experiments.

Chapter 3

Physical scale model

3.1 Introduction

With experimental research the influence of the stone diameter on surface roughness and flow in the armour layer can be determined. Also, the influence of a permeable core on the run-up and flow in the breakwater can be determined by experimental research. In this chapter the four geometries placed in the flume are elaborated. These are the smooth impermeable slope, rough impermeable slope, permeable top (armour layer) on an impermeable core and permeable core. Within each geometry changes in stone diameter, slope angle or grading of the core are made. In total this leads to ten different set-ups which are elaborated in this chapter, and an overview is given in Table 3.1 In section 3.2 from each of the geometries the basic dimensions, material properties are given. During the experiments the wave height varies between $0.065 \leq H \leq 0.15$ m and the wave period between 0.85 s – 3.0 s. Next, the measuring equipment and method of analysis are considered. In section 3.4 the four different geometries are elaborated alongside the expected results. In appendix L pictures of the physical scale models are showed.

Geometry	1:1.5	1:2	$d_{n50;a}$= 0.067 m	$d_{n50;a}$= 0.09 m	d_{85}/d_{15}= 1.5	d_{85}/d_{15}= 4
Smooth slopes	√	√				
Rough impermeable slope*	√	√	√	√, only 1:1.5		
Armour layer on impermeable core	√	√	√	√, only 1:1.5		
Armour layer on permeable core		√	√		√	√

Table 3.1: Overview geometries and the structural properties

** In literature with a geometry "rough impermeable slope" is often meant an armour layer on an impermeable core, in this study this is not the case.*

3.2 Physical model

The experimental research is performed in the wave flume in the Water laboratory ('WaterLab') of the faculty of civil engineering and geosciences of the TU Delft in the Netherlands. The wave flume has dimensions of L x b x h = 45 x 0.8 x 0.95 m^3. The wave generator in the flume is equipped with active wave absorption and can generate wave periods from 0.85 s till at least 4 s. Also, the wave generator has a control function to minimize or avoid second order effects in the wave field. The active wave absorption almost totally reduces the reflection of the wave from the vertical wave paddle.

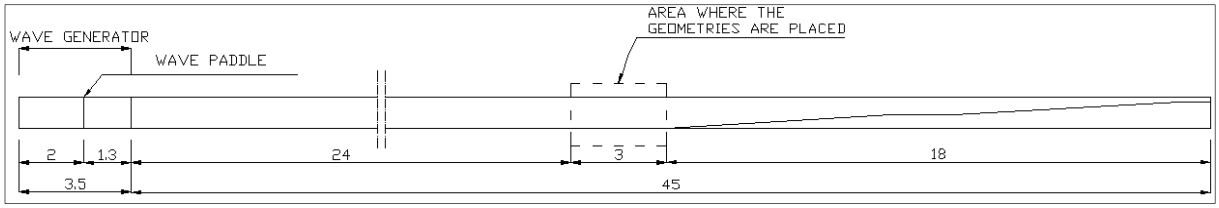

Figure 3.1: Side view of the wave flume

In the physical test program test are conducted with four different geometries. In Figure 3.2 drawings of the geometries are shown. The left drawing depicts the run-up tests on smooth slope, this slope is the reference slope. In the middle drawing, the model that only takes the slope roughness into account is shown. In this case the armour layer is not permeable. In the right (Third) geometry a permeable armour layer is placed on an impermeable core.

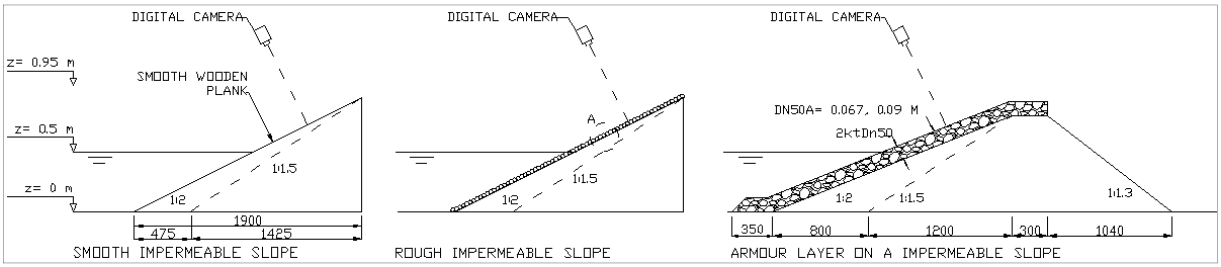

Figure 3.2: Geometries were experiments are conducted on

A fourth scale model representing a breakwater with a permeable core is also one of the geometries, see Figure 3.3. The configurations of this scale model are according to the notional permeability factor *P*= 0.5. The volume exchange model is in its current form only valid for this type of configurations. Therefore, this geometry is necessary to improve the volume exchange model.

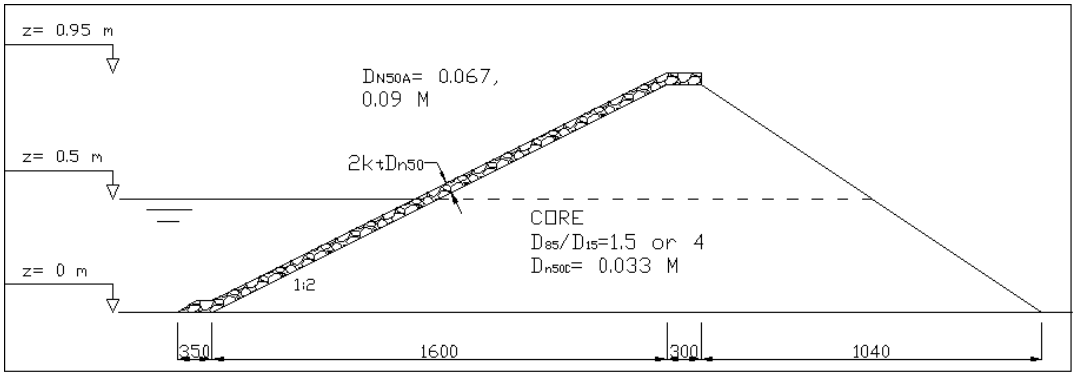

Figure 3.3: Armour layer on permeable core

3.2.1 Design of the scale model

The scale models are not directly related to a prototype breakwater. However, in order to have a notion of the dimensions in prototype a scale factor is determined. Stable rock breakwaters (without a berm) are economical feasible in situation with a design wave height H_s between 2 – 3 m. For the design of the breakwater it is important to understand that the breakwater should not be damaged during the experiments. Different types of geometries are under research, but the governing experiment is the impermeable slope with a permeable armour layer with an irregular wave field. To determine the required stone diameter in the armour layer, the formula of VAN DER MEER [1988] for surging waves is used.

$$\frac{H_s}{\Delta d_{n50}} = 1.0P^{-0.13}\left(\frac{S}{\sqrt{N}}\right)^{0.2}\xi_m^P\sqrt{\cot\alpha} \qquad \text{eq. 1.2}$$

Variable	Value	units
Maximum wave height H_s	2	[m]
Iribarren number ξ	3.3 – 7.0	[-]
Notional permeability P	0.1	[-]
Damage level S	1	[-]
Number of waves N	1000	[-]
Slope angle α	1:1.5 or 1:2	[°]
Relative density ρ	1.61	[-]
Required d_{n50}	1.33	[m]

Table 3.2: Parameters VAN DER MEER formula

The dimensions of the wave flume allow a scaling factor of 1:20. This scale factor depends on the width of the flume. Sufficient stones should be placed over the width of the flume to mimic a prototype slope properly. This leads to a choice of a minimum armour stone of d_{n50}= 0.067 m. Using a significant wave height of 3 m (in scale 0.15 m) leads to too large stone diameters. Moreover, the emphasize on the experiments lays on test with regular waves. For this type of wave field, experiments can be performed till at least H= 0.15 m without damaging the slope.

3.2.1.1 Dimensions

In section 2.2.2 the influence of the stone diameter on the combined roughness is mentioned. Therefore, it is interesting to vary the stone diameter in the armour layer, to be able to say something about the influence of d_{n50}. In the experiments two different d_{n50} are used, 0.067 and 0.09 m. Between the different stone diameters the shape/roundness is no different. The layer thickness varies with the stone diameter, a two layered armour layer has a thickness of $2k_t d_{n50}$ where $k_t \approx 0.9$, see CUR/CIRIA [2007]

The diameter of the stones in the toe is the same as in the armour layer. The toe is less heavily attacked than the stones in the armour layer, therefore the stability of the stones in the toe is guaranteed when using the same stones as in the armour layer.

During the experiments no wave overtopping is allowed. The largest wave run-up is expected during the experiments with a smooth impermeable slope, in Figure 2.3 it can be seen that the largest wave run-up is three time the significant wave height. When regarding significant waves of 0.1 (prototype scale of H_s= 2 m) the maximum run-up is around 0.30 – 0.40 m and for regular waves with H= 0.15 also around 0.40 m. The effective height of the flume is 0.95 m. The regular waves vary between 0.075 – 0.15 m, in order to have a good spreading of the ratio d_{n50}/H. A water depth 0f 0.5 m is used, in order to avoid influence of the water depth on the run-up. When d/H > 3 the water depth has no influence on the run-up height. So, with a construction height of 0.95 m no overtopping is expected.

In order to have a good representation of a prototype breakwater design guide lines are used. One of these guidelines is that the core width is at least three times the stone diameter in the armour layer, k_t d_{n50}. The physical model has a crest width B_c of approximately 0.30 m.

Beneath the armour layer, no filter layer is present, as is in corresponds with the notional permeability factor of 0.5. The CUR/CIRIA [2007] guidelines, state that in rubble mound breakwaters the layer beneath the armour layer is,

$$\frac{d_{n50;a}}{d_{n50;c}} = 2.2 - 2.5 \qquad \text{eq. 3.1}$$

In practice the above guideline is often used, however, for the scaling of the core stones other criteria become more important and also the availability of the material is of importance. For the core stones the scaling law as stated in BURCHARTH ET AL. [1999] is applied. For the scaling a Froude scaling is applied. For the case of the core stones using a Froude scaling can lead to too small Reynolds numbers which implies too large viscous forces, that is not in corresponds with reality. In appendix F this method is elaborated. However the Reynolds number is dependent on among others the porosity and the stone diameter. Also, for the armour stones the Reynolds number is not scaled "correctly", but this gives no problems.

3.2.1.2 Grading armour layer and core

The porosity of the armour layer and core is important for the permeability of the layers. The porosity depends on the grading , shape and method of placing. The latter two factors are not varied, thus in this case only the grading has influence on a different porosity, see also section 2.4.1. For the grading of the armour layer a narrow grading is chosen, as also most of the cases in practice. The stones for the armour layer are handpicked, and resulted in a grading of $d_{n50;a}$= 0.067 m with a grading of 1.2 and $d_{n50;a}$= 0.09 m with a grading of 1.2. The mean density of the armour stones is 2610 kg/m^3 with a deviation of 20 kg/m^3. The porosity of the two types of armour stones in "bulk" situation is 0.41 for $d_{n50;a}$= 0.067 m and 0.40 for $d_{n50;a}$= 0.09 m. This latter only shows that the porosity of the armour layer varies not significantly, it tells nothing about the actual porosity of the layer. For the core stones, a sample is taken, and of each of the stones in the sample the individual weight is measured. This resulted in the following properties of the stones, $d_{n50;c}$= 0.033, ρ_c= 2590 kg/m^3 with a grading of 1.5. This was matching with the specifications of the stones given by supplier which was later acquired. Also, a grading of 4 is used in the experiments; however, the grading is based on the specifications of the supplier. The porosity of the grading 1.5 is after 'compaction' 0.43 ±0.02 and for the core with a grading of 4 n=0.36. In appendix E a more detailed description regarding the material properties is given. In appendix ## a method is elaborated to determine the flow properties in the core under the governing situations. The requirement is that Re > 300, in Table 3.4 it can be seen that the flow properties in the core meet this requirement.

H_{m0}	T_p	δ (SWL/-y)	α (or α')	β (or β')	Re
0.11	4.0	4.47/4.00	360	3.6	690
			1007	0.63	970
			0	3.6	620
			0	2.7	720

Table 3.3: Computed Reynolds numbers with the method of BURCHARTH [1999]

3.2.1.3 Overview of the parameters

In Table 3.4 the relevant parameters for the geometries are given and Figure 3.3 represents the overall lay-out graphically.

Parameter	Value	Dimension
Structural parameters		
Armour stones, $d_{n50;a}$	0.067, 0.09 m	[m]
Core stones, $d_{n50;c}$	0.033	[m]
Grading armour, d_{85}/d_{15}	1.2	[-]
Grading core, d_{85}/d_{15}	1.5 and 4	[-]
Hydraulic parameters		
Surf similarity, ξ	1.7 – 9	[-]
Wave steepness, s	0.01 – 0.90	[-]
Wave height, H	0.075 – 0.15	[m]
Significant wave height, H_s	0.075 – 0.11	[m]
Wave period, T	0.85 – 3.0 (3.5*)	[s]
Geometrical parameters		
Slope angle, α	1:1.5 or 1:2	[-]

Table 3.4: Important parameter experimental program

** In some experiments wave periods till 3.5 seconds were generated by the wave paddle. This leads to cnoidal waves and cannot be accurately described by the linear wave theory.*

3.2.1.4 Scale effects

As a consequence of scaling, phenomena that are negligible in prototype situations could become more of influence. In this sub-section these phenomena/ forces are briefly considered.

In PULLEN et al. is stated that surface tension on wave propagation can be neglected if the wave period is larger than T > 0.35 s and H > 0.02 m, which is the case for the proposed experiments. In VAN DE WALLE [2003] is stated that for small run-up the surface tension is of influence. For R_u> 0.022 m surface tension is negligible. In theory when We > 10 and Re > 10^3 surface tension or viscous forces are negligible. According to this latter the influence of surface tension can be regarded as negligible in the proposed experiments.

Scaling of the core material can lead to non-negligible viscosity forces; this can be avoided by using the scaling method of BURCHARTH ET AL. [1999]. For the core in the proposed experiments this method, see section 3.2.

3.3 Measuring and observation techniques

During the experiments the incoming waves, reflected waves and run-up are measured. Below, the measurement equipment and techniques used in the experiments are considered. In appendix A more information about the video analysis and accuracy of the measurements is given. The principle and measurements of the resistance wires are elaborated in appendix C.

3.3.1 Camera observations

The run-up height of the regular waves is measured by using a digital camera (Panasonic HDC-HS300) with a resolution of 1920 x 1080 pixels. By using a frame the camera is placed directly above the slope with an angle of 2:1 above the slope 1:2 and 1.5:1 above the slope of 1:1.5. The camera is rotated such that 1920 pixels are in the direction of the run-up. In this way the run-up parallel to the slope is measured with sinus α the run-up height R_u is determined. The slope angle for the smooth slope and rough impermeable slopes is exactly (negligible difference) 1:1.5 and 1:2, for the other slopes this give a variation in accuracy

Next, to a video camera above the slope also a camera was placed on the side of the flume. The observations made with this camera may improve the knowledge on the inflow of water into the breakwater. Also, the breaker shape of the wave is recorded with this camera, and aspects of wave run-up. No quantitative measurements are made with the 'side-camera'.

3.3.1.1 Run-up measurements with the camera

For the actual measurements with the camera at least three aspects of the recordings must be known to be able to measure the actual parallel run-up. First, the level of the still water line in the recordings must be known. This is done by starting a recording during still water and read out the average pixel of the still waterline. Second, the number of pixels per millimetre must be known and last, of course, the average maximum pixel of the run-up must be determined. The pixel height of every water line is always determined by taking multiple points over the cross section, and determining the average pixel of these points. For the second aspects, two methods are used,

1. For the first couple of experiments it was quite accurate to measure the distance between the edge of the slope and the waterline (at multiple longitudinal sections). From recordings with the still water line the number of pixels over these distance can be determined, this leads values '*x [mm/pixel]'*
2. The second method is by placing a ruler on the slope and pointing out markers on the slope at known distances. The number of pixels between the markers leads also to a calibration value 'x [mm/pixels]'.

In appendix A a more elaborated explanation is given of the methods together with the accuracy (and precision) of the measurements. The frame that is depicts the maximum run-up situation is determined by observing the recordings frame by frame.

To ease the observations of the water motion tracers are poured into the water. Two types of tracers are used, wooden beads with a diameter of 8 mm, and black plastic pieces with a diameter of ±3 mm, see Photo 1. The wooden beads were sprayed with red paint to improve the visibility of the tracers. The amount of red tracers, however, was limited and after the first experiments were conducted several red tracers were sunk to the bottom. Therefore, the second type of tracers is also used.

Photo 1: Left red wooden tracers 8 mm and right plastic tracers

In case of a rough slope multiple points are needed to give a good estimation of the run-up. Otherwise the run-up is influences to much by local influences. Local influences can be, a 'channel' that is formed by stones lying close together in which the water surges up much higher than without. Also, without the tracers the edge of the water line was visible, especially when comparing the different frames.

The analysis of the run-up height in an irregular wave field, $Ru_{2\%}$, could not be observed/ measured. To be able to follow the water movement with the help of software tracers with enough contrast should be visible on the video recordings. In the case of the smooth slopes the tracers were gradually

dispersed over the flume, after a couple of surging waves the tracers moved away from the structure ,and with plunging waves some came back to the structure. After a couple of minutes only a few tracers (one or two) are visible on the footage. In the case of experiments conducted with irregular waves and the rough impermeable slopes also the second type of tracer is used. However, neither of the two tracers was transported to the top of the wave tongue. It seems that in the top part of the run-up tongue the upper water layer does not move forward.

3.3.2 Run-up measurements with resistance wires

For measuring the run-up of 2% of the highest waves in an irregular wave field (JONSWAP spectrum) camera observations were not the ideal measuring equipment. Therefore, the traditional method of measuring the run-up with a resistance wire is used. These resistance wires are custom made in the Waterlab. One resistance wire was placed on the surface of the armour layer, and a second one between the armour layer and the core of the breakwater. The resistance wires were only used in the experiments with the armour layer on an impermeable core and the complete permeable breakwater.

For these geometries the run-up due to regular waves is measured by using the camera's and the resistance wires. For the last geometries the relation between the different measuring methods can be determined. Resistance wires on the surface of the armour layer are always placed some millimetres above the slope. This leads to a lower run-up, because the water can flow under the wire without detection. Next, to this a resistance wire is also more influenced by local stone configuration were as with the camera observations a lot of points can be determined over the width of the slope. Third, the camera is positioned directly above the slope, thus the water line that is visible is partly between the stones.

3.3.2.1 Theoretical error on a smooth slope

On a smooth slope the error made by the resistance wire is dependent on the distance between the resistance wire on the slope *d,* the wave steepness of the incoming wave *s* and the slope angle *α* of the slope. In Figure 3.4 a graphical presentation of the under estimation of the run-up made by the resistance wire is given. For the given approach it is assumed that the run-up tongue is a straight line.

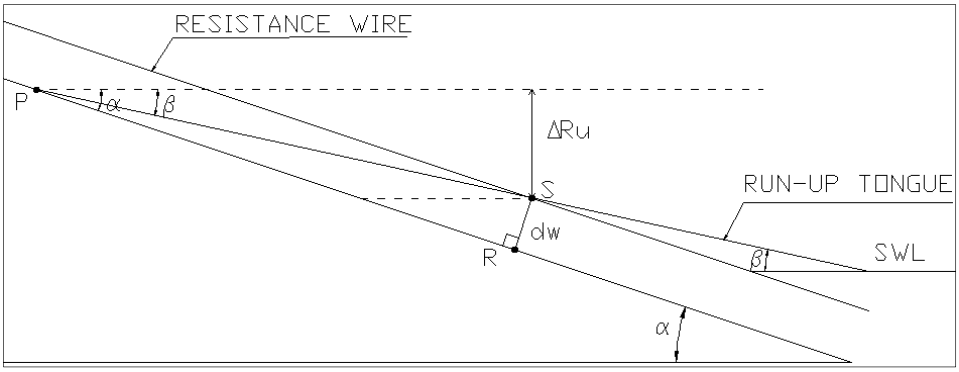

Figure 3.4: Theoretical error ΔR_u made by the resistance wire on a smooth slope

VAN DE WALLE [2003] stated the error made by the resistance wire can be determined by,

$$\Delta R_u = |PS| \sin\beta$$

With β has been determined by BRANDTZAEG [1962] (VAN DE WALLE [2003]),

$$\beta = \alpha - 5s$$

With the above figure this leads to the following equation for the run-up error made by a resistance wire on a smooth slope,

$$\Delta R_u = d_w * \frac{\sin(\alpha - 5s)}{\sin(5s)}$$

eq. 3.2

So, for a wave with low wave steepness the error is larger and can increase to large proportions. This approach is valid for surging and collapsing waves. However, also the upper parts of run-up tongue of breaking waves do not touch the resistance wire. However, the error made by surging waves is still (a lot) larger than for plunging waves.

3.3.3 Wave measurements

In front of the structure the wave conditions are measured by three wave gauges *WG*, more information about the gauges can be found in appendix C. The gauges measure the water elevation in time by measuring the voltage over the gauge. The wave height in front of the structure is influenced by the reflected wave. In KLOPMAN and VAN DER MEER [1999] (reference VAN DE WALLE [2003]) is stated that the wave gauge, nearest to the structure must be placed at a distance of $x \geq L_p/4$ in order to measure the reflection correctly. The wave gauges are placed at a distance of $x_{1\text{-}2}$=0.30 m and $x_{2\text{-}3}$=0.40 m for measuring an irregular wave field with the JONSWAP spectrum. The analysis of the data is done by the method of ZELT AND SKJELBREIA [1992] in case of irregular waves. For analysing the spectrum the measurements of the three WG are used. A more elaborated description of the wave analysis see appendix J.

For regular waves a 2-gauge method is used. The ideal distance between the wave gauges is L/4. In general the gauges are placed at a distance of $x_{1\text{-}3}$= 0.95 m and $x_{1\text{-}2}$= 0.30 m, however, for long waves the gauges are placed further away from each other, with a maximum distance of $x_{1\text{-}3}$= 1.8 m. The method for analyzing the water elevations measurements is developed by applying the linear wave theory on monochromatic waves, see GODA AND SUZUKI [1976](reference FUNKE AND MANSARD [1980]). Singularities exist for $x_{1\text{-}2}/L=n/2$, where *n* is an integer, to avoid these singularities the distance between the gauges must be in the range of $0.05L \leq x_{1\text{-}2} \leq 0.45L$.

3.4 Geometries and expectations

Based on previous studies and theory expectations of the experiment results are given. These expectations are helpful for determining possible errors in the analysis of the results and if not indicate possible interesting furthers research topics. In Figure 3.5 the general positioning of the slopes is given. In this case rough impermeable slope is situated in the flume, but as described this can be a smooth, rough impermeable slope or a physical scale model of a breakwater (impermeable or permeable).

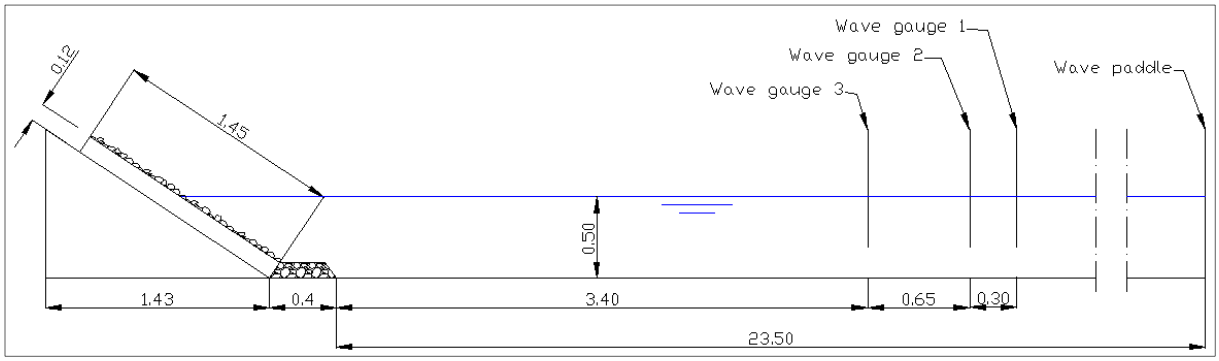

Figure 3.5: Side view of the flume with one of the slope placed in the flume, in this case rough impermeable slope 1:1.5 with d_{n50}= 0.067 or 0.09 m.

3.4.1 Smooth impermeable slopes

One of the geometries that are placed in the flume are smooth impermeable slopes (1:1.5 & 1:2). Theoretically the slope does not induce any friction and therefore no energy dissipation takes place on the slope. Only the wave motion itself results in energy dissipation, for example plunging breakers have large energy dissipation. No difference is expected between the wave run-up on the different slope angles, since no friction, and regarding the relative wave run-up as a function of Iribarren number (ξ) the influence of the slope angle is included in the Iribarren number.

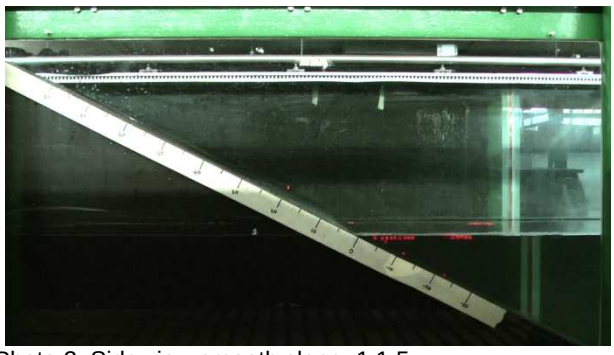

Photo 2: Side view smooth slope, 1:1.5

The energy of an incoming wave consists of the potential energy and the kinetic energy. When waves encounter the slope this energy is used to run-up the slope. When assuming that during maximum run-up the water has no velocity and no energy dissipation will take place, than the total energy is converted into potential energy. In JUMELET [2010] it is determined that in theory run-up of $R_u = 2.36$ H, see appendix H. Assuming a triangular wave run-up and sinusoidal shape of the incoming wave. This value gives an upper value in the case of surging, always some dissipation will occur, the waves cannot be described by the deep water equations and the shape of the wave run-up on the slope is not a triangular wedge.

In the seventies, BRUUN AND GÜNBAK [1977] did experiments with smooth slopes, quarry stone and rubble mound slopes. In this research experiments were performed with wave heights between 0.04 m and 0.15 m and periods from 0.8 to 2.43 s. The slope angle varied from 1:1.5, 1:2 and 1:3. Resulting in a covering range for the Iribarren number of $1.33 < \xi < 7.96$ (only till ξ=6.5 is presented), but for $\xi >$ 6 a constant range of values is found. The water depth was constant at 0.5 m depth. In their results a resonance peak was found between $2 < \xi < 3$. Resonance occurs, “when run down is in a low position and wave breaking takes place simultaneously and repeatedly close to that location”. The impact force of breaking waves is not damped, because the run-down motion is almost completed. So on the impact point no considerable water layer is present. For $\xi <$ 2.2 the run-down is not below SWL, the remaining water layer will damp the impact force and the wave run-up is therefore lower. For $\xi >$ 4 the wave run-up is approximately constant, according to BRUUN AND GÜNBAK [1977].

A second research on the wave run-up on smooth slopes is that of SCHÜTTRUMPF [2001]. In this research a multiplex plate was used to construct the smooth slope. The hydraulic parameter varied from H= 0.07 -0.20 m and T= 1.50 – 4.24 s. Three slope angles were used 1:3, 1:4 and 1:6, in combination with the hydraulic conditions, this result in an Iribarren number between 0.8 – 6.9.The water depth varied from 0.70 – 0.80 m, however, when d/H > 3.0 the water depth has no influence on the wave run-up. No peak was found between $2.0 < \xi \leq 3$ and a constant value of R_u/h =2.25 for high Iribarren numbers was found. In Figure 3.6 the results of the above considered studies are shown.

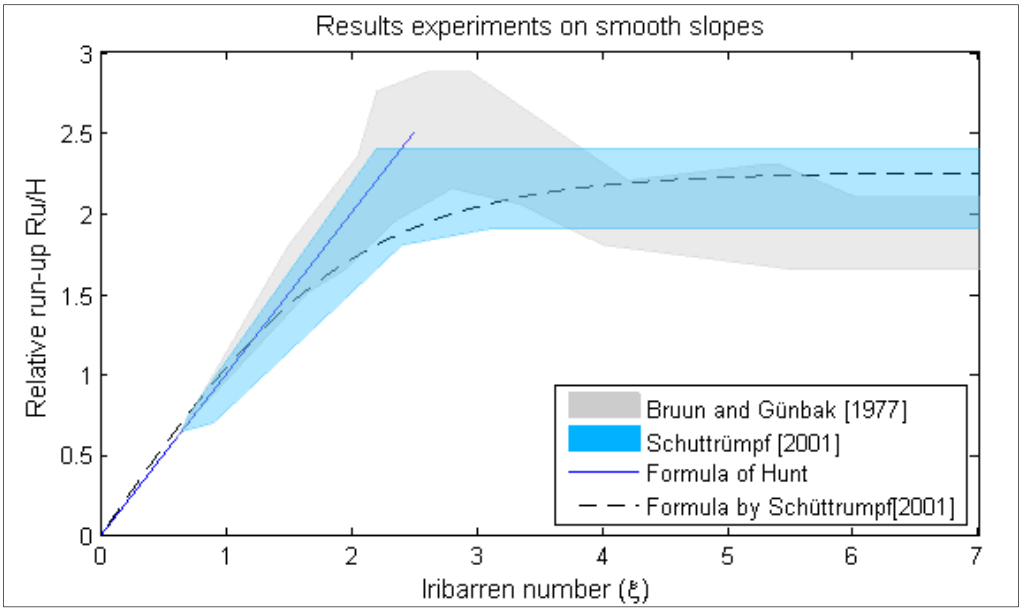

Figure 3.6: Previous results experiments on smooth slopes.

In Figure 3.6 it can be seen that the formula of Hunt eq. 2.6 gives a good approach of the run-up for ξ ≤ 2.5. This was also concluded in the research of ROOS and BATTJES [1976]. LOSADA and CHIMINEZ-CURTO (eq. 3.3) stated that the following equations could be used for the results of Bruun and Günbak,

$$\frac{R_u}{H} = \xi \qquad \xi \leq 2.5$$

$$\frac{R_u}{H} = 2.5 - \frac{2.5 - \xi}{3} \qquad 2.5 < \xi \leq 4.0 \qquad \text{eq. 3.3}$$

$$\frac{R_u}{H} = 2 \qquad \xi > 4.0$$

The formula of SCHÜTTRUMPF [2001] (eq. 3.4) is a hyperbolic function to have a smoother transition between the different breaker types.

$$\frac{R_u}{H} = 2.25 \tanh(0.5\xi) \qquad \text{eq. 3.4}$$

3.4.2 Rough impermeable slopes

The rough impermeable slope models only slope (surface) roughness of the armour layer, and not the permeability. During the experiments with the rough slope two stone diameters are used. The ratio d_{n50}/H varies between 0.43 – 1.2. In Figure 3.7 are cross sectional part of a rough impermeable slope is shown.

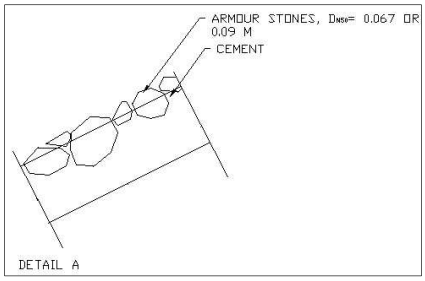

Figure 3.7: Sketch of the rough surface

Photo 3: Rough impermeable slope (outside the flume)

For practical reasons it is chosen to place the stones in a layer of cement. The first idea was to place a normal armour layer (two stones thick) and fill the pores with cement. However, the binding between the two layers was not strong enough. This could give complications when the slopes are lifted into the flume, due to the momentum in the slope. Moreover, the cement influences also the packing of the layers. Therefore, it would not make a lot of difference if the stones are placed as is shown in Figure 3.7 or in the two layer variant. Three different configurations of this geometry are tested in chronological order of testing,

1. 1:2 rough slope with d_{n50}= 0.067 m
2. 1:1.5 rough slope with d_{n50}= 0.067 m[1]
3. 1:1.5 rough slope with d_{n50}= 0.09 m

No other studies have investigated only the influences of roughness of rock material, however studies with blocks placed on smooth slopes and normal armour layer slopes are performed. In general the influences of the roughness decreases with increasing Iribarren number. In Table 3.5 the combined roughness factor of different types of geometries are presented. These factors belong to test with irregular waves; however, the physical processes that occur are the same as with regular waves. The reduction factors in the table are for low Iribarren numbers ($\xi \leq 2$). With increasing Iribarren number the reduction coefficient increases gradually to one. Physically this can be seen as, for a long wave (large Iribarren number) the layer thickness over the slope is large, the influence of the stones on the flow is therefore relative small. For example, in case of a collapsing breaker the layer thickness is small and therefore the flow of water is relatively more hindered by the stones. The forces of stones in bed protection are also lower in the case of increasing wave length, which indicate a reduction in roughness, see section 2.2.2.

The ratio d_{n50}/H varies between the different test runs, due to varying wave height and stone diameter. This will lead to a spreading of the relative run-up. A larger wave height has a lower reduction than smaller wave height. This should be more pronounced in the case of a d_{n50}= 0.09 m. For the test with a d_{n50}= 0.067 m it is expected that the ratio d_n/H causes only a slight difference. In De Waal et al. [1992] the same ratio is tested and no large difference was found. For plunging waves the situation is different, because the influence of the wave height on the layer thickness is smaller due to the breaking of the wave on the slope.

The curve that is expected will have an average maximum of $R_u/H \approx 1.9$ for Iribarren numbers larger than 4 – 5, based on literature study. For the stones of $d_{n50;c}$= 0.09 m a larger difference is expected

[1] *This slope is created by shortening the 1:2 version. Thus, the surface texture is identical for the first two slopes.*

between the different wave height. In Figure 3.8 the above statements are graphically presented. The following formula is used,

$$\frac{R_u}{H} = 2.0 * \tanh(A * \xi_0) \qquad \text{eq. 3.5}$$

Where A is lower in the case for $d_{n50}/H > 1$.

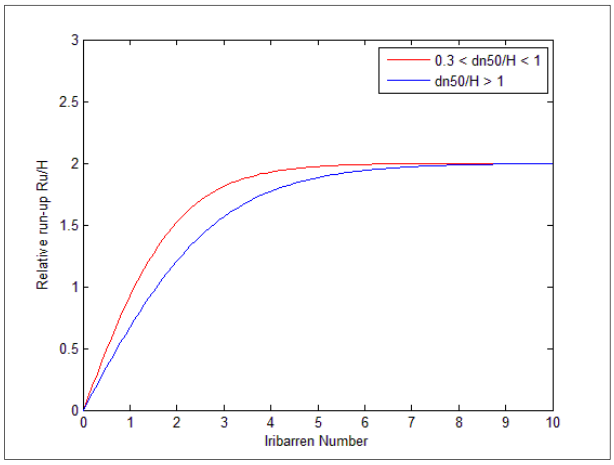

Figure 3.8: sketch of the expectations of a rough slope

3.4.3 Armour layer on an impermeable core

The next geometry that is constructed in the flume is a core with a permeable armour layer, where the core is made impermeable by placing a plastic sheet over the core surface. The plastic sheet is flexible, so that the armour layer follows the rough surface of a rubble mound core. This latter is needed for stability reasons and to represent the porosity of an armour layer correctly on the boundary with the core. Also, in this case three slopes are tested, a slope with an angle of 1:1.5 with $d_{n50;a}$= 0.067 or 0.09 m and a slope angle of 1:2 with $d_{n50;a}$= 0.067 m. This slope is placed at approximately the same place as the rough impermeable slope, see Figure 3.5.

Photo 4: Side view armour layer on impermeable core, plastic sheet fixed at the sides by tape.

For regular waves the hyperbolic function probably gives the best representation of the results. The transition between the breaker types is more ‘naturally’. From Table 3.5 the roughness coefficient for an armour layer on an impermeable core is 0.55 for low Iribarren number (ξ). However, this reduction

value is determined for irregular waves, the principle is the same. For increasing Iribarren number (ξ) the relative run-up will increase, but not till the level of the smooth slope, see Figure 3.9. For an impermeable core estimations are made in relation to test of BRUUN AND GÜNBAK [1977] on rubble mound breakwaters and the above statements. For high Iribarren numbers the average maximum is R_u/H = 1.3.-1.4. The shape coefficient is in the order of 0.4, this in relation with figure 4.10, since for low Iribarren numbers the permeability has a negligible influence.

$$\frac{R_u}{H} = \gamma_{f;c} * 2.0 * \tanh(A * \xi)$$

where,

$\gamma_{f;c}$ = combined roughness (≈ 0.7)

$A \approx 0.4$

3.4.4 Permeable slopes

Two different permeable slopes are tested, with a grading of 1.5 and a grading of 4. The breakwater has a slope of 1:2 and armour layer of d_{n50}= 0.067 m. The breakwater is constructed in approximately the same location as the previous geometries, see Figure 3.5.

Photo 5: Armour layer on a permeable core, with a grading of 4

In BRUUN AND GÜNBAK [1977] tests are stated about rubble mound breakwaters, with a filter layer of d_{50}= 20 mm and core material of d_{50}=4 or 10 mm. Hydraulic condition were 0.038 ≤ H ≤ 0.16 m and 0.8 s ≤ T ≤ 2.43 s. The wave run-up measurements in this study and other studies have led to Figure 3.9. The scale of the core stone in this research is small, leading to a flow that is more laminar than in prototype breakwaters occurs. For ξ> 4.0 the relative wave run-up is approximately constant at a value of $R_u/H \approx$ 1.2.

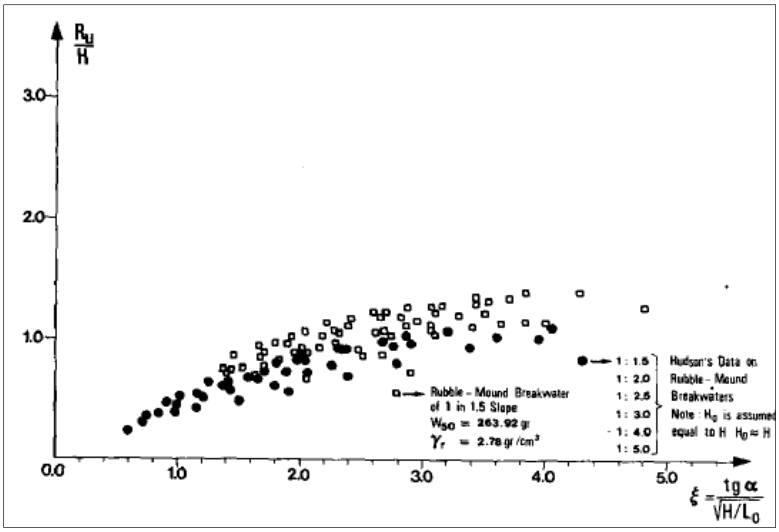

Figure 3.9: Results rubble mound breakwater, ○results BRUUN and GUNBAK [1977] and ●results Hudson, BRUUN AND GÜNBAK [1977]

Expected is that for ξ≤ 3.3 the relative run-up is similar as for the impermeable slope. For larger Iribarren numbers the influence of the permeable core should be noticeable. In Figure 3.10 the values computed with the Volume exchange model are compared with the expected results of the armour layer on an impermeable core. However, a small modification is made in the volume exchange model. The roughness factor of 0.75 is removed, because of the expectation of small influences of the roughness for large Iribarren numbers. The reduction for large Iribarren numbers is in the order of 5 %.

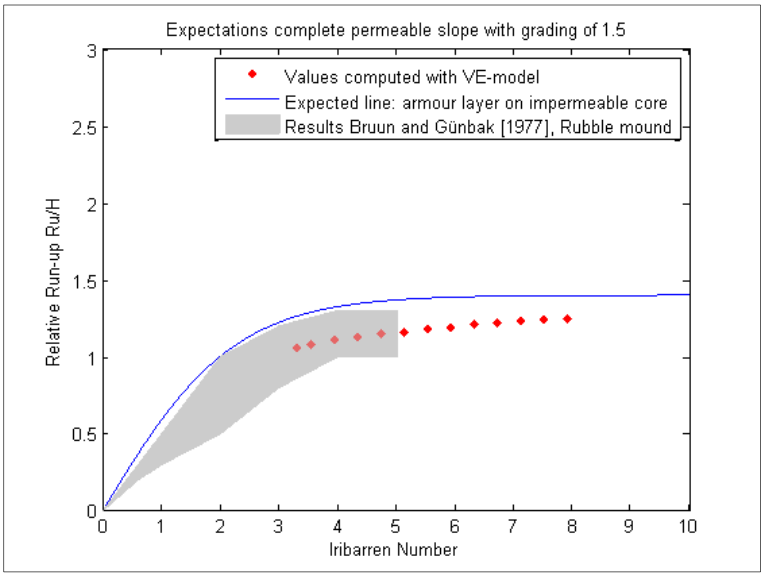

Figure 3.10: Expectations permeable slope computed with the volume exchange model.

3.4.5 Expectations on Irregular waves

For the expectations of the experiments with irregular waves, eq. 2.7 is used. In Table 3.5 the roughness coefficient based in previous studies are listed.TAW [2002] give guidelines for designing coastal structures. The rough impermeable slope is not equal to a single layer armour layer, due to the permeability of this armour layer. The coefficients are valid for ξ< 2.0 and thereafter the coefficient increases linearly till one for the range of 2 till 10. The expectations for the irregular wave experiments for the smooth slope and impermeable core are showed in Figure 3.11.

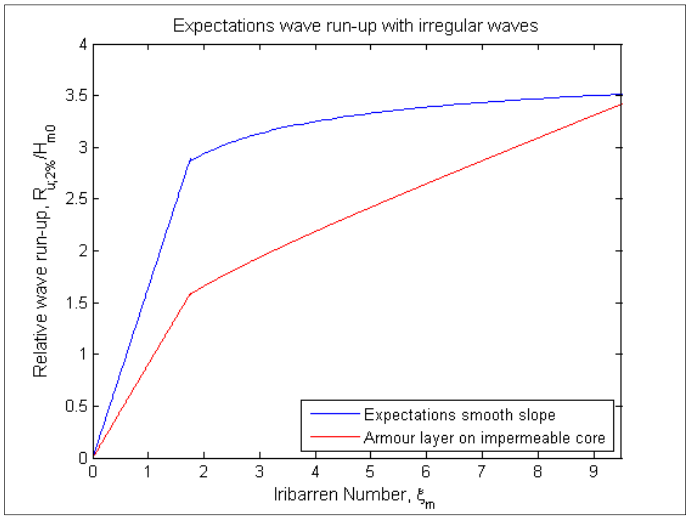

Figure 3.11: Expectations $R_{u2\%}/H$ for an impermeable core and a permeable core

Type of slope	d/H_s	Literature	$\gamma_{f;c}$	Remark
One rubble layer	0.33 – 0.67	De Waal et al. [1992]	0.55 – 0.60	Valid for 1 < ξ < 4
Two or more rubble layers	0.17 – 0.67	De Waal et al. [1992]	0.50 – 0.55	
Rock, one layer permeable core	- (unknown)	Bruce et al. [2006]	0.45	Valid for 1:1.5 slope.
Rock, two layers permeable core	-		0.40	
Rock, one layer impermeable core	-		0.60	
Rock, two layers impermeable core	-		0.55	
Single armour rock	-	TAW [2002]	0.70	
Two layers rock	-	TAW [2002]	0.55	
Ribs (optimum distance)	-	TAW [2002]	0.75	

Table 3.5: Combined roughness coefficients of different researches or literature

Chapter 4

Comparison of measuring equipments

4.1 Difference between video observations and resistance wire

For the last series of experiments the run-up was measured by a resistance wire and video recordings. Resistance wires ('RW') are the traditional measuring equipment for measuring run-up on a slope. This method uses two steel wires, through which alternating current flows. The output of the equipment is a voltage, which is larger if the wire is under water. So a higher voltage indicates a higher run-up. The calibration factor is then determined by raising the water level in the flume slowly and using the wave gauges as a reference, see appendix C. The method described is easy in use, especially in the way it processes the data. In practice however, some problems with this method took place. First of all the RW had to be placed at a distance d_w above the slope. In this way the run-up tongue of a wave was able to surge up beneath the wire without making physical contact, leading to a lower measured run-up than actually occurred. Secondly the wire measured a local run-up that could deviate from the average run-up over the width. This problem could result in both overestimations and underestimations, but could easily be avoided by placing multiple wires on the slope.

The main method of measuring the run-up, used in this study (video recordings), was not influenced by the previous problems. Through video recordings the water was directly visible on the slope and also in the first centimetres of the slope. So, the difference between the RW and video recordings results is partly caused by measuring the water line inside the armour layer with the video observation method.. Moreover, the average wave run-up over the width can be determined, see also appendix A. This method, however, has other disadvantages. Processing of the video recordings into actual run-up measurements is labour intensive. Furthermore it was not possible to automate the process, because the contrast between the water and the slope was not large enough (except for a smooth slope). This lack of contrast not only avoided automation, but it also made the measurements sensitive for inaccuracies and misinterpretations.

During the experiments with the permeable and impermeable core the wave run-up of regular waves was measured by the two different measuring equipments. The average distance d_w between the stones and wire was 11 mm (the area of interest). Surging waves and the run-up tongue of breaking waves were able to flow under the wire without detection. In the experiments only one resistance wire was placed on the slope, which led to large influence of the local stone configuration.

4.1.1 Measured differences

In Figure 4.1 till Figure 4.4 the differences between the two methods are graphically presented. In general no large differences were found when regarding the surging waves. However, in the case of plunging waves a significant difference was observed. The difference between the two methods can have four different causes,

- Accuracy of the measurements
- Distance of the wire till the slope
- Video recordings show the water line on and slightly in the slope
- Local stone configuration

The first cause is elaborated in appendix A and C and the second cause is discussed in section 3.3.2.1. By placing a video camera directly above a slope with relatively large stones, led to a view that recorded the water line at the surface and between the stones. The water level could not be

determined, since the recordings were made directly from above (perpendicular to the slope). The combination that the resistance wire, was placed 11 mm above the slope and the view inside the layer has led to a difference in the measured run-up. The influence of the local stone configurations was also introduced above. Only the third cause is not a model or measuring error, but a principle difference between the two measuring methods.

For surging waves the structural error has a slight influence on the difference between the two different measurement methods. The variation is always within the accuracy band width of the measurements. Moreover, the measured values by RW_{arm} are also often higher, which give indications that the local stone configurations are more of influence. One of the factors that are important for this is that the run-up tongues not a clear run-up tongue as in the case of a smooth slope. The wave run-up tongue (on the surface) that is not detected by the resistance wire has a small thickness, which is easily stopped by a stone. This leads to a 'more abrupt' end of the run-up, which leads to a more equal value for both measuring equipments.

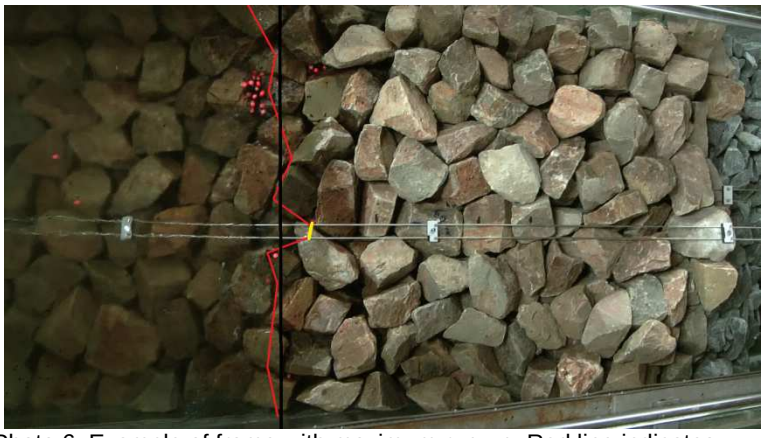

Photo 6: Example of frame with maximum run-up. Red line indicates water line, yellow line: measurement run-up level by RW_{arm} and black line is average wave run-up level. Experiment no.: E197

The measurement with the resistance wire was mostly influenced by the local stone configuration. The theoretical error on a smooth slope was not directly applicable for measurements on a geometry with an armour layer. This was caused by using only one resistance wire. Moreover, the resistance wire influenced the placing of the stones, which resulted in a less randomly placement beneath the wire. For example, in Figure 4.3 the resistance wire did not indicate a reduction due to the infiltration of water into the core. In Photo 6 the frame with maximum run-up is given. Clearly visible is the difference between the measured levels. In other words, the local influences were an important factor for the measurements done with the resistance wire unlike the ones done with the video observations. Nevertheless, for surging waves (and collapsing) the measurements had the same "shape".

With respect to plunging waves ($1.5 < \xi < 3$) a large difference was visible, not only between resistance wire and video recordings, but also between the different geometries. Where the video observations gave consequently values around $R_u/H \approx 1$, the values obtained by RW_{arm} fluctuated between $R_u/H \approx 0.5 - 0.9$. In Figure 5.13 results of a wave run-up measurements on a semi-permeable breakwater are given, which indicate that in these measurements also a scatter was visible between $R_u/H = 0.5$ -1. These results, however, originate from an old research which most likely used a resistance wire as measuring device. The measurements done for the video observations, compared with the resistance wire, "overestimate" the run-up. Still, this is a (possible) good example of the influence of recording the water line not only at the outer surface but also inside the armour layer. When the plunging wave is broken down on the slope, then the maximum run-up is practically reached. But during breaking it was difficult to recognize the water line (turbulent and splashing water),

and after the wave was broken down the water line was mostly situated between layers or inside the armour layer. The latter situation could be measured by the video recordings, but not with the RW.

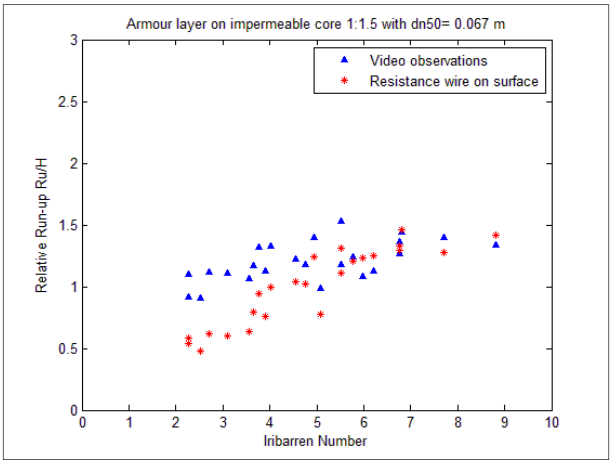

Figure 4.1: Comparing measurement methods, Impermeable core, 1:1.5 with $d_{n50;a}$= 0.067 m

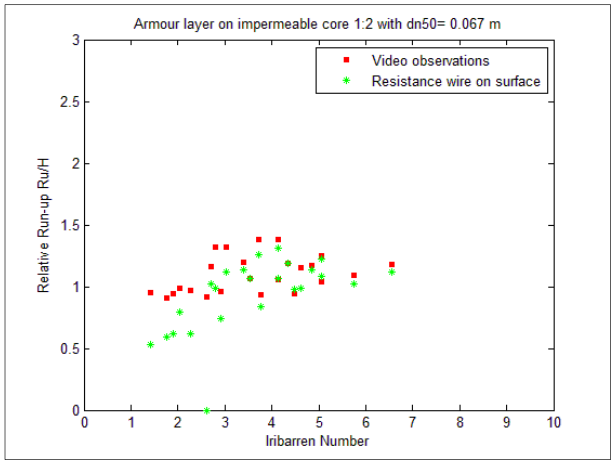

Figure 4.2: Comparing measurement methods, impermeable core, 1:2 with $d_{n50;a}$= 0.067 m

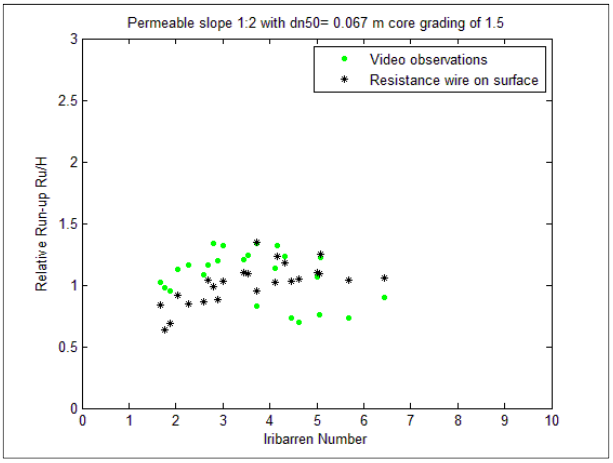

Figure 4.3: Comparing measurement methods, permeable core, grading of 1.5

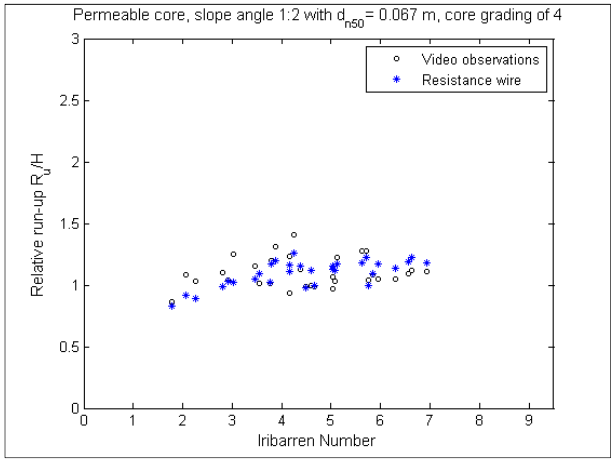

Figure 4.4: Comparing measurement methods, permeable core, grading of 4

In short, for the measurements done with surging waves no large differences were found. Two main reasons could be given for this. Firstly, the wave run-up tongue was less pronounced on an armour layer than in the case of a smooth slope. Secondly, the local stone configuration had a large influence on the measurement compared to the values averaged over the width of the slope. When regarding the plunging waves the video recordings gave a more constant value of the plunging waves (which were not influenced by a permeable core). This was probably caused by the video observation method which allowed a measurement of the visible water line between and on the slope. However, measurements of plunging waves were more sensitive for misinterpretations due to the turbulence and splashes of breaking waves.

4.2 Resistance wire error with irregular waves

In Figure 4.5 the results of the experiments conducted with irregular waves are given. The difference between the expected and the measured values is clear. In this section the results are not analysed, but a probable cause of the underestimations is given.

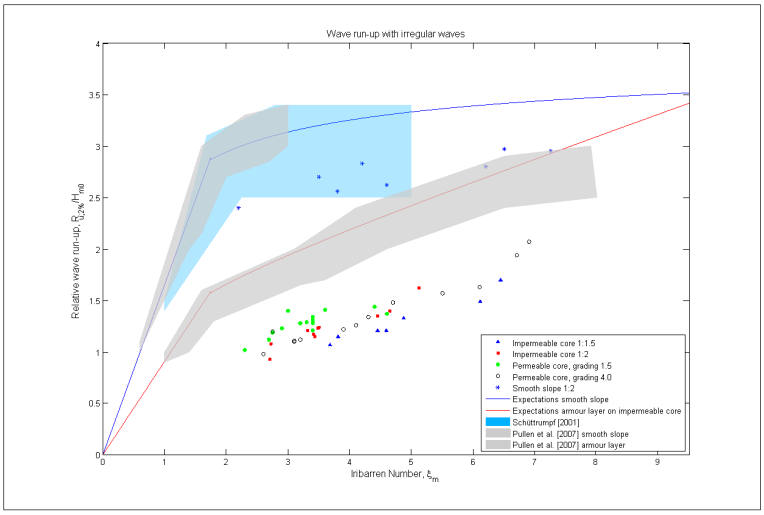

Figure 4.5: Results irregular waves

In section 3.3.2.1 it is discussed that on a smooth slope the underestimation caused by flow under the wire can be computed by using eq. 3.2. In the results of the regular waves (see Figure 4.1 - Figure 4.4) no structural underestimation of the measurements with a RW is visible. One may say that for armour layer slopes this error is negligible. However, for regular waves the local stone configuration has more influence on the measurements, as is also discussed. The local stone configuration for irregular waves is of less importance, since every wave(and run-up) is different. In VAN DE WALLE [2003] the difference between a resistance wire and a digital wave run-up gauge is determined. Wave run-up values measured by the resistance wire where always lower than measured with the digital wire gauge. On average a underestimation of 8 %, with a maximum of 25 % was found.

The underestimations by the resistance wire is not the only cause of the underestimation, see Figure 4.6. The adjusted values are determined by adding the computed wave run-up error to the measured values. In appendix D the measured values and the error computed with eq. 3.2 are given.

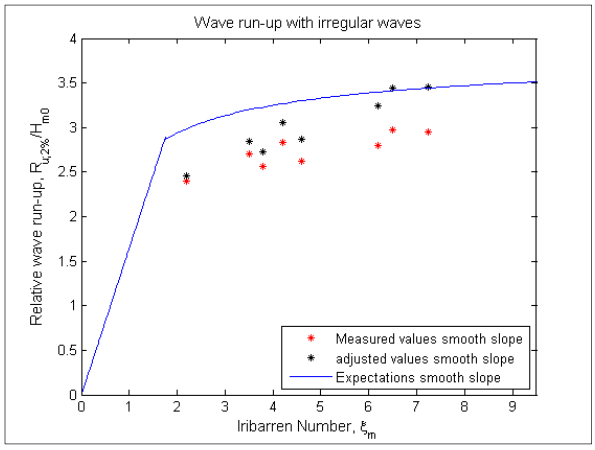

Figure 4.6: Adjustments results smooth slope with measurement error

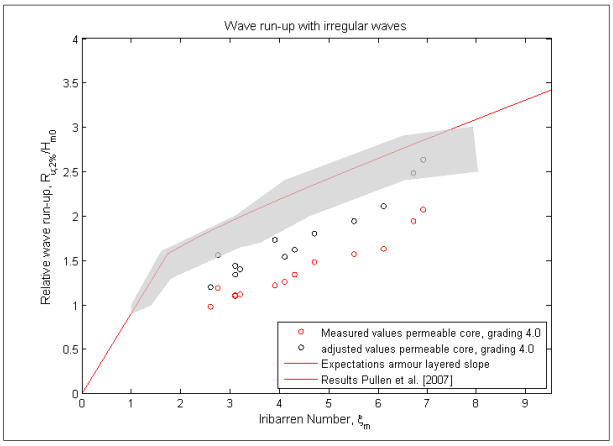

Figure 4.7: Adjustments results permeable core with measurement error

It seems that the measurement error is not the only cause of the underestimation of the wave run-up. In VAN DE WALLE [2004] is stated that the low spectral width of the JONSWAP spectrum in the laboratory experiments is a probable cause of the underestimation of wave run-up, $R_{u2\%}$. This statement was based on experiments conducted in the GWK with $\varepsilon \approx 0.60$. However, in the current experiments the values are also in the range of $\varepsilon \approx 0.60$, and show lower values run-up values than

expected, see appendix D. So, here no relation is found between a low spectral width and a lower wave run-up. Generally, when the spectral width increases also the wave run-up increases. In appendix I more information about difference between small scale laboratory and large scale experiments are given.

In DE ROUCK ET AL. [2007] an elaboration is given about the comparison between full scale measurements and the laboratory measurements. It was concluded that in the case of the Zeebrugge breakwater the wave run-up was underestimated in the laboratory experiments. The exact cause of the model effects is still not fully understood. However, the model effects should not deviate a lot between the structures, since the models are built and scaled in the same manner.

First, the error made by the resistance wire is added by the measured $R_{u2\%}/H$. For the situation with the smooth slope the theoretical error can be computed with most precision, because the distance between the wire and slope is almost constant. In Figure 4.6 the adjustments of the measurements error are shown. Using these values to curve fit the values to the expected line, leads to the following multiplier,

$$C = 1.41 * \xi^{-0.17} \qquad \text{eq. 4.1}$$

For the RW on the slope a distance between the slope of d_w=10 – 15 mm. Based on the measurements of d_w on the slope with a grading of 4.0 and impermeable slope 1:2. However, these are average values over the length of the slope. These adjustments lead to the graph in Figure 4.8.

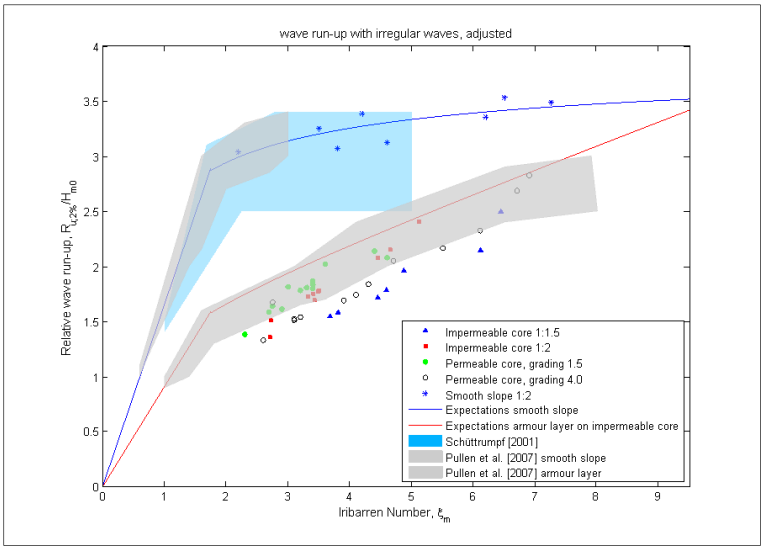

Figure 4.8: Adjusted values for the irregular wave experiments

In Figure 4.8 the adjusted values of $R_{u2\%}/H$ of the experiments performed in this study are given. Also, results of other studies are given. It seems likely that the underestimations are caused by a combination of the error made by the resistance wire and model effects.

Chapter 5

Analysis experiment results

5.1 Introduction

In the chapter 4 the experiment program is considered. One of the objectives of this experimental program is to be able to determine the influence of the surface roughness and permeability of the armour layer on the run-up height. Also, the influence of the core permeability of the run-up is of interest regarding the Volume exchange model. Furthermore, also for the volume exchange model it is interesting to know the run-up at the surface of the core (between armour layer and core).

The experimental program consists of four different geometries. The first geometry is a smooth slope with an angle of 1:1.5 or 1:2. The second geometry is a rough impermeable slope, this slope models only the roughness of an rock armour layer. Third, a scale breakwater was built in the slope consisted of an armour layer on an impermeable core. Finally a geometry with a permeable core was tested with armour stones of d_{n50}= 0.067 m and slope angle of 1:2. The core material consisted of a d_{n50}= 0.033 m and a grading of 1.5 or 4. The measurements of the run-up height are done with video recordings and resistance wires on the surface of the armour layer and on the surface of the core. In chapter 4 the physical scale model has been elaborated. The wave height used in the experiments can be categorized in three categories, see Table 5.1.

Name	Wave height range [m]
Small wave range	0.065 ≤ H ≤ 0.075
Medium wave range	0.085 ≤ H ≤ 0.110
Large wave range	0.130 ≤ H ≤ 0.150

Table 5.1: Wave height ranges

In this chapter the results obtained during the experiments are presented and analysed. In appendix B the results of the measurements done with the video recordings and in appendix D the values measured with the resistance wire are given. This chapter is divided in an analysis of each geometry, starting with the smooth slopes, and continuing in chronological order. In the second part the influence of the roughness of the armour layer is elaborated. In section 5.4 the influence of the core permeability on the run-up is discussed. Followed, by the influence of the stone diameter which is included in the relative wave run-up to reduce the scatter in the graphs. Finally, the imposed core run-up on an impermeable and a permeable core is considered.

5.2 Analysis per geometry

5.2.1 Smooth slope

In section 3.4 previous experiments with regular waves on smooth slopes are considered. In this thesis experiments were conducted with smooth slopes with slope angle 1:1.5 or 1:2. Here, a comparison is made between the current experiment results, the findings of BRUUN AND GÜNBAK [1977] and SCHÜTTRUMPF [2001]. This indicates if the measuring method with video recordings gives reliable results and which reference is best to use.

In Figure 5.1 the results of previous studies to wave run-up on smooth slopes are shown. The current test program has more similarities with BRUUN AND GÜNBAK [1977] than with SCHÜTTRUMPF [2001]. This is also visible in the results, the results of this thesis coincide very well with the results of Bruun and Günbak.

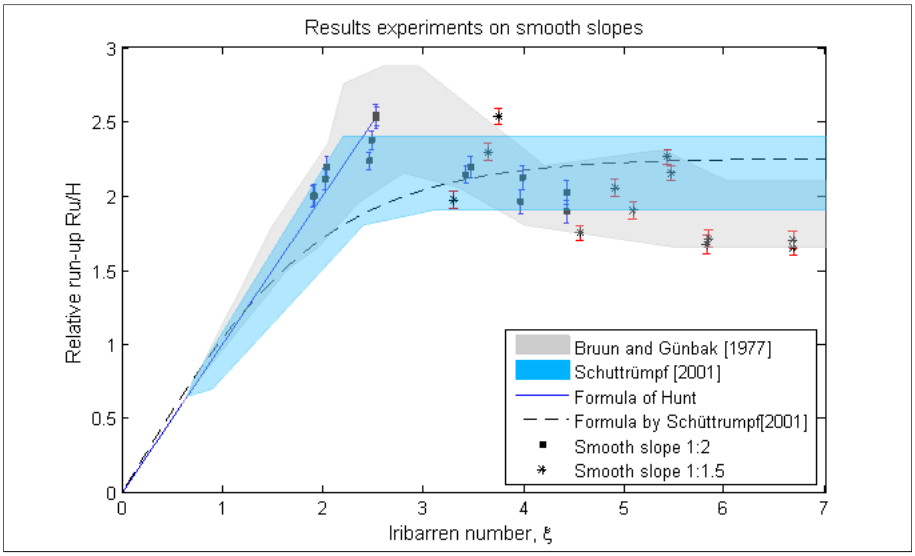

Figure 5.1: Results smooth slopes compared with previous studies.

The main difference with SCHÜTTRUMPF is the slope angle (1:4 and 1:6). The large scatter that is visible in the graph and the difference between the two previous researches cannot be explained by the only accuracy of the measurements. It may be possible that the slope angle has an influence in another way than it is incorporated in the Iribarren numbers. For the explanation of the scatter it is important that a difference is made between types of breaking. The analysis is not only based on the measurements, but also on the side view video recordings.

In the area of the plunging waves ($\xi < 2$) little scatter is found. In this area the impact force of the breaking wave is reduced due to the remaining water layer of the previous run-up. In this range the run-down motion is not completed, before the next wave breaks on the slope. The impact on the remaining water layer leads to large turbulence in the layer and energy dissipation. Between $2 \leq \xi < 3$ this run-down motion is for a large part completed, therefore the remaining water layer is smaller, thus the dissipative effect is less. After studying the video observations of the plunging waves in this Iribarren range, the effect of the remaining water layer was visible. After every high wave run-up a smaller wave run-up followed, and vice versa. So, within the same experiment the run-up varied between two consecutive wave run-ups. This was not visible for the surging waves, were the wave run-up was the same after the equilibrium situation was reached. After breaking of the wave, the shape of the wave run-up had a quite clear triangular wedge shape.

For surging between $3.5 < \xi < \leq 6.0$ the wave run-up shape had a more concave shape. For low Iribarren numbers this was a more pronounced concave shape at maximum run-up than for larger Iribarren numbers. A difference was visible between different wave heights. For a slope angle of 1:1.5 the following holds, the concave shape is caused by a phenomena, which best can be described as a "whip" effect. With a large wave and short period this effect is larger. For a surging wave this effect starts higher up on the slope and for a collapsing wave this starts below SWL. The run-up starts as an triangular wedge shape, but is reshaped turns in a concave shape. For a slope with 1:2 this effect was not visible, but it were not a lot of measurements for large Iribarren number (ξ).

For $\xi > 6.0$ a lower relative wave run-up is measured. In SCHÜTTRUMPF [2001] no reduction is visible in the results and BRUUN AND GÜNBAK did not comment on the reduction for large Iribarren numbers. For surging waves their only comment was: "It attains an approximately constant level for high Iribarren numbers (ξ) values ($\xi > 4.0$)". In GRANTHEM [1955] (reference HUGHES [2004]) one of the tested slopes had an angle of 1:1. For this slope from $\xi > 3.5$ the relative run-up was distinctive lower than for the gentler slopes. Probably, the same phenomenon is the cause for this reduction as for the large

Iribarren number (ξ) for a slope 1:1.5. In HUGHES [2004] and JUMELET [2010] it is mentioned that surging waves or waves on steep slopes have a more concave shape. Plunging waves have a triangular wave run-up wedge. The weight of the wave per unit width, in case of a triangular run-up wedge is theoretical determined in HUGHES [2004] (eq. 5.1)

$$W_{wave} = \frac{\rho g}{2} \frac{R^2}{\tan\alpha} \left[\frac{\tan\alpha}{\tan\beta} - 1 \right] \qquad \text{eq. 5.1}$$

The weight of the run-up or the volume of the wave run-up determines the run-up height, since no energy dissipation takes place on the slope. Regarding an energy balance, an incoming wave rushes up the slope till the incoming energy is transferred in potential energy, in the form of the wave run-up volume. In appendix H the triangular wave run-up wedge approach used by JUMELET [2010] is given. With this theory and assuming a sinusoidal incoming wave a R_u/H= 2.36 has been determined. This is not in agreement with the current measurements and results, because analysis shows a lower relative wave run-up for a triangular wedge shape run-up. A probable cause in the difference is the assumed value for the incoming wave and the potential energy of the triangular wedge.

So, from the side-view video recordings it became clear that the wave run-up shape for ξ≥ 6, has a more wedge shape than a concave shape. In these experiments the local wave steepness was lower than 0.03. For values 3.5 < ξ <6 the shape is a more concave shape. With decreasing Iribarren number it has an increasing pronounced concave shape, however, this shape is also influenced by the wave height (run-up) and period. For ξ > 6 only small waves with correspondingly low run-up are tested, so the relation with the breaker parameter may be the cause of this. Regarding the energy balance, it is possible that a concave shape run-up has a higher run-up and still has the same weight/ volume as a wave that has a triangular wedge run-up. The hypothesis is that with a more pronounced concave shape the relative run-up is higher than in the case of a triangular wedge shape at maximum rub-up due to a difference distribution of volume in the run-up shape for a slope angle of 1:1.5.

The analysis behind the scatter in the results of the smooth slopes experiments is not the main research topic of this thesis. With the current obtained results the above made statements cannot be conclusively determined. More research should be done to the (cause) shape and volume of the wave to be able to make conclusive remarks.

5.2.2 Rough impermeable slope

The rough impermeable layer is made out of stone of d_{n50}= 0.067 or 0.09 m, that are placed with half of their diameter in a cement layer. These slopes are placed on the former smooth slopes, and have an angle of 1:1.5 or 1:2.

In section 2.2.2 is mentioned that with increasing breaker parameter the influence of the surface roughness decreases, and also with larger wave heights the influence of the roughness on the run-up is less. In the results these phenomena are clearly visible. In Figure 5.2 the results of the measurements performed with the video recordings are presented. In Figure 5.3 the same results are given only the width the bandwidth of the accuracy of the measurements. Between 2 ≤ ξ < 3 no resonance peak is visible, this was expected since the stones absorb the impact forces of the breaking wave and drag forces in the run-up tongue. For ξ > 4 the relative run-up is constant with the scatter is caused by the variation of d_{n50}/H. However, for values for ξ > 7 seems to be an extra reduction. This can also be a consequence of a higher ratio of d_{n50}/H, however, the surface roughness has less influence for large Iribarren numbers. Another explanation is that, for large ξ values the rough slope acts as a smooth slope. So, the same phenomena can occurs as was seen in the results of the smooth slope 1:1.5. Overall, the scatter in the results is mainly caused by the ratio d_{n50}/H.

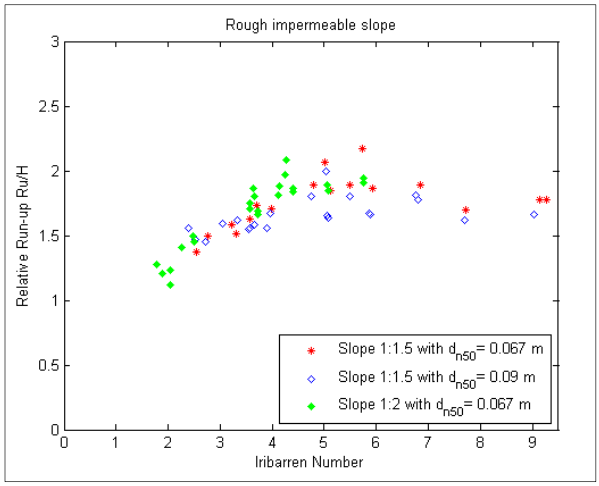

Figure 5.2: Results rough impermeable slope

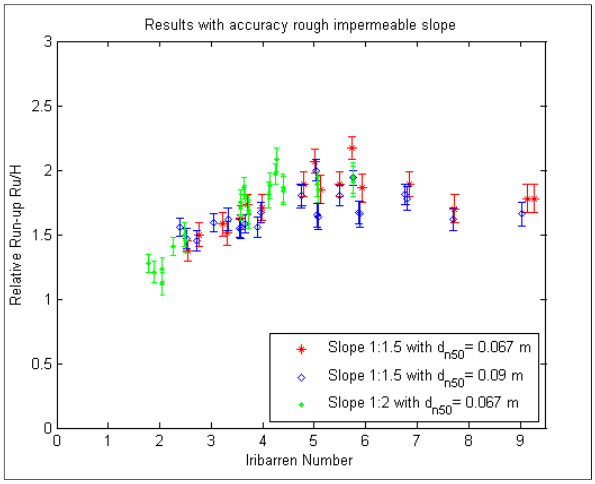

Figure 5.3: Results rough impermeable slope with bandwidth

Figure 5.3 shows the results with their bandwidth, this result in an unclear graph. Figure 5.2 is the results of interpolation between the error bars. The results follow the shape expected line, only the reduction for low Iribarren numbers for d_{n50}= 0.09 m, was expected to be larger. Apparently the difference in reduction in the run-up tongue has almost no effect. For surging waves a larger reduction is found for the test conducted with d_{n50}= 0.09 m. So, the roughness has an influence for larger Iribarren numbers (ξ). The graph can be divided according to types of breaking and trends in the graph. Between ξ = 4 – 5 the interpolation leads to a biased image. When regarding the trend of only the slope with d_{n50}= 0.09 the R_u/H values in this range would be approximately 1.7.

- Plunging breaker, from 1.5 < ξ < 2.8
- Collapsing waves from 2.8 < ξ ≤ 3.3 (3.6)
- Surging waves from 3.6 ≤ ξ < 7.0
- Surging waves from 7.0 ≤ ξ < 9.5

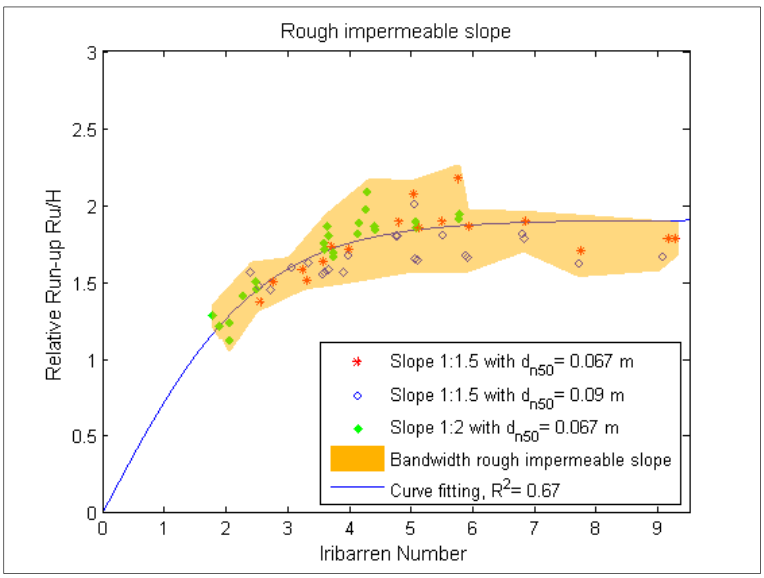

Figure 5.4: Results rough impermeable slope with the hatch area depicts the accuracy of the points.

The sudden 'break' at (ξ, R_u/H)= (6,2) is the result of performing experiments for the large wave range till ξ <6. A slight difference in increase of the R_u/H with increasing Iribarren number between the plunging and collapsing waves is found. Both the water layer that runs up the slope is relatively small, but the plunging waves dissipate a lot of energy due to the wave impact. For surging no significant increase of R_u/H with increasing breaker parameter is found. The slope of the graph and the transition between the different breaker types can best be approached with a hyperbolic functions, as in eq. 3.4. The blue line in Figure 5.2 is the curve fitted line with the properties as shown in eq. 5.2.

$$\frac{R_u}{H} = a * \tanh(b * \xi)$$

eq. 5.2

$$a = 1.86$$

$$b = 0.42$$

$$R^2 = 0.67$$

5.2.2.1 Influence of the stone diameter

The scatter in the graph is mainly caused by the difference in d_{n50}/H ratio. The run-up is in principle a function of the wave height, Iribarren number and the stone diameter. In section 2.2.2 the influence of the water layer thickness on the influence of the combined roughness is described.

In the above figures it becomes clear that with a d_{n50}= 0.09 a slightly larger reduction of the run-up is found. In Table 5.2 some experiment results are shown. When comparing the two slopes, it becomes clear that only the stone diameter influences the roughness, since the other parameter are not varied, see also appendix B.

No.	Wave height [m]	Reflection coefficient [-]	Measured run-up [m]	Relative run-up [-]	Wave period [s]	Wave length [m]	Wave steepness [-]	Iribarren number [-]
Results rough impermeable slope 1:1.5 with d_{n50}= 0.067 m								
E050	0.070	0.72	0.130	1.86	1.88	3.77	0.019	5.9
E051	0.065	0.65	0.121	1.85	1.57	3.00	0.022	5.1
E052v2	0.065	0.86	0.116	1.78	2.80	5.90	0.011	9.1
E053	0.085	0.82	0.161	1.89	2.40	5.00	0.017	6.8
Results rough impermeable slope 1:1.5 with d_{n50}= 0.09 m								
E071	0.071	0.70	0.120	1.67	1.88	3.76	0.019	5.9
E072	0.067	0.66	0.110	1.65	1.57	3.00	0.022	5.1
E069	0.067	0.83	0.110	1.66	2.80	5.93	0.011	9.0
E073	0.087	0.80	0.158	1.81	2.40	4.99	0.017	6.7

Table 5.2: Some results of the experiments on a rough impermeable slope

The energy loss over the wave run-up period can be determined by using the run-up velocity in the Morison equation. This determines the force on the stone, which can be used to determine the energy dissipation on the slope, see section 2.2.2. This resulted as energy dissipation as a function of d_{n50}/(Hξ). For surging waves the influence of the Iribarren number is small, as is visible in Figure 5.4. So, in the case of a rough impermeable slope the scatter is mostly caused by the ratio d_{n50}/H. The difference between plunging and surging is logical when regarding the impact force of the plunging breaker and the layer thickness after the impact on the slope. Also, the resonance phenomenon does not occur on a rough slope. However, the reduction was based on the wave height and the Iribarren number. in this case a division is made based on the breaker type. This has led to a factor of d_{n50}/H which led to a quite a reduction of the scatter, see Figure 5.6

Figure 5.5 is based on the results of the slopes 1:1.5 and 1:2 with d_{n50}= 0.067 or 0.09 m. For the reduction the theoretical values for the smooth slope (eq. 3.3) are used. This gives the reduction to the theoretical value of run-up on smooth slopes for an angle of 1:1.5 and 1:2. The values do not give the

actual reduction, but allows the determination of the influence of the stone diameter and will be consequently used in this study.

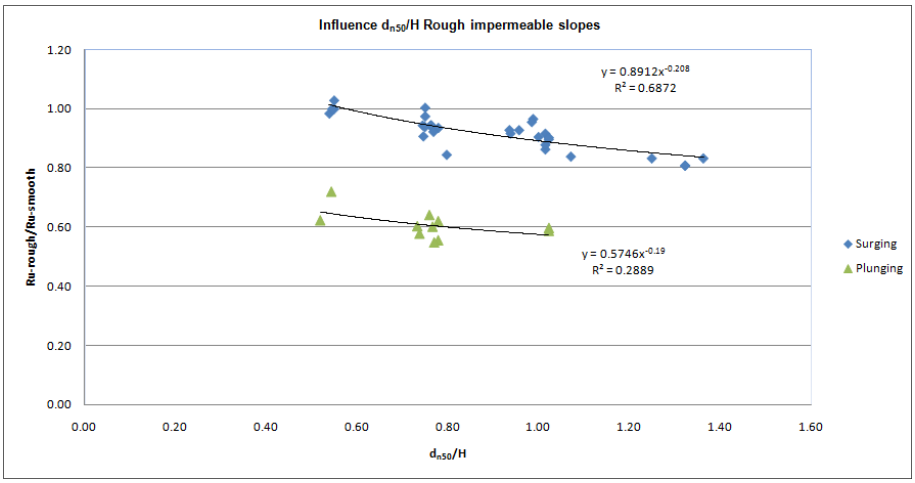

Figure 5.5: Influence relative stone diameter, on rough impermeable slope

The trend line is chosen to be a power function, because with a small diameter the rough layer acts as an smooth slope. For example a concrete plate or asphalt is in the theory seen as a smooth slope. Next, to this the influence of the stone diameter has a maximum value for very large stones. Large stones act as an wall and the run-up is in this case equal to the wave heights (assuming no standing wave). Comparing with the result of the smooth slopes, this leads to an theoretical bottom value of 0.50. So, with two asymptotic lines are best represented with a negative power function.

The influence of the Iribarren number will be taken into account by putting this parameter on the 'x-axis'. The values in the power function can be used to reduce the scatter in the graph. This leads to the following figure.

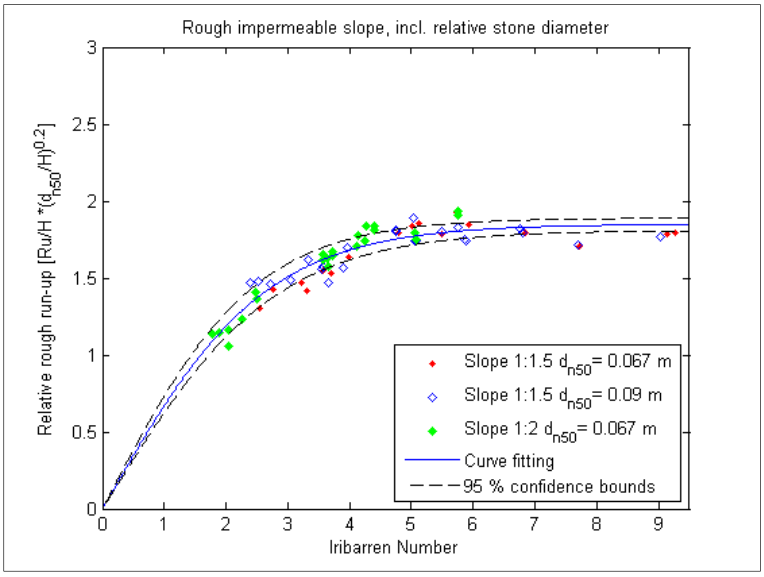

Figure 5.6: Results including the relative stone diameter.

The curve fitting leads in the form of a hyperbolic function, leads to the following,

$$\frac{R_u}{H} = a * \tanh(b * \xi)$$
$$a = 1.85$$
$$b = 0.38$$
$$R^2 = 0.88$$

eq. 5.3

The shape of the graph is maintained, see eq. 5.2. By taking the roughness into account clearly reduces the scatter. For ξ > 7 still an extra reduction is found, and based on the effect that multiple points have a lower value accuracy of the measurements is not a likely cause. So, the ratio d_{n50}/H and accuracy of the measurements is not the cause of the reduction for ξ > 7. Most probably, the same phenomenon occurs as causing the reduction for a smooth slope 1:1.5. Moreover, the rough impermeable slope acts more as a smooth slope for large Iribarren numbers.

5.2.3 Armour layer on an impermeable core

The impermeable core is created by placing a rubble mound core in the wave flume. Over this rubble mound structure a flexible plastic sheet is placed. On top of the plastic sheet an armour layer is placed with a stone diameter of d_{n50}= 0.067 m or 0.09 m, both layers have the same grading. The slope of the structure was standard 1:1.5, and for the armour layer with d_{n50}= 0.067 m also a slope angle of 1:2 was made. In this section the results are presented and the processes occurring a connected with the results.

In chapter 3 the phenomena about the influence of hydraulic and structural parameters are described, below a short summary is given. With an armour layer energy dissipation takes place in the pores of the layer and not only due to the surface roughness of the layer, see section 5.2.2. With larger stone diameters also the pores are larger, which lead to more energy dissipation. Also, the layer thickness (dependent on the stone diameter, $2k_t d_{n50}$) increases with increasing armour stone diameter. This leads to an increase in storage volume inside the armour layer. By increasing the stone diameter an increase in dissipation is obtained, due to the more turbulent flow. For short and small waves the storage volume increase has relative a larger influence. A general trend is that, with increasing wave steepness the dissipation of energy in the armour layer also increases. In TROCH [2000] pressure measurements showed, pressures on the core decreases when the wave steepness increases. So, wave damping is larger for large wave steepness, see also section 2.2.3.

In Figure 5.8 the results of the experiments done on the geometry “armour layer on an impermeable core” are shown. The “bleu hatched area” is an interpolation between the error bars of the given points. No transition point is visible between the different types of breaking. The scatter in the graph is the results of a varying d_{n50}/H ratio, as visible this ratio is more of influence for surging waves. The thickness of the water layer on the slope for plunging waves differs not a lot with the wave height. Most dissipation (40 %) is caused by the breaking of the wave on the slope, see section 2.2.3. Overall a slight increase of the relative wave run-up for increasing Iribarren number is visible. After analysing the observations done with the side camera the following division can be made between the breaker types.

- Plunging between 1.7 ≤ ξ < 3.0
- Collapsing between 2.7 < ξ ≤ 3.1
- Surging from ξ > 2.9

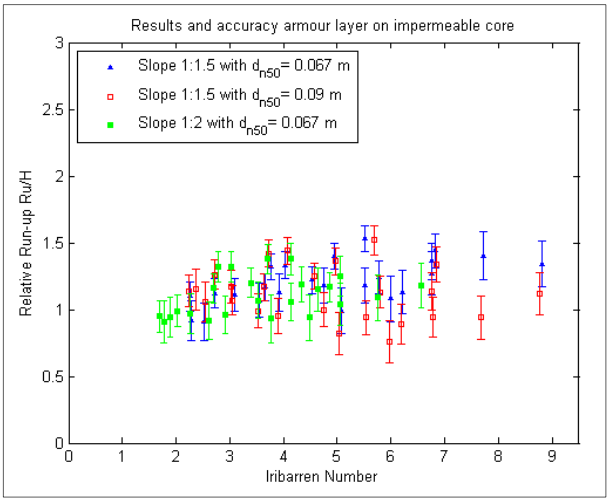

Figure 5.7: Results of experiments conducted on armour layer on impermeable core.

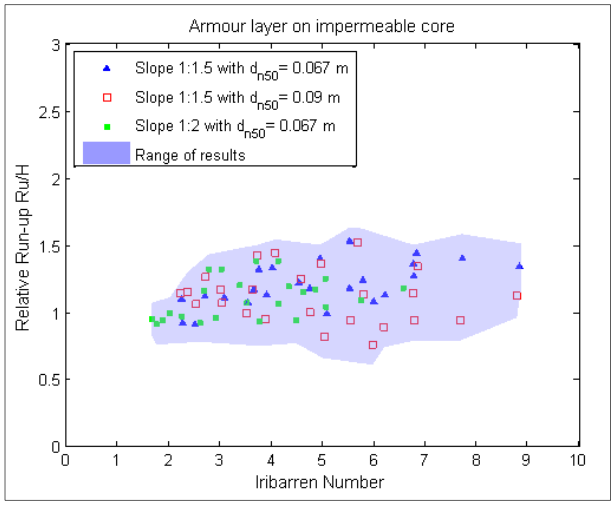

Figure 5.8: Interpolation between the error bars

In Figure 5.8 a large scatter is visible, especially for the slope with d_{n50}= 0.09 m. The scatter is caused by experiment with different wave height series. The relative stone diameter is important for the amount of reduction of the run-up. A larger relative stone diameter leads to more reduction. Also, the armour layer thickness is of influence. It is difficult to separately describe these phenomena, with an equal d_{n50}/H ratio for the two different stone diameters the volume of the incoming waves also vary.

For determining a curve fitted line for the results, a hyperbolic function can be used as in the previous geometry was done. However, a hyperbolic function does not include the increase the relative wave run-up for increasing Iribarren number. Moreover, no difference is visible between different breaker types. Therefore, a linear trend represents the shape best; however, a curve fitting including the larger armour stones was not possible, regarding the accuracy.
The linear line is, valid between 1.7 < ξ < 9.5 and only for the results with d_{n50}= 0.067 m.

$$\frac{R_u}{H} = 0.058\xi + 0.91$$
$$R^2 = 0.30$$

eq. 5.4

The scatter in the graph will lead eventually in a large scatter in the reduction coefficient caused by the armour layer.

With increasing Iribarren number (decreasing steepness) the trend is that less reduction of wave run-up occurs. In Figure 5.9 till

Figure 5.11 this behaviour is more clearly depicted. In these graphs a distinction is made between different wave heights, so that the influence of the steepness is more clearly visible.

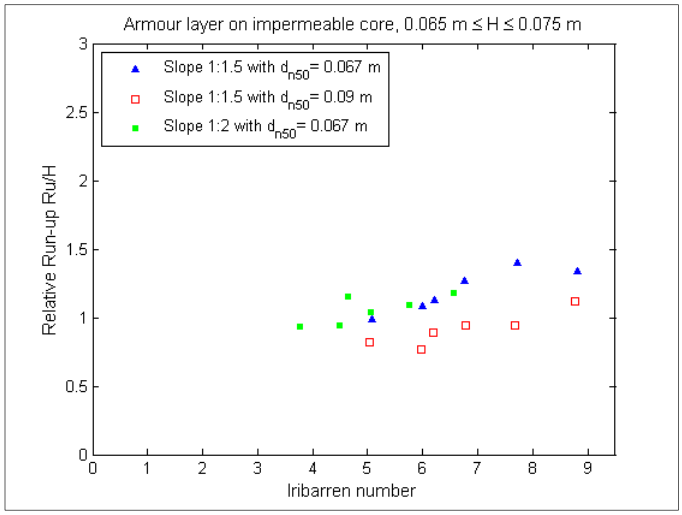

Figure 5.9 shows the results with wave's ±0.07 m. Within this wave range the stone diameter has a large influence in the reduction. Caused by extra dissipation or the extra storage area. The steepness of the three trend lines is approximately equal. For the large stone diameter the extra reduction is caused due to the 'extra storage' and by a 'jump' in the ratio d_{n50}/H. It can be concluded that a ratio of $d_{n50}/H > 1$ has a considerable influence on the wave run-up. For the slope 1:1.5 It seems to be a constant value for $\xi > 7$, however, this can also be the cause of the spreading in accuracy of the measurements.

Figure 5.9: Impermeable core, wave height range 0.065 ≤ H ≤ 0.075 m

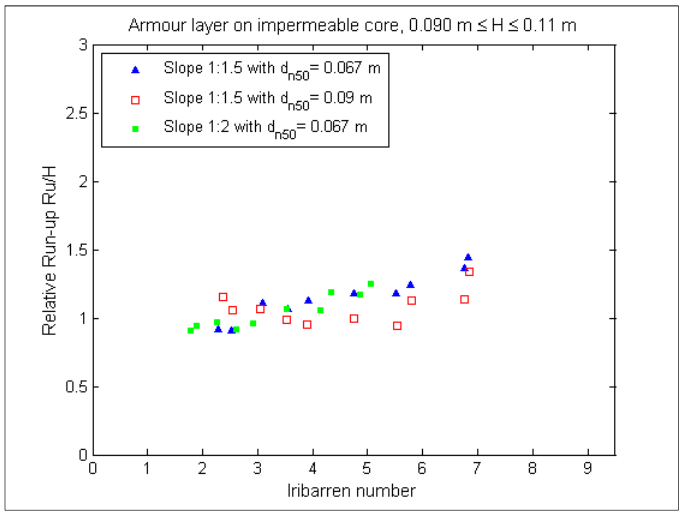

The figure on the left shows the wave range around $d_{n50}/H = 1$ for d_{n50}= 0.09 m. For the waves smaller or equal than the stone diameter a relative large reduction is visible. For waves larger than 0.09 m no significant difference is visible between the slopes with different stone diameter. Most probably the increase of the relative run-up for low Iribarren numbers is due to the accuracy of measurements. For $d_{n50}/H < 1.0$ almost no difference in reduction between the stone diameters is visible.

Figure 5.10: Impermeable core, Wave height range 0.09 ≤ H ≤ 0.11

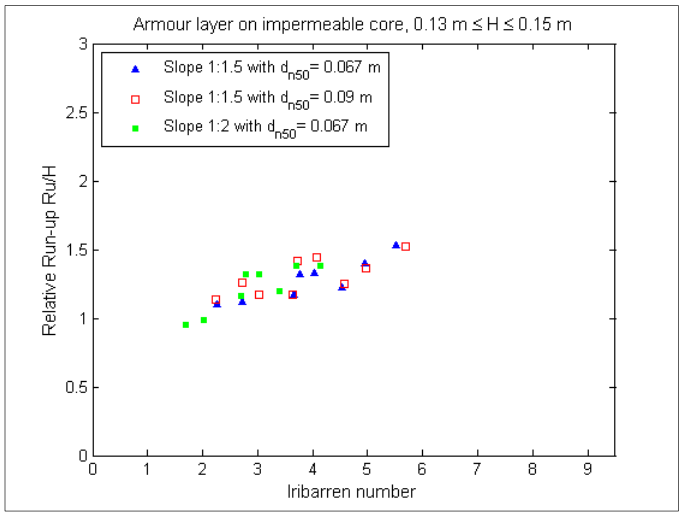

Within the wave range depicted in the figure on the left no difference is visible between the slopes with different stone diameter. So, for a ratio of $d_{n50}/H \leq 0.70$ no influence of the stone diameter is visible. Roughness has an influence, but the actual size of the stone diameter is negligible. In Figure 5.10 the relative stone diameter is for all the slopes larger than 0.70.

Figure 5.11: Impermeable core, wave range 0.013 ≤ H ≤ 0.015

From the above figures it can be concluded, for a relative stone diameter values smaller than 1.0, a larger stone diameter does no lead to a smaller wave run-up. So, a value of 0.70 or 0.50 gives (almost) the same reduction. For the small wave range the reduction was caused by a combination of porous flow dissipation and a combination of the increased volume of the layer. Nevertheless the ratio d_{n50}/H is still a good measure to describe the influence of stone diameter, see Figure 5.12. This figure represents the same d_{n50}/H ratio, so for the results of d_{n50}= 0.09 m a larger wave range is chosen.

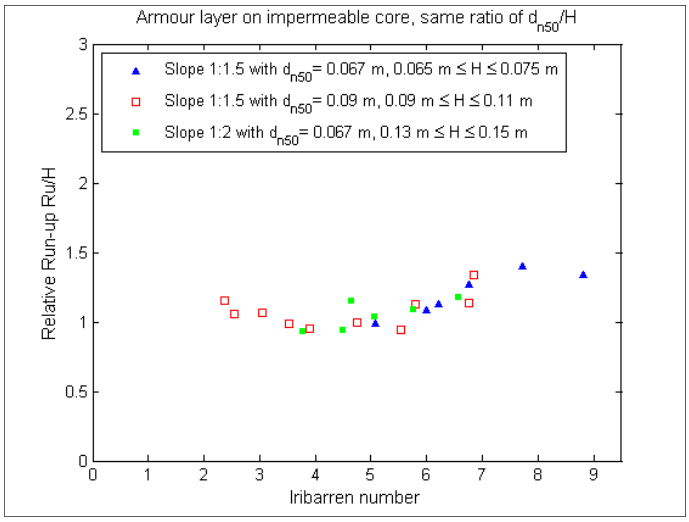

Figure 5.12: Results with (almost) similar d_{n50}/H values.

5.2.4 Armour layer on a permeable core

The geometry with a permeable core has a slope angle of 1:2 with an armour layer with d_{n50}= 0.067 m or 0.09 m. The core is build out of stones of d_{n50}= 0.033 m with a grading of 1.5 or 4. The porosity of the two cores is respectively 0.42 and 0.36 see also appendix E.

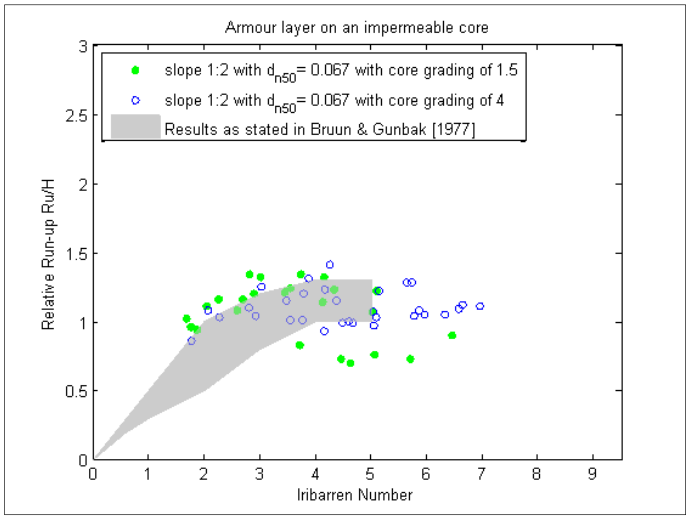

Figure 5.13: Comparison with semi-permeable breakwater

In Figure 5.13 the current results are compared with the results stated in BRUUN and GÜNBAK [1977] for a semi-permeable rubble mound breakwater. Expect, from the plunging waves and the values around R_u/H=0.7, a good match is visible. The plunging wave shows different results, this can be the cause of the difference between the method of measuring and accuracy, and is considered in chapter six. The values around R_u/H=0.7 are probably caused by a different amount of infiltration of water into the core, as will be discussed below.

With respect to the different breaker types, three different areas can be distinguished. In the transition zone is not always clear which type of breaking occurs, and also small wave heights act different from the larger waves. Therefore, an overlap of the breaker types occurs. In appendix B from every experiment the type of breaking is given.

- Plunging from $1.65 < \xi \leq 3.0$
- Collapsing from $2.8 < \xi \leq 3.0$
- Surging for $\xi > 2.9$

In Figure 5.14 & Figure 5.15 the results are shown with their bandwidth of accuracy. The left figure shows the results with their error bar and the right figure is the interpolation of these error bars resulting in a hatched area.

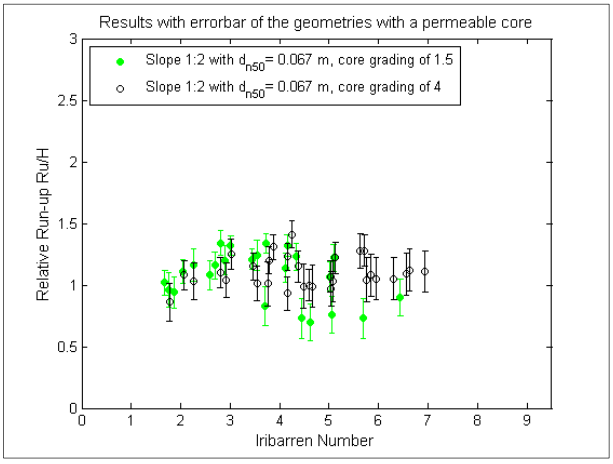

Figure 5.14: Result of the geometry with a permeable core including error bars

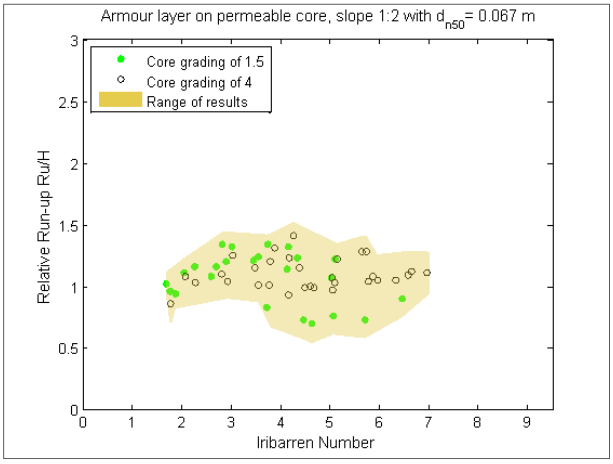

Figure 5.15: Results with interpolation between the error bars.

For the grading of 1.5 two different areas can be distinguished. An area around $R_u/H = 0.6 – 0.7$, in this area a reduction is visible as a consequence of infiltration. In the second area, less reduction of the run-up is visible; in this area the larger waves are situated. This may indicate the importance of the flow velocity on the slope. With larger waves and equal wave period the run-up velocities on the slope are large which reduces the inflow into the core during the run-up period. For the core with a grading of 4 no large difference is visible within the different wave ranges and between the larger wave heights for the grading of 1.5. In Figure 5.13 till Figure 5.15 a division is made between the different wave heights ranges, this gives a better view on the influence of the wave height (and implicitly wave steepness).

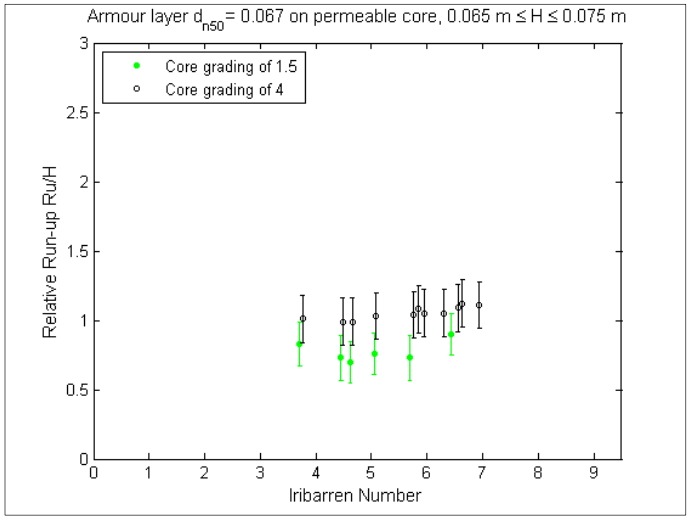

Figure 5.16: Results of geometry with a permeable core, 0.065 ≤ H≤0.075 m

In the figure on the left the influence of the small wave heights is visible. It can be seen that the run-up is lower for the narrow graded core (grading 1.5). This is only possible when during the run-up period water is infiltrated into the core. The results are so consequent that this is unlikely, that the accuracy of the measurements will influence this conclusion.

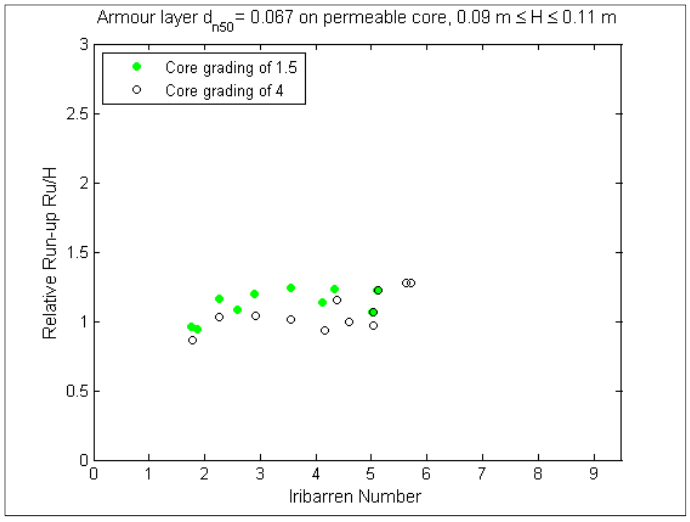

permeable core, 0.09 ≤ H ≤ 0.011 m

In this figure the results of the medium large wave heights are shown. In this figure no significant difference is visible between the two different grading. It seems a larger reduction for the wide grading occurs, however, this has no physical basis. This is a difference due to the accuracy of the measurements.

Figure 5.17: Results of geometry with a

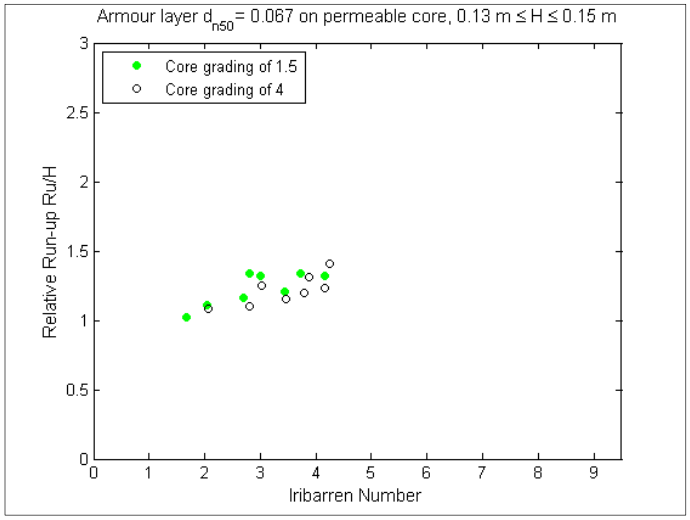

Figure 5.18: Results of geometry with a permeable core, 0.13≤H ≤0.15 m

Figure 5.18 the relative run-up for large wave heights are given. The results show that there is no difference between the different grading of the core. However, the most infiltration occurs in the case of long waves, and in this graph the maximum value of ξ= 4.3.

So, when regarding the influence of the different core grading on the reduction of the run-up. The following can be said for a permeable core with a slope angle of 1:2.

- For small waves with a low wave steepness more reduction of the wave run-up in the case of a narrow graded core (more permeable core) is visible. The only physical explanation for this is that during the run-up period more water has infiltrated into the narrow graded core due to the larger permeability.
- For medium large wave heights no difference between two grading is visible. The infiltration during the run-up period is not considerable larger for the narrow graded core.
- For the large wave height series no conclusive remarks can be done, based on only the graph. However, based on the previous statement it can be concluded that also for the larger wave height series no difference for larger Iribarren numbers will occur.

A possible explanation for the difference between the different wave height series is that the flow velocities on the slope for low waves are smaller. The run-up height is lower in the case of smaller waves, in combination with an equal wave period this results in a difference in velocity on the slope. With a larger velocity on the slope less inflow occurs. The influence of the gravity on the water volume is relatively small when an upward velocity is large.

5.3 Influence of the roughness

In the previous section an analysis is made of the results per geometry. Below, a comparison is made between the results of different geometries to separate the combined roughness. The influence of the surface roughness $\gamma_{f;s}$ is determined by comparing the results of the smooth slope with results for the rough impermeable slope. In the second part of this section a comparison of the latter slope with the armour layer on an impermeable core, leads to the influence of the permeability.

5.3.1 Comparison rough impermeable slope with smooth slope

In section 5.2.2 the results obtained by the experiments with the rough impermeable geometry are briefly described. Also, the influence of the stone diameter is described. The best fit line for the rough impermeable core was given in 5.2.2 by eq. 5.2, in this fit the influence of the d_{n50}/H is not included.

$$\frac{R_u}{H} = 1.86 * \tanh(0.42\xi) \qquad \text{eq. 5.2}$$

The results of BRUUN AND GÜNBAK [1977] are used to compare it with the rough impermeable slope. The equations stated in section 3.4.1 can be used as a best fit for smooth slopes. One can argue that for a smooth slope with an angle of 1:1.5 the set of equations of eq. 5.5 gives a better fit. Using a constant value of two (as in eq. eq. 3.3) leads to an overestimation for a slope 1:1.5. The range of the values lies between R_u/H= 1.65 -2.05, and the spreading is evenly. Also, this relates better with the findings in this thesis. Moreover, it is likely that the reduction is caused by the shape of the wave run-up which differs not between a smooth slope and a rough impermeable slope.

$$\begin{aligned}
&\frac{R_u}{H} = \xi && \xi \leq 2.5 \\
&\frac{R_u}{H} = 2.5 - \frac{2.5 - \xi}{3} && 2.5 < \xi \leq 4.0 \\
&\frac{R_u}{H} = 2 - (0.075 * (\xi\text{-}4.0)) && 4.0 < \xi < 6.0 \\
&\frac{R_u}{H} = 1.85 && \xi > 6.0
\end{aligned} \qquad \text{eq. 5.5}$$

When one will compare the results with the results of SCHÜTTRUMPF [2001] eq. eq. 3.4 can be used. This is not done in this report, because the results match better with the results of BRUUN and GÜNBAK [1977].

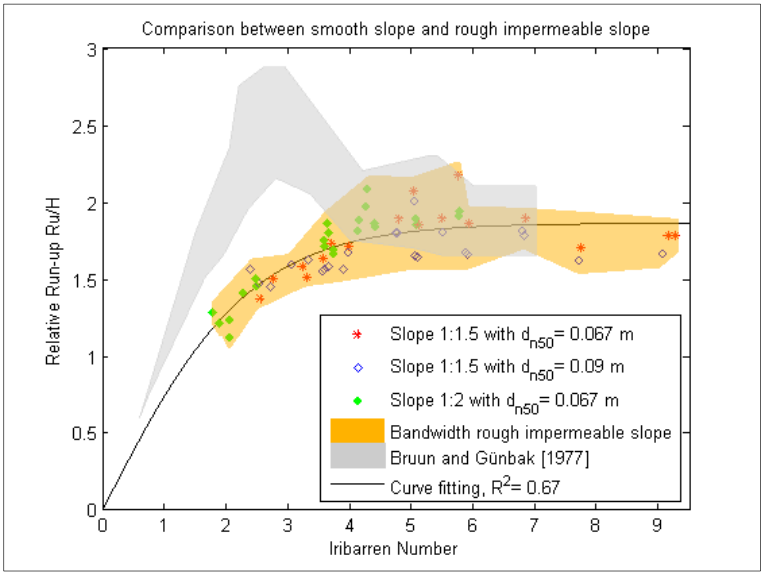

Figure 5.19: Smooth slope vs. rough impermeable slope

Figure 5.19 shows; for ξ > 4.0 the rough layer does not have a significant influence on the reduction of the run-up. The values fit in the range that was found for wave run-up on smooth slopes. So, the reduction due to the surface roughness of the slope is nil. The interpolation between ξ= 4 to 5 gives a biased image. The measured values in this range are all in the smooth slope area, as can be seen in the figure.

Below ξ ≤ 4.0 a considerable reduction is found, mostly because the resonance phenomenon does not occur on the rough slope. For ξ> 3.6 surging waves, start to occur (which look similar to collapsing waves). The layer thickness of these surging waves with low Iribarren numbers is still quite small and the reduction is similar as with collapsing waves. Due to the roughness the peak is not visible in the results of the rough impermeable slope. The impact force is taken up by the stones. Run-up tongue that follows has approximately a maximum thickness of the stone diameter (the stone are placed $0.5d_{n50}$ in the cement), which leads to a very turbulent flow. This latter is based on analysis of the side view recordings.

When comparing the results with the formula of Hunt (valid till ξ≤ 2.5), a reduction factor of 0.8 – 0.6 (±16 %) from 1.7 ≤ ξ ≤ 2.5 can be derived. Hunt's formula has an accuracy of 10% and the current experiments have a deviation of 4 – 8 % for plunging waves.

Between 2.5 < ξ < 4.0 the reduction factor is 0.6 for ξ≈ 2.5 which linearly increases till 1.0 for ξ≈ 4.0 (±0.15). Around ξ≈ 4.0 the influence of the stones is negligible, due to the increasing layer thickness. Between 3.6 and 4.0 the waves can be surging or collapsing waves, nevertheless the wave run-up tongue has a small thickness, and the flow is highly turbulent.

5.3.2 Comparison rough impermeable slope with armour layer on impermeable core

Comparing the results of the rough impermeable slope with the results of the armour layer on an impermeable core give insight in the importance of the surface roughness $\gamma_{f;r}$ and permeability of the armour layer $\gamma_{f;p}$ on the reduction of the run-up.

For a smooth slope and a rough impermeable slope the influence of the Iribarren number is clearly visible till ξ =4.0 For higher values of the Iribarren number this influence is almost constant For situations with an armour layer no influence of the Iribarren number is visible.. This is partly due to the fact that the ratio wave height and stone diameter is also of influence. So, one can question if R_u/H is a proper dimensionless number for the wave run-up on rubble mound breakwaters In the next section the stone diameter is included in the relative wave run-up parameter. Also, the layer thickness can be the parameter that is influencing the scatter. In this study this cannot be determined, since the layer thickness was dependent on the stone diameter.

In Figure 5.20 the limits of the relative wave run-up are fairly good visible. A value of R_u/H= 3 is an upper limit for wave run-up of regular waves. The lower limit R_u/H= 0.5, is related to the amplitude of the wave. Wave height is the sum of the amplitude below and above SWL, and wave run-up is defined as the vertical distance between SWL and maximum run-up on the slope.

In the previous sections it could be noticed that the transition point (or zone) between plunging and surging waves occurs for lower values of the Iribarren number, when the slope became more permeable (armour layer and/or core). This should have an effect on the roughness coefficient, however, this cannot be determined in certainty within this test program.

In section 5.3.1 the results of the rough impermeable slope experiments were compared with the results of experiments on smooth slopes. No reduction found for surging waves was found, which occurred from $\xi > 4.0$. For collapsing ($3.0 \leq \xi < 3.6$) and plunging waves ($1.5 \leq \xi < 3.0$) the surface roughness reduces the run-up. The transition between surging and plunging has changed from ±3.6 to ±3.0 between the rough impermeable slope and the armour layer on an impermeable core.

When comparing the influence of the surface roughness with the influence of permeability of the armour layer, see Figure 5.20, it leads to the conclusion that for surging waves ($\xi \geq 4.0$) dissipation of energy due to turbulence in the pores is the governing factor. The surface roughness does not have an influence. The influence of the permeability of the armour layer on the reduction of the wave run-up can be quantified by using eq. 5.4.(linear fit). However, this fit is only valid for armour stones d_{n50}= 0.067 m. Including the larger stone would only lead to an increase in the variation of the reduction coefficient. So, by computing the difference between the maximum value for smooth slopes $R_u/H \approx 2.0$ for $4.0 \leq \xi < 9.5$, this leads to an reduction factor of 0.6, which increases linearly for increasing Iribarren number till a value of 0.73 compared with the smooth slope. In the case of a slope 1:1.5, for $\xi > 6.0$ an upper bound value of 0.8 is found. The above values represents the roughness coefficient that is the result of the dissipation due to the permeability of the armour layer, $\gamma_{f;p} = \gamma_{f;c}$.

For $1.7 \leq \xi < 4.0$ both the surface roughness and the permeability has an influence. The armour layer represents the combined roughness of both phenomena. Compared with the smooth slopes the armour layer has a combined roughness coefficient of 0.55 to 0.4 from ξ = 1.7 till ξ= 2.5. For the range 2.5 till 4 a roughness coefficient of 0.40 with a variation of 0.08 is found. In literature a combined roughness value of 0.55 for ξ=1.8 is found which linearly increases till 1 for ξ=10. This matches the current result, because the coefficient in the literature has reference to irregular waves, were the resonance peak does not occur.

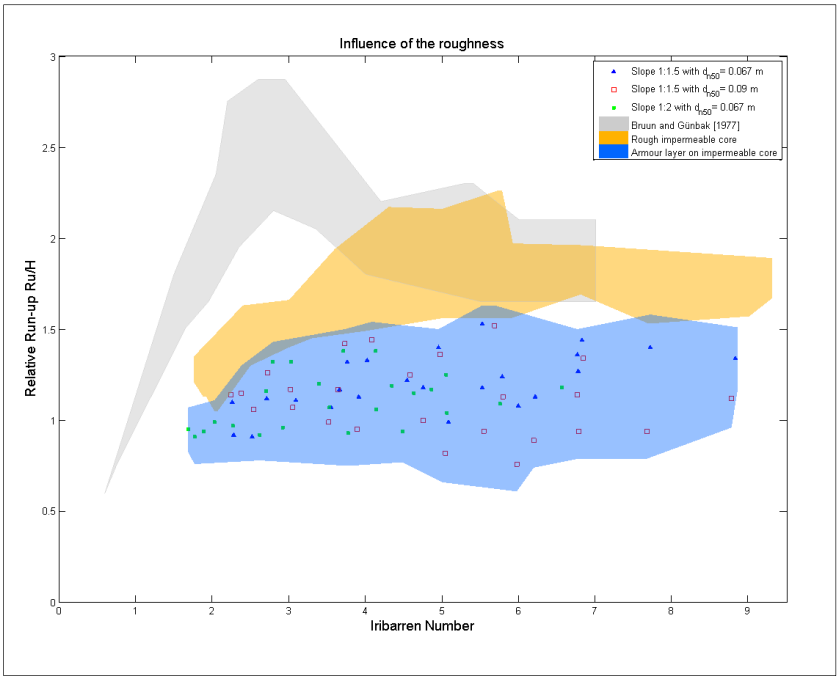

Figure 5.20: Comparison between the results of the smooth slope, rough impermeable slope and armour layer on impermeable core.

Above, for 1.7 ≤ ξ < 4.0 the combined roughness is determined, it is now also possible to determine the roughness only caused by the permeability $\gamma_{f;p}$ by using the fit lines of eq. 5.1 and eq. 5.4. This lead to $\gamma_{f;p}$ from 0.88 – 0.65 which reduces with a power function. However, in the previous section it is discussed that for surging waves the influence of the surface roughness is less, and due the shift of the transition between the breaker types the value of 0.65 will reduce till 0.57. So, the permeability coefficient decreases from $\gamma_{f;p}$ = 0.88 till 0.6 from 1.7 < ξ < 4.0 and $\gamma_{f;p}$ = 0.6 till 0.8 from 4.0 ≤ ξ < 9.5.

5.3.2.1 Influence relative stone diameter

In 2.2.2 is discussed that the influence of the stone diameter is relative from the wave height and the Iribarren number, $d_{n50}/(H\xi)$. In Figure 5.21 this factor (for 2.0 ≤ ξ <9.5) is put out against the reduction caused by the surface roughness or the armour layer and compared with the theoretical values of the smooth slope, see eq. eq. 3.3. For the rough impermeable slope this does not give representative reduction values. However, for the comparison between the two geometries this is useful. The distance between the trend lines of the two slopes does not deviate over the tested range from each other. According to Figure 5.21 the stone diameter has no influence on the amount of dissipation inside the pores for the tested range in this study. Leading to a preliminary conclusion that the extra reduction for the small wave range is caused by an increase in storage volume.

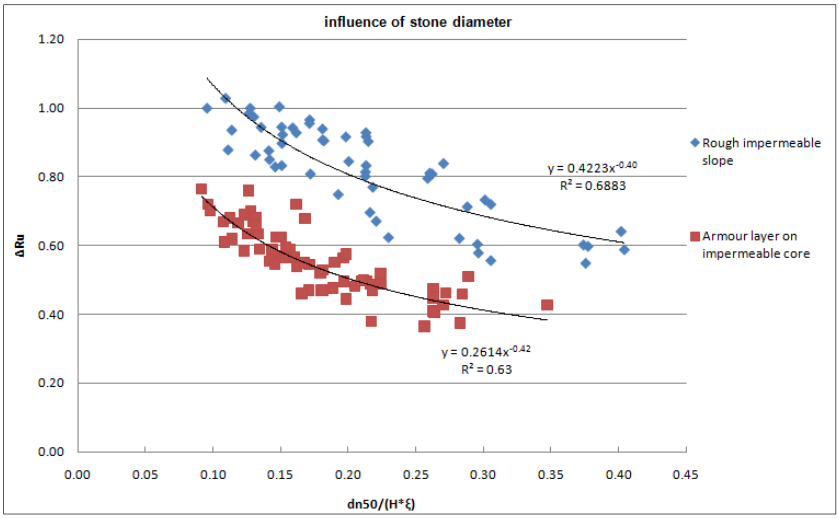

Figure 5.21: influence of the stone diameter of the rough impermeable slope and armour layer on impermeable core.

When one rewrites the above equations into a function dependent on the Iribarren number one can find the influence of the relative stone diameter.

$$\Delta R_u = \left(\frac{d_{n50}}{H\xi} \right)^{-0.4}$$

$$\Delta R_u^{2.5} \frac{d_{n50}}{H} = \xi$$

eq. 5.6

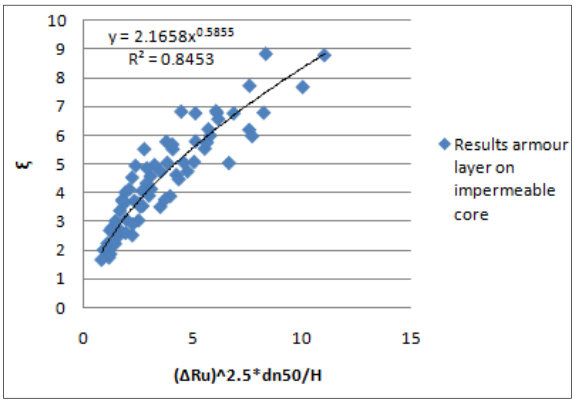

Figure 5.22: Influence of the stone diameter dependent on the Iribarren number

The scatter in the results of the rough impermeable slope is not been reduced. The manner in which the stone diameter is included in Figure 5.5 leads to a better reduction of the scatter. As was visible in the results the influence of the Iribarren numbers is limited. The type of breaking and the wave height is more of influence. The processes of water flowing over the rough impermeable slope and armour layer are different. Therefore, it is not strange that $d_{n50}/(H\xi)$ is a better parameter to describe the roughness for a permeable armour layer. For the geometry with the armour layer the scatter is reduced. Also, the scatter Figure 5.21 is larger for the rough impermeable slope. So, it seems $d_{n50}/(H\xi)$ is more related to a permeable armour layer. Moreover, both graphs show a lowering of the values, including the relative stone diameter with a power function is not the best way of removing the scatter.

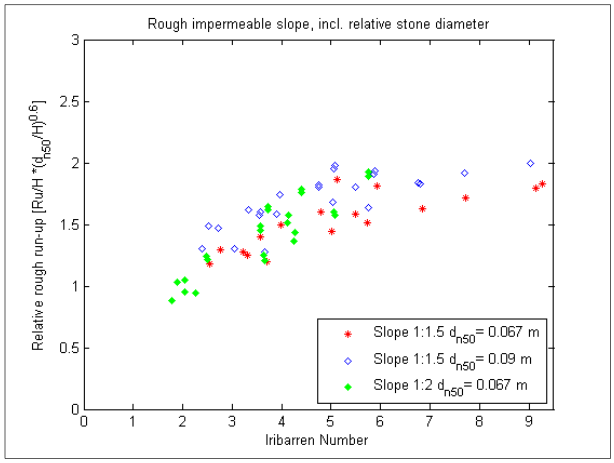

Figure 5.23: Results rough impermeable slope including relative stone diameter

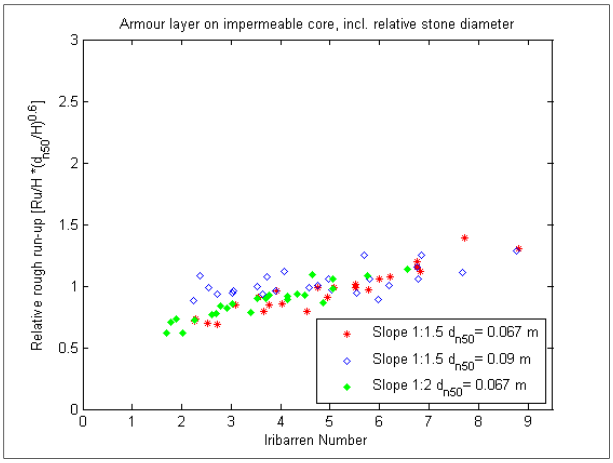

Figure 5.24: Results armour layer on impermeable core including relative stone diameter

5.4 Influence of the core permeability on the run-up

One of the main interests of this research is the influence of the core permeability on the run-up. The Volume Exchange model determines the permeability factor P based on the reduction of the run-up due to infiltration of water into the core. The reduction can be determined by comparing the results obtained by the experiments conducted on an impermeable core with the permeable core. The experiment with the permeable core are only performed with d_{n50}= 0.067 m. Therefore, only the results of the impermeable core with d_{n50}= 0.067 m are used. In section it was concluded that only a difference between a grading of 1.5 or 4 in case of the small wave series (H≈ 0.07 m) happens. In Figure 5.25 and Figure 5.26 the results of the geometries are shown.

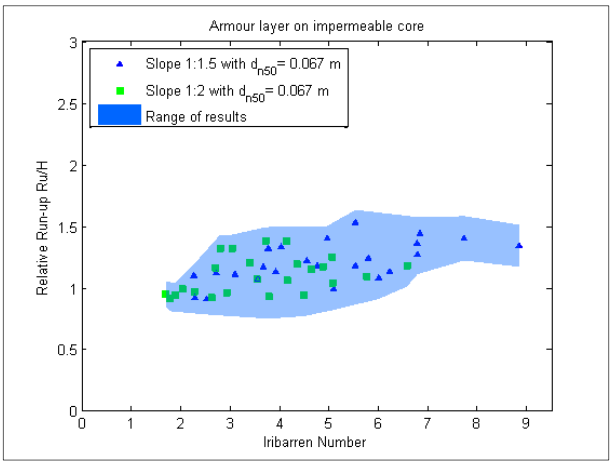

Figure 5.25: Results impermeable core with d_{n50}= 0.067 m, with accuracy range

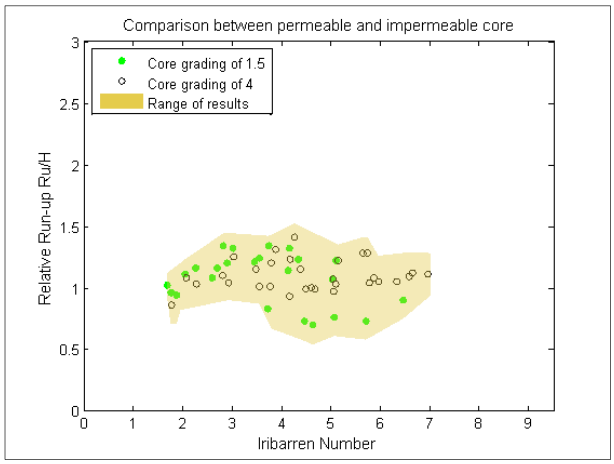

Figure 5.26: Results with permeable core with accuracy range

For ease of comparison both graphs are plotted on each other, see Figure 5.27. The data points of the impermeable core are not plotted in this figure. For a core grading of 1.5 a reduction is found for the small waves with a long period, see also Figure 5.28. In combination with a high porosity (n= 0.42) this leads to a considerable infiltration of water during the run-up period that it reduces the run-up height. For the rest of the experiments no significant reduction can be found. With respect to the grading of 4 no significant reduction can be found of the wave run-up as a consequence of a permeable core. So, a porosity of 0.36 is already not permeable enough to lead to any reduction of the wave run-up.

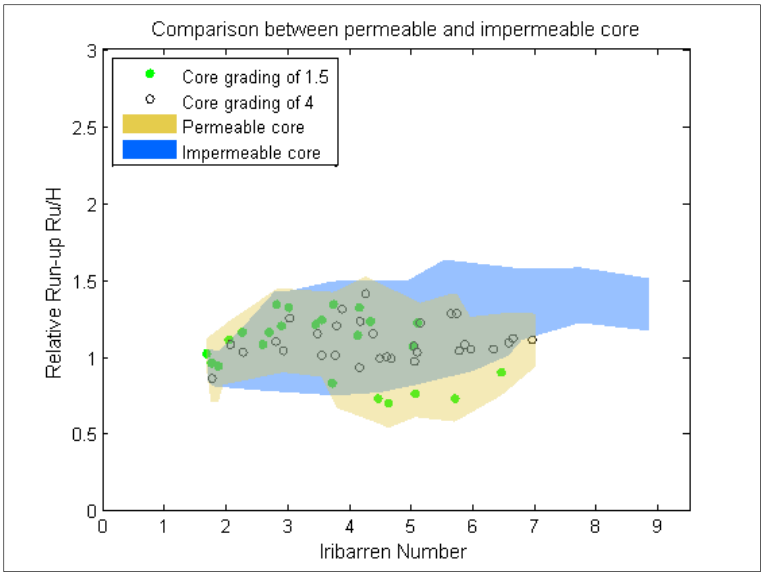

Figure 5.27: Comparison between impermeable core and permeable core.

As mentioned in the previous sections the wave height and period is of importance for the run-up in two ways. First, for the reduction of the run-up by the armour layer the wave steepness and relative stone diameter are of importance. Secondly, the infiltration and/or the wave damping inside a core are dependent on the (local wave steepness). When analysing the results on basis of the different wave height ranges, than it becomes clear that overall the wave run-up is not reduced by infiltration of water into the core. The only exemption of this rule is in a narrow graded core with a low wave height, resulting in low wave run-up that has a relative long run-up period. Another process that has influence of the run-up is the run-down motion. For an impermeable core the rushed up volume of water retreats entirely via the armour layer, and this give hindrance to the coming wave run-up. With a permeable core this volume retreats via the armour layer and the core, leading to less hindrance of the coming wave run-up.

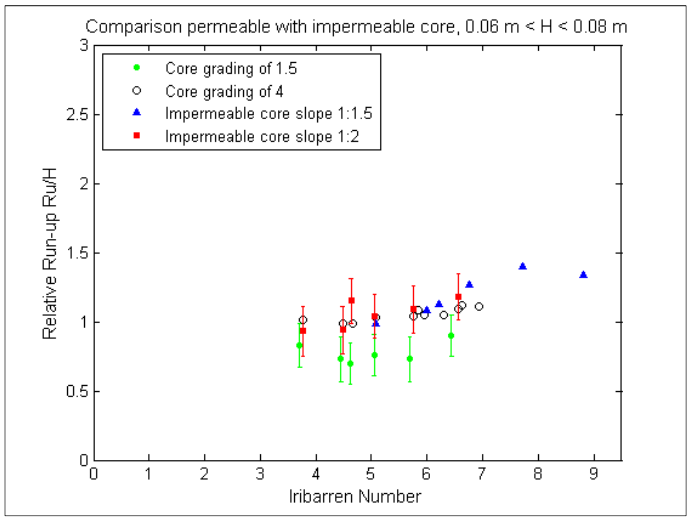

Figure 5.28: Comparison between impermeable and permeable core with wave height range of 0.065 m ≤ H ≤ 0.075 m.

Figure 5.28 the results belonging with small wave heights are shown. It is clear that no reduction of the relative wave run-up for a core with a grading of 4 compared with the impermeable core is found. For a grading of 1.5 a reduction is visible for ξ> 4.0. One might put the boundary at ξ> 4.5 due to the accuracy of the measurements.

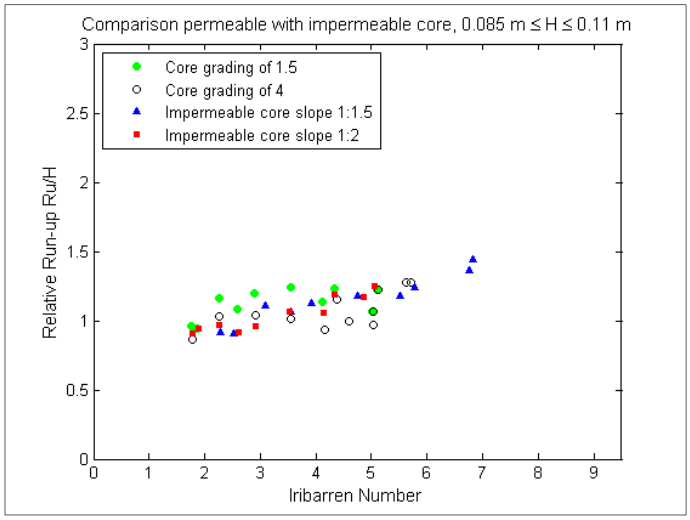

Figure 5.29: Comparison impermeable core with permeable core, wave height range 0.085 ≤ H ≤ 0.11 m

From Figure 5.29 it can be concluded that for this wave height range the core has no influence on relative wave run-up. The more permeable core shows slightly higher results than the impermeable core, however, this is the consequence of the accuracy of the measuring method. The same holds for the slightly lower results for the core grading of 4.

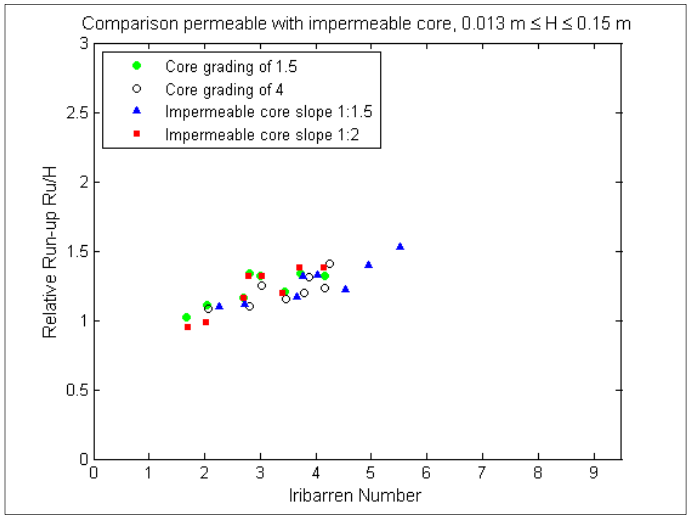

Figure 5.30: Comparison impermeable core with permeable core, Wave height range 0.013 ≤ H ≤ 0.015 m.

From Figure 5.30 it becomes clear that a permeable core induces no extra reduction of the wave run-up. The infiltration of water into the core does not influence the run-up height. The amount of infiltration is not determined. However, in this graph for the permeable core only values of $\xi < 4.5$ are measured. Regarding the physical processes of infiltration it is unlikely that for longer waves a reduction is found, since this was also not found in Figure 5.29.

When using the same method as in 5.3.2.1 by including the relative stone diameter the same conclusions is drawn, with a permeable core the surface run-up is not reduces compared to an impermeable.

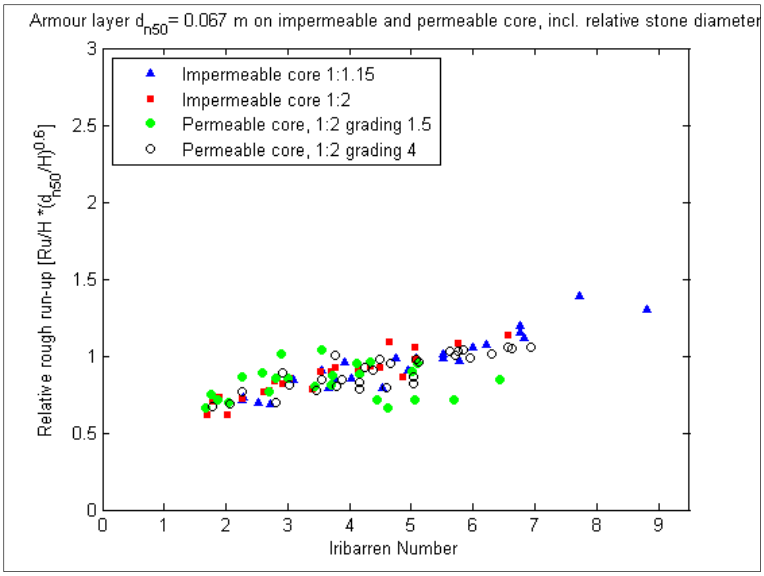

Figure 5.31: Results armour layer on (im)permeable core including the relative stone diameter.

In this section is has become clear that the core with a grading of 4 (n= 0.36) show the same (relative) wave run-up as an impermeable core. Therefore, the infiltration of water into to core is negligible small that is has no influence on the wave run-up. A quantitative amount of infiltration is not known.

For a core with a grading of 1.5 leading to a porosity of 0.42, a reduction is visible when the wave heights are small, however, for medium and large wave heights no reduction is visible. An explanation is, the run-up is related to the wave height (A large wave height leads to larger run-up), and the period of the run-up is related to the wave period. A smaller wave height leads to a proportional smaller run-up, when the wave period is equal this leads to smaller slope velocities. The gradient of the water flowing into the core is depended on the slope velocity. For a lower slope velocity the infiltration is larger and this leads to the reduction of the wave run-up.

Also, the process of run-down may have a considerable influence on the following wave run-up. With an impermeable core the rushed up volume retreats entirely back via the armour layer. Whereas, with a permeable core this volume flows back via the core and the armour layer. Therefore, the return flow on an impermeable core can give more hindrance to the following wave run-up.

5.5 Imposed core run-up

In the Volume exchange model the run-up at the surface of the core is used to compute the infiltrated volume. In the Volume Exchange model this core run-up (or imposed core run-up) was assumed to be only dependent on the maximum surface run-up with a (imposed core run-up factor γ_{ru}) factor of 0.5. In reality this is not a constant value, but varies with the hydraulic properties and the structural properties (porosity, stone diameter). In the current experimental program the armour layers have a constant porosity. Only the armour stones and permeability of the core is varied. Disconnection of the water line will not occur, however, due to the resistance in the layer the water line in the armour layer will lag behind. In Figure 5.32 a graphical presentation of the imposed core run-up is given.

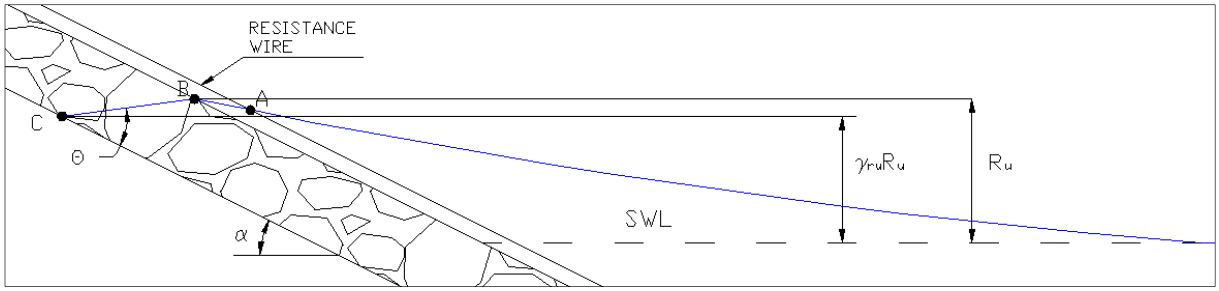

Figure 5.32: Definition imposed core run-up

During the experiments the wave run-up is not only measured by a resistance wire on the surface of the slope, but also by a resistance wire between the armour layer and the core, $RW_{core.}$ Also, a qualitative analysis is possible using the video recordings of camera placed next to the slope. Due to problems with calibration and measurements with the RW_{core} (see appendix C) it is not expected that the resistance wire gives reliable results. Therefore, a mainly qualitative analysis is performed based on the side view video recordings.

The notations A, B and C in Figure 5.32 indicate the definition of the different run-up heights. The resistance wire measures a wave run-up height indicated by A. The video analysis measures the run-up height directly on the surface of the armour layer and with the resistance wire on the core the run-up height at C is measured. One can argue what the best definition of the wave run-up height is. When regarding wave overtopping, the height at C is normative, since there is wave overtopping when water flows over the top of the core.

5.5.1 Side view recordings analysis

At the side of the flume a camera was placed which recorded the wave run-up and the flow in the core. Tracers were placed on the slope to have a better view on the maximum run-up, since the tracers were small they, could travel unhindered into the core. This latter made it possible to analyse the flow directions inside the core.
During up-rush of the wave till maximum surface run-up, the run-up at the core is lagging behind due to the resistance of the porous armour layer. For incoming waves with low wave steepness the gradient is relatively small. The outside water motion can easily be followed by the water line in the armour layer, most probably due to the longer period of run-up. For steep waves a maximum gradient in the armour layer is found. The maximum gradient in the armour layer makes an almost perpendicular angle with the slope. The water line in the armour layer on top of the impermeable core had an estimated angle of $40 < \Theta < 90^{\circ}$ between the slope and the surface run-up during rush-up. In case of a permeable core an estimated angle of $30 < \Theta < 60^{\circ}$ was found. The difference in gradient is probably the cause of the connection of the wave run-up with the water inside the core. On an impermeable core the rushes up in a complete dry armour layer. However, this connection does not reduce the surface run-up height, see section 5.4.

With a permeable core it was not visible that during the run-up infiltration into the core took place. At breaking or surging of the wave on the slope, the flow direction in the core followed the wave motion upwards/outwards, due to the suction force of the wave. During rush-up the flow in the core was parallel to the slope angle and only at/after maximum surface run-up the flow was directed into the core, see also Figure 5.33.

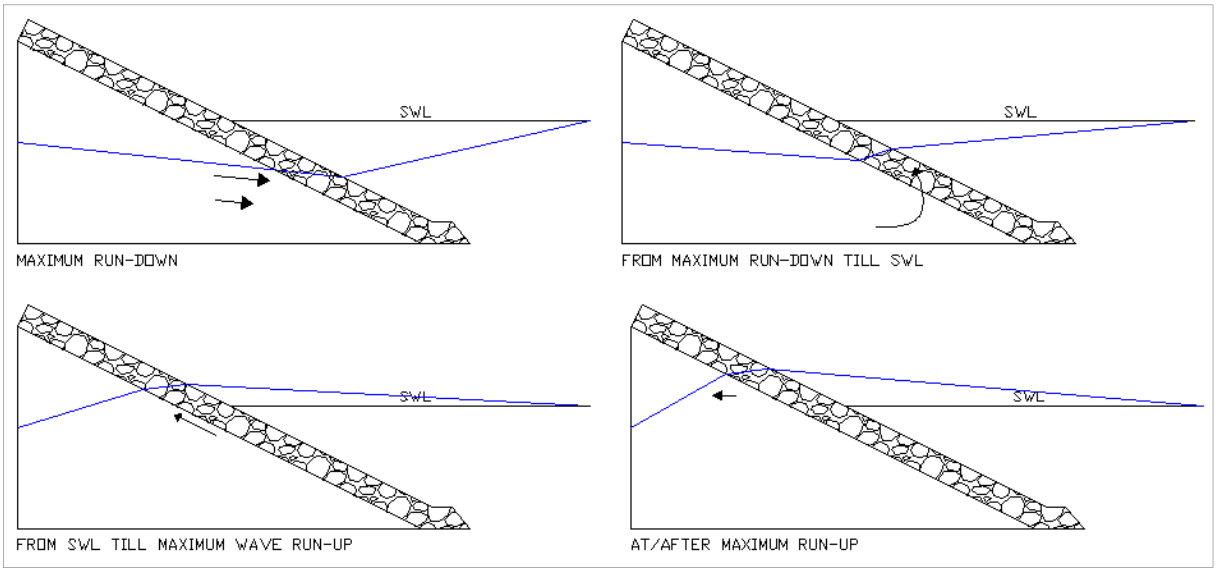

Figure 5.33: Sketches of the general flow directions inside the core during a run-up period.*
*The arrows are not vectors, but indicate only a direction

At maximum (surface) wave run-up the water at the surface stands still, however, inside the armour layer it is still a flow in 'upward' or in horizontal direction. At this moment an important difference is visible between a permeable and impermeable core. The water in the armour layer on the impermeable core has not reached its maximum level and continues for a couple tenths of a second in upward direction. Before the core run-up reaches its maximum the surface run-up has sank into the armour layer and is already retreating. The period between the maximum surface run-up and the maximum core run-up varied between 0.1 – 0.4 s and is different between the different wave height ranges. This is probably dependent on the wave steepness, due to the rough estimations this could not be determined with certainty. The run-up at the core will go one till the water line at the surface is retreated below the vertical height of the core run-up at that moment. With a steep water gradient (large wave steepness) in the armour layer core run-up cannot reach the theoretical maximum height (same as surface run-up), because the water is retreating more quickly.

For a permeable core the run-up height at the core does not increase significantly after the maximum run-up. At the moment of maximum run-up and thereafter, water flows into the core. However, for steep waves a slight increase of the imposed core run-up was visible after the maximum surface run-up. The gradient during rush-up in the armour layer for low steepness ($s < 0.03$) is a good estimation for the gradient between the maximum run-ups (surface and imposed core run-up). For larger wave steepness the (steep) gradient slightly decreases after the maximum surface run-up.

5.5.2 Imposed core run-up coefficients

During the analysis of the video recordings for some experiments estimation are made for the factor γ_{ru}, order to have an idea of the imposed core run-up coefficient γ_{ru}. Only for surging waves the video analysis gave reliable estimations. Also, the results of the resistance wire on the core are used, however for the experiments conducted with an impermeable core the measurements are very reliable, see Figure 5.35. For the impermeable core ranges of γ_{ru} are estimated and are between 0.6 – 1.0. A (linear) decreasing trend for γ_{ru} is visible for increasing wave steepness. The results of the resistance wire and video analysis did not match, although a same trend is visible. The resistance wire gave values that had a coefficient of γ_{ru}= 0.2 higher, see Figure 5.34. These factors give only an idea of the influence of the wave steepness no quantitative conclusions can be drawn from these

estimations. No clear difference is found between the two armour layer ($d_{n50;a}$= 0.067 m or d_{n50}= 0.09 m), mainly to the unreliable measurements.

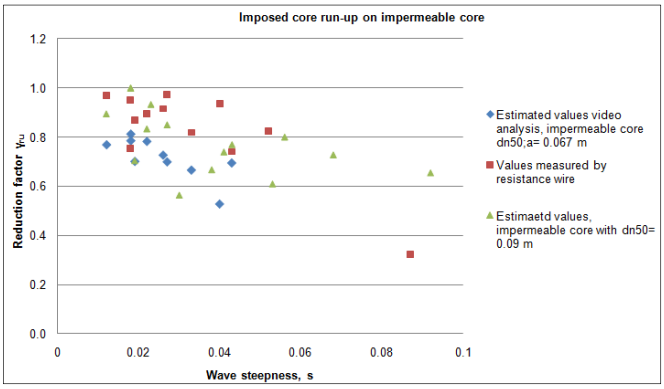

Figure 5.34: Imposed core run-up factors for the experiment conducted on an impermeable core with d_{n50}= 0.067 m and d_{n50}= 0.09 m.

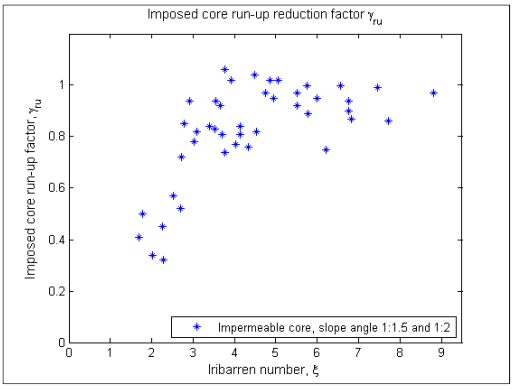

Figure 5.35: Imposed core run-up factor based on measurements with RW_{arm} and RW_{core}

For the permeable core the results of the resistance wire match the video analysis quite good. Moreover, with a permeable core the water has come better in contact with the resistance wire which increases the reliability of the measurements. Therefore, the measurements obtained from RW_{core} on a permeable core are reliable measurements. In Figure 5.36 the reduction factors γ_{ru} is given. The same trend was visible as with the impermeable core only with γ_{ru} values between 0.4 -0.7. For a grading of 1.5 a lower reduction factor is found for $\xi > 2.5$. The trend lines of the measurements intersect at s= 0.054. So, as was expected only for surging waves the permeability of the core has an influence and for a more permeable core more infiltration occurs.

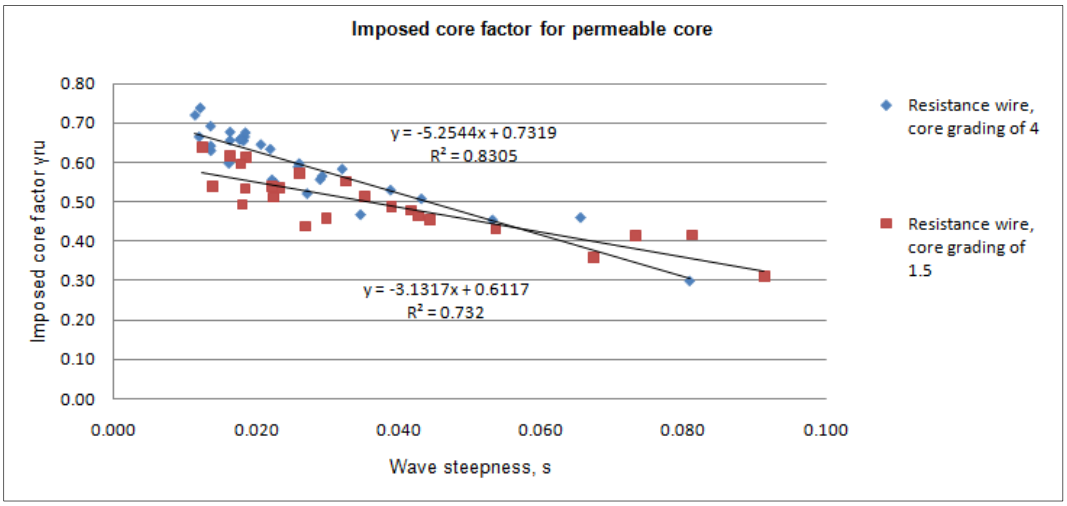

Figure 5.36: Reduction factors γ_{ru} for geometries with permeable core;

In section 5.4 is concluded that there is no difference in surface run-up between an impermeable core and a permeable core. So, no significant infiltration took place during the run-up period as was concluded in this latter section. In this section it is determined that the difference between a non-permeable and (more) permeable occurs after maximum surface run-up. With an impermeable core the imposed core run-up will increases after maximum run-up, were in case of a permeable core the water flows into the core. This leads to lower imposed core factor γ_{ru} for geometry with a permeable

core. Figure 5.37 shows the results of the RW_{arm} and RW_{core}. It shows clearly that the run-up height at the core is lower and the reduction is larger for a more permeable core (grading 1.5).

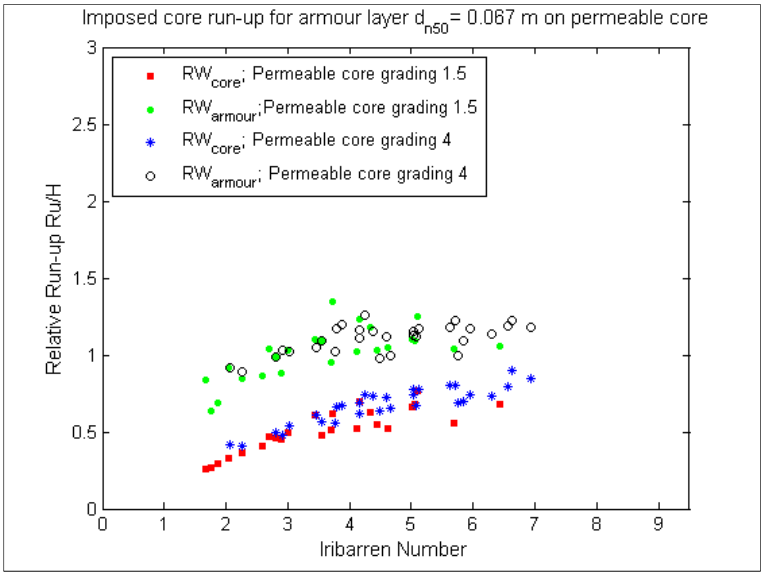

Figure 5.37: Results RW_{core}, relative run-up between armour layer and permeable core and RW_{arm}, relative surface run-up of the experiments with the permeable core

5.5.3 Remarks about armour layer stability

In this chapter it is concluded that the maximum surface run-up is not lower in the case of a breakwater with a permeable core (slope 1:2). In setting up the Volume Exchange model it was discussed that a lower run-up height would lead to smaller velocities in the slope during run-down. The run-up height at the surface was not lower, but on the core the maximum run-up is lower in case of a permeable core. Over the thickness of the armour layer the water will rush down in average from a lower height. Moreover, even important is the fact that for an impermeable core the entire rushed-up volume flows back via the armour layer. With a permeable core a part of the rushed-up volume flows first into the core and then to 'seaward-side' or aft-side of the breakwater. So, the force on the stones during run-down is smaller in the case of a more permeable core. In Figure 5.32 definitions of the different run-up height are mentioned. For the stability of armour layer it is more useful to know the run-up at the core than at the surface. Another approach for determining the influence of the core permeability is regarding the pressure gradient below the armour layer is less when the core is more permeable, see Bruun and Günbak [1977].

5.6 Results irregular waves

Experiments are performed with irregular waves on three different geometries. These geometries are the smooth slope, armour layer on impermeable core and permeable core. The measurements are performed with a resistance wire on the surface of the armour layer or smooth slope. For the irregular wave field a single peaked JONSWAP spectrum is used with shape values σ_a= 0.07, σ_b= 0.09 and γ_p= 3.3. The wave sequence (so called, 'seed') is a fixed value so the random generator produces every test the waves in the same order. The water depth is $d/H_{m0} > 4$, so a relative deep water situation is created in the flume. For every experiment with irregular waves the duration was long enough to create at least 1000 waves. In general between 1400 and 1600 waves are generated during each experiment. The number of waves is based upon the length of the time series and the average wave period $T_{0,1.}$ For the conversion of the peak wave period T_p in the spectral period $T_{m-1,0}$ a relation of $T_p=1.1T_{m-1,0}$ is used, see PULLEN et al. [2007]. The analysis of the value $R_{u2\%}$ is done according to the

Bayesian estimator (VAN DE WALLE [2003]), when the run-up events are placed in descending order then $R_{u2\%}$ is the run-up value of, $N_{th}/(N_{total}+1)= 0.02$.

In Figure 5.38 the results of the measurements are given as well as the expectations that are based on previous studies. In section 4.2 the adjustments made on the results are elaborated. The difference between measured and expected values is caused by a combination model effects and a measurement error related to the placing of the resistance wire. The results support the earlier made conclusions that a permeable core does not have an influence on the reduction of the wave run-up. This is partly supported by the video recordings made from the side of the breakwater. In the recordings it was visible that for the largest wave heights a disconnections occurred between the water in the armour layer and the core with a grading of 4.0.

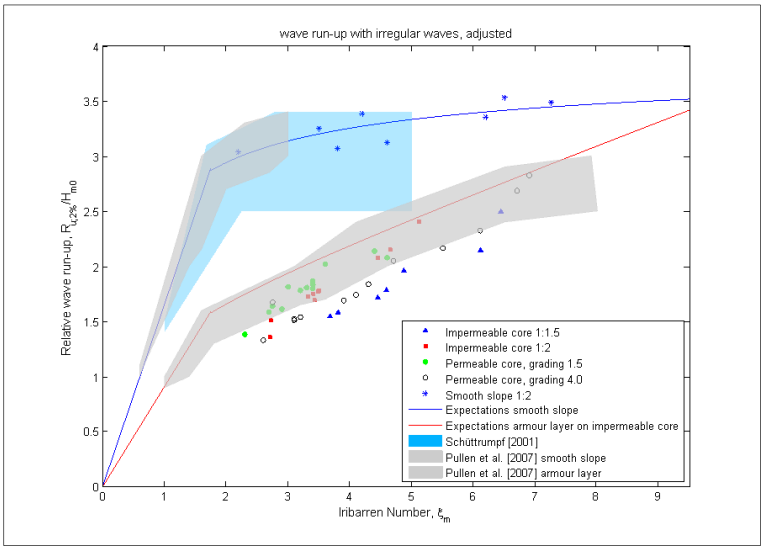

Figure 5.38: Results of the experiments with irregular waves, next to the expectations

Chapter 6

Results related to the volume exchange model

6.1 Introduction

In chapter 1 the principle of the volume exchange model has been elaborated. This model is based on the exchange of volume between the external wave volume and the internal core volume. The notional permeability coefficient *P* could be determined by computing the difference in wave run-up due to the infiltration of water during the run-up period. This P-factor was introduced in VAN DER MEER [1988] to implement the permeability of the breakwater in stability formulae of armour stones. The volume exchange model has as a basis that inflow of water into the core would reduce the run-up on the slope.

$$c_r = \frac{R_{u;s,r}}{R_{u;s,f}} \qquad \text{eq. 1.5}$$

Where $R_{u;f}$ is the run-up reduced by the surface roughness of the armour layer and $R_{u;r}$ is the run-up reduced by the surface roughness and permeability of the breakwater. The surface roughness had an assumed value, $\gamma_{f;r}$= 0.75 in JUMELET [2010]. A relation of γ_{ru}= 0.5 between the surface run-up and the core run-up was assumed. The inflow into the core was based on the porous flow as described by the Forchheimer equation and the duration of the inflow was assumed to be equal to the run-up period, which is approximately a quarter of the wave period.

In this study wave run-up experiments are performed with among other the geometry representing the P-factor of 0.5. The results are analysed in chapter 5, but the outcome is not yet related to the volume exchange model. In JUMELET [2010] rough assumptions were made about the slope surface roughness and the imposed core run-up that are both used in the VE-model. In this study these two assumption are investigated and more reliable values instead of these assumptions can be used in the VE-model. Moreover, run-up reduction values can be determined based on the measurements and compared with the computed values with the VE-model. This has led to a couple of adjustments in the VE-model that are elaborated in the following section.

6.2 'Improvement' volume exchange model

With the results obtained in chapter five, the volume exchange model has been adjusted. Also in a qualitative manner the knowledge about the influence of the permeability is increased. In this section the adjustments made in the VE-model are elaborated. The fundament of this model is stated in JUMELET [2010] only minor changes are proposed here.

In this study it is determined that the influence of the surface roughness is negligible for surging waves for $\xi > 4$, see Figure 5.20. Since, the volume exchange model is only applicable for surging waves the following holds,

$$R_{u;f} = R_{u;\max} \qquad \text{eq. 6.1}$$

In this study the shape of the wave run-up has not been investigated in a quantitative manner. Although in a qualitative manner can be said that for very large Iribarren values $\xi > 7$, the shape is a triangular wedge, and for lower Iribarren numbers the shape will have an increasingly more pronounced concave shape. Also, the shape of the run-up wedge varies with the slope angle.

However, for a first approach eq. 6.2 is still a proper assumption. For a more precise wave run-up volume the concave run-up shape stated in JUMELET [2010] can be used, see also appendix H. A problem is that with the use of this wave shape the error made comparing with reality varies over the range of the Iribarren number.

$$V_{ru} = \frac{1}{2}\chi R_u \qquad \text{eq. 6.2}$$

** A different notation is used in JUMELET [2010] for the distance χ.*

The run-up reduction factor is based on the infiltration of water into the core during the run-up period. In section 5.4 is concluded that the core permeability had no influence on the surface wave run-up for a slope angle of 1:2. Using the surface run-up to determine the amount of infiltration into the core and consequently to determine the permeability factor P is not the solution.

In JUMELET [2010] an imposed core run-up factor of 0.5 was used. Based on the measurements of the resistance wire on the core estimated imposed core run-up factors are derived, Figure 6.1. It shows that the imposed core run-up factor is dependent on the Iribarren number and is not a constant value. The maximum core run-up for general cases can be determined by making a trend line for the imposed core run-up factor γ_{ru}. Based on the measurements on the impermeable core the following relation is found:

$$\gamma_{Ru} = 1.0 * \tanh(0.31 * \xi) \qquad \text{valid for } 1.8 \leq \xi \leq 8.8 \qquad \text{eq. 6.3}$$

The above equation is based on measurements with a RW that had some difficulties in measuring the wave run-up height. This equation is determined in order to give a general indication of the imposed core run-up factor. For the VE-model the values of $\xi > 3.0$ are of interest. In Figure 6.1 the imposed core run-up factors are given, based on the measurements on an impermeable core. Figure 6.2 shows the measured values of the relative wave run-up on the surface of the core.

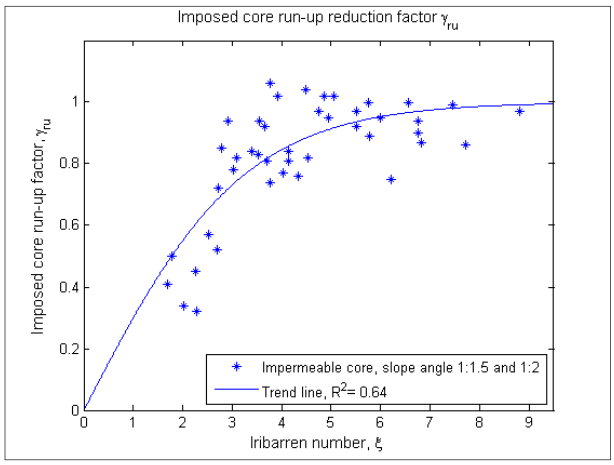

Figure 6.1: Imposed core run-up factor (impermeable core)

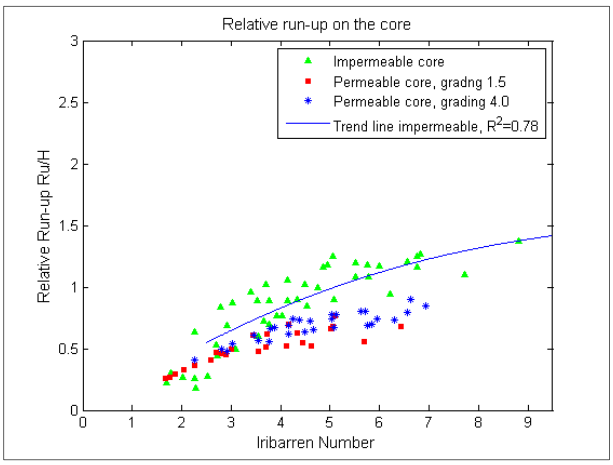

Figure 6.2: Measured values of wave run-up on the core surface

During the run-up period, the run-up at the core is slightly influenced by the permeability of the core. However, after maximum run-up the flow is directed into the core and the permeability of the core had a large influence. In case of an impermeable core, the run-up at the core increases after the maximum run-up has taken place. For a permeable core the water can flow into the core and a small increase of the core run-up after maximum surface run-up is visible in the video observations. Also, a difference visible between the core with a grading of 1.5 and 4 is visible. A more permeable core has a lower imposed core run-up. This leads to the notion that the imposed core run-up can be used as a measure

to determine the permeability factor. The reduction factor c_r must be redefined for a breakwater with a slope 1:2.

$$c_r = \frac{R_{u;c;r}}{R_{u;c;imp}}$$ Run-up reduction factor : eq. 6.4

The value of $R_{u;c;imp}$ is not constant, but varies with the wave steepness (or Iribarren number). For the reference level of $R_{u;c;imp}$ the trend line showed in Figure 6.2 is used, in formula:

$$\frac{R_u}{H} = 1.63 * \tanh(0.14\xi) \qquad \text{with } R^2 = 0.78$$ eq. 6.5

For the permeable core also a trend line could be determined. For the core grading of 1.5 this yields:

$$\frac{R_u}{H} = 0.76 * \tanh(0.24\xi) \qquad \text{with } R^2 = 0.80$$ eq. 6.6

For the core grading of 4.0 the trend line is given by the following formula:

$$\frac{R_u}{H} = 0.89 * \tanh(0.23\xi) \qquad \text{with } R^2 = 0.82$$ eq. 6.7

Based on the trend lines the run-up reduction factor can be derived. The run-up reduction factors are related to a 'notional' permeability factor of P= 0.5 structure. In Figure 6.3 the reduction factor c_r is given based on the curve fitted line of the measurements of RW_{core}.

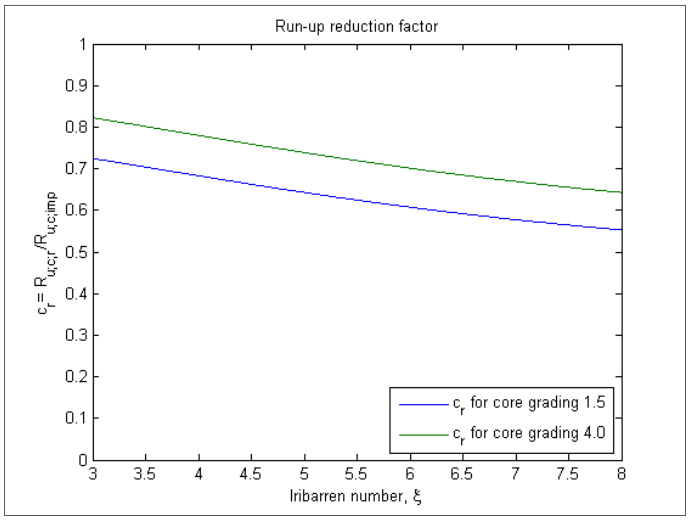

Figure 6.3: Run-up reductive factor based on the measurements

For the period of inflow into the core a quarter of the wave period was used in the volume exchange model. In fact the inflow does not take place during the wave run-up period, but during a part of the run-down period. Approximately between maximum run-up and till the water outside the breakwater is dropped below water level in the core (or SWL). At least the period of inflow is shorter than a quarter of the wave period. When regarding a sinusoidal wave motion the estimated inflow period T_{inf} is between one fifth and one eighth of the wave period. In eq. 6.4 the determination of the gradient as presented in JUMELET [2010] must be adjusted for an inflow period of $0.12\ T_0 \le T_0 \le 0.2T_0$ (γ_{inf}= 5 - 8)

$$\frac{1}{2} * n * \left(\frac{1}{l}\right) * R_{u;c;N}^2 = \frac{1}{\varpi}\sqrt{l/b} * \frac{R_{u;c;N}}{\sin\alpha}\left(1 - \cos\left(\varpi \frac{T_0}{\gamma_{inf}}\right)\right)$$ Determination of the gradient: eq. 6.8

Where *I* is the water level gradient with only the turbulent term *b*, see eq. 3.13. The reduction of the volume is determined by computing the volume of the body, increase of the volume in the core, see eq. 7.5,

$$V_b = \frac{1}{\omega}\sqrt{\frac{I}{b}}\frac{R_{u;c}}{\sin\alpha}\left(1-\cos\left(\omega * \frac{T_0}{T_{\inf}}\right)\right)$$ Volume body: eq. 6.9

The reduction of the imposed core run-up can now be determined based on the computed inflow.

$$R_{u;c;r} = \frac{V_{ru;c} - V_{b;N}}{V_{ru;c}} * R_{u;c;imp}$$ Reduced core run-up eq. 6.10

The volume exchange model is still based on the same assumption as mentioned in chapter two, except for the assumptions investigated in this study. In the adjusted VE-model eq. 6.5 multiplied by the wave height is used to determine the external volume V_{ru}. Computing the reduction factors for the structure used in the experiments, results in Figure 6.4 and Figure 6.5. See also appendix K.

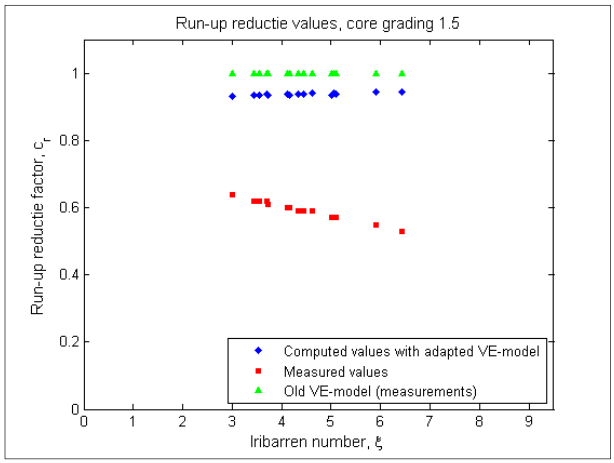

Figure 6.4: Comparison between measured and computed c_r values, core grading 1.5

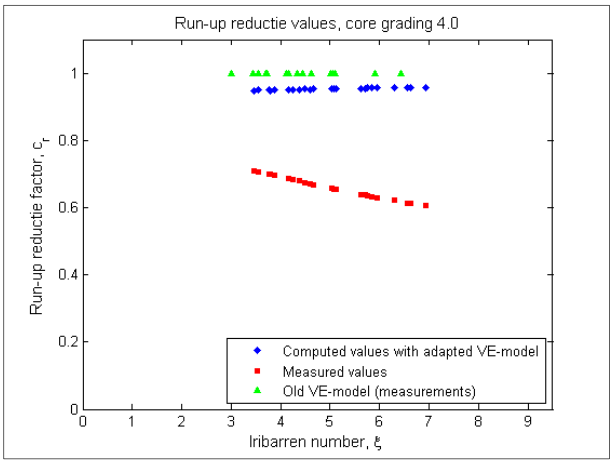

Figure 6.5: Comparison between measured and computed c_r values, core grading 4.0

The VE-model not only computes too large values of c_r, but also the trend with increasing Iribarren numbers is different. A plausible cause is a wrong assumption of the external run-up volume. This is in reality not a triangular wave run-up wedge, but has a concave shape. Especially for longer waves this influences the ratio between inflow volume and external volume. The base of the triangle is dependent on the wave length, and therefore the external volume increases with increasing Iribarren number. If the inflow volume does not increase proportionally an upward trend will be visible. Also, the difference between the two grading is not well reflected by the VE-model. When a curve fitting is used with a constant value in front of the Iribarren number (without the influence of the porosity) then it is not a proper fit, see Figure 6.6.

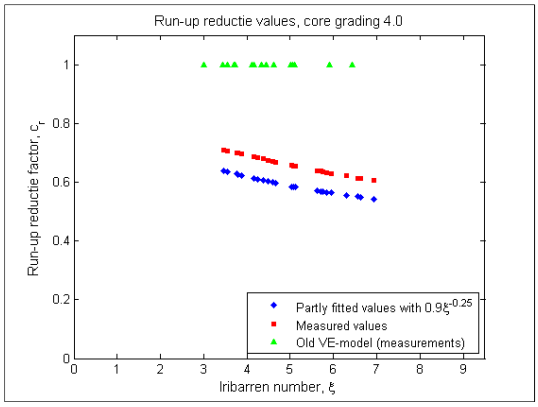

Figure 6.6: Values with a fit only including the Iribarren number

Using a reduction factor based on curve fitting, the computations with the model can be fit on the measurements. The reduction factor has a correlation of 0.940, and is given by,

$$\gamma_{cr} = 1.60 * (1-n)\xi^{-0.25} \qquad \text{eq. 6.11}$$

In the above equation the Iribarren number and the porosity of the core is included. The external volume is not modelled correctly, and also the inflow into the core is not correctly modelled by the VE-model. The reduced core run-up in the adjusted volume exchange model is now given by,

$$R_{u;c;r} = \left(\gamma_{cr} \frac{V_{ru;c} - V_{b;N}}{V_{ru;c}} \right) * R_{u;c;imp} \qquad \text{eq. 6.12}$$

		P=0.6	P=0.5	P=0.1	Core grading 1.5	Core grading 4.0
Armour layer	d_{85}/d_{15} [-]	1.25	1.25	1.25	1.2	1.2
	d_{n50a} [m]	0.036	0.036	0.036	0.067	0.067
	Porosity *n* [-]	0.4	0.4	0.4	(0.41)	(0.41)
Filter layer	d_{n50a}/d_{n50f} [-]	-	-	4.5	-	-
	d_{85}/d_{15} [-]	-	-	2.25	-	-
	Porosity *n* [-]	-	-	0.38	-	-
Core	d_{n50a}/d_{n50c} [-]	-	3.2	-	2.0	2.0
	d_{85}/d_{15} [-]	-	1.5	-	1.5	4.0
	Porosity *n* [-]	-	0.4	-	0.43	0.36

Table 6.1: Values of the Van der Meer [1988] tested structures, values for the porosity are assumed and structural properties of the structures tested in this study.

A relation between the run-up reduction factor and the notional permeability coefficient is found. To derive this relation the VE-model is adjusted by including eq. 6.5 and eq. 6.11 in the model. Computations for the run-up reduction factor are made with the structural properties of the tested structures by Van der Meer [1988], see Table 6.1. This leads to a difference with d_{n50}/H compared to the experiments performed in this study, therefore the wave heights are proportional reduced. This has lead to a relationship between $c_{r;\gamma}$ and the permeability coefficient P with the following formula:

$$P = 0.37\xi^{-0.8} c_{r;\gamma}^{-3.4} \qquad \text{eq. 6.13}$$

In appendix K the derivation of the formula for the permeability coefficient *P* is elaborated. eq. 6.13 is used to determine the P-factors for the geometries with a permeable core. For the grading of the core this has lead to a P-factor of 0.70 and for the core with a grading of 4.0 to a P-factor of 0.43. The

larger P-factor is caused by a larger porosity for the core with a grading of 1.5 than is used to compute the reduction factor for the homogenous structure. In fully turbulent flow the porosity is more of influence on the hydraulic gradient than the stone diameter. Moreover, the homogenous structure in the study of Van der Meer [1988] has a d_{n50}= 0.036 m, which deviates not a lot from the core stone diameter ($d_{n50;c}$= 0.033 m) used in this study.

The derived formula for the permeability coefficient is cannot be directly used in the stability formulae, due to the curve fitting of these formulae. A new curve fitting of the stability formulae with the results of Van der Meer [1988] must be done if eq. 6.13 is used for the P-factor. Moreover, in the model a reduction factor γ_{ru} is used that is related to the measurements on a P=0.5 structure. The other configurations of the notional permeability coefficient are not tested in this study.

Chapter 7

Conclusions and recommendations

7.1 Conclusions

The main objective of this thesis is to improve the knowledge on the influence of the core permeability on the stability of armour stones in rubble mound breakwaters. Within the main objective a theoretical model (so called: "Volume exchange model") was derived in JUMELET [2010]. This theoretical model needed improvements on specific points and more knowledge was needed on the influence of the core permeability on the wave run-up. A sub-objective is to improve the knowledge of the physical processes regarding the reduction of the wave run-up by the armour layer. With the current Volume Exchange model a very rough estimation of the wave run-up at the core of the breakwater is made. For further use of this model more information was needed about the run-up at the core. To meet the objective an experimental program was performed leading to the following conclusions.

The slope (surface) roughness and permeability of the armour layer were separately investigated in the experimental program. This will improve the knowledge of the physical processes that causes the reduction of the wave run-up by the armour layer. The following conclusions are valid for the tested slopes, 1:1.5 and 1:2, together with values of d_{n50}/H between 0.45 – 1.38.

- For (regular) surging waves above $\xi > 4.0$ the surface roughness has a negligible influence on the reduction of the wave run-up. The roughness coefficient γ_f in the Volume Exchange model has a value of 1 for $\xi > 4.0$.
- The reduction in the case of surging waves is entirely caused by the dissipation of energy in the pores of the armour layer. Compared to a smooth slope the mean reduction coefficient due to energy dissipation in the pores is $\gamma_{f;p}=0.6$ for $\xi=4$, which linearly increases till 0.8 for $\xi=9.5$.
- For $\xi < 4.0$ both the surface roughness and the permeability of the armour layer have an influence. This is for a large part caused by the absence of the resonance peak. From $\xi= 2.5$ till $\xi= 4.0$ the surface roughness reduction coefficient increases from 0.6 – 1.0. So, for the roughness coefficient in the Volume Exchange model a value of 0.8 can be chosen for $\xi= 3.3$
- For values $d_{n50}/H < 0.7$ the stone diameter has no influence on the reduction of the relative wave run-up. This led to less scatter in the graphs of relative wave run-up that complied with this condition. For values of d_{n50}/H between 0.7 – 1.0 a slight difference is visible, and for $d_{n50}/H > 1.0$ large differences occur.
- The parameter $d_{n50}/(H\xi)$ appears to describe the influence of the roughness of a permeable armour layer very well. On the basis of this parameter the scatter in the results of experiments conducted with an armour layer could be reduced.

Regarding the influence of the core permeability on the wave run-up the following conclusions can be drawn, based on experiments with a physical model breakwater with a slope angle of 1:2, an armour layer consisting of stones with a $d_{n50;a}= 0.067$ m, and a permeable core made out of core stones $d_{n50;c}= 0.033$ m with grading of 1.5 or 4.0. The results of the experiments conducted with a permeable core were compared with an impermeable core, while holding the armour stones the same.

- Generally, a permeable core has no influence on the reduction of the (surface) wave run-up. In the results of the experiments no reduction was found in the case of a core grading of 4,

and above a wave height of 0.075 m also no reduction was found with a core grading of 1.5. Most probably this was caused due to a negligible amount of infiltration of water into the core during the run-up period. This theory is supported by the video analysis, which showed that the flow inside the core during run-up was directed parallel to the slope (in upward direction). Another process that might have an effect was the reducing effect of return flow on the coming wave run-up. The entire run-up volume flowed back via the armour layer for the case of an impermeable core, which affected the coming wave run-up.

- The wave run-up height at the core is related to the surface wave run-up and to the Iribarren number of the incoming wave. More importantly; the run-up height at the core is influenced by the permeability of the core. After the maximum surface run-up is reached the flow is directed into the core. This is not possible with an impermeable core, in which consequently a higher run-up was observed. For low wave steepness the increase of the core run-up after maximum surface run-up was negligible. For $\xi > 2.5$ a difference was measured between the run-up heights at the core between the two cores with different grading.
- The previous statement led to a change in the Volume exchange model. In the improved model the run-up reduction factor c_r was defined as the ratio between the surface wave run-up, reduced by the surface roughness, and the surface wave run-up, reduced by the friction and the permeability. Eventually this study led to the conclusion that for a slope angle of 1:2 the run-up reduction factor must be written in the form,

$$c_r = \frac{R_{u;c;r}}{R_{u;c;imp}} \qquad \text{Run-up reduction factor : eq. 6.4}$$

  In this form the reduction factor is the ratio between the imposed core wave run-up on a permeable core and the wave run-up at the core on an impermeable core.
- In case of an impermeable core the entire run-up volume flows back via the armour layer after maximum run-up. With a permeable core the water flows back via the core and the armour layer. Furthermore, the run-up height at the core is lower in the case of a permeable core. So, this will negatively affect the stability of the stones on an impermeable core.
- With the increased knowledge on the influence of the core permeability on the wave run-up the Volume Exchange model is adjusted. Based on the adjusted VE-model a formula for the permeability coefficient *P* was made. It showed that the P-factor is not only dependent on the structural properties of the breakwater, but also on the Iribarren number, see eq. 6.13.

In this study with two different methods (video analysis and resistance wire) the run-up of regular waves was measured. The following conclusions can be drawn regarding the different measuring methods for regular waves.

- For surging waves the difference between the results of the video observations and the resistance wire measurements are within the accuracy band width of the measuring equipments. This is mainly caused by the local stone configurations, which influences the run-up measured by the resistance wire. The measurements with the video observations were not influenced.
- For plunging waves the results of the video observations show both a larger relative run-up and less scatter than the measurements with the resistance wire. In the video analysis the water line on an in the upper layer of the armour layer is visible. After the wave has broken down on the slope the water line that can be measured by the video observations is higher than the line measured with the resistance wire.

- On a smooth slope the scatter in the results are partly caused by a different wave run-up shape. For a steep slope (1:1.5) this shape varied between different wave heights and wave periods. On a slope of 1:1.5 the more concave shape wave run-up had a higher relative wave

run-up than a triangular wedge shape run-up. At a gentler slope (1:2) this situation did not occur resulting in a more constant wave run-up.

7.2 Recommendations

This study into the influence of the core permeability together with the other research objectives has led to the following recommendations. First, the recommendations are given regarding experiments that can improve the insight into the core permeability. Secondly, some recommendations are made about data that is not used in this study. Finally, some recommendations are made about the external volume, wave run-up on armour layers and type of wave breaking.

- Regarding the imposed core run-up more investigation is needed to determine the core run-up at an impermeable core. The measurements done in this research are not reliable enough to make conclusive statements. Also, the influence of the stone diameter on the core run-up could not be accurately determined.
- In this study only estimations of the inflow period could be made. Further research is needed to determine this period. With the help of velocity indicators in the slope the direction of the flow can be determined.
- More investigation is needed to the influence of the core in the case of a slope angle 1:1.5 and 1:3. With a steeper slope the flow during run-up may be directed into the core leading to a reduction of the surface wave run-up. The notional permeability factor was derived for slopes between 1:1.5 and 1:3, so the reduction factor must be applicable for these ranges of slope angles.
- In this study test were conducted on a breakwater made out of an armour layer on a relatively narrow graded core. In comparison to the grading of core material in practice. It is recommended to perform the tests also for very wide graded core material in order to determine the influence of the infiltration of the core run-up. Also, other configurations of breakwaters should be tested.
- The results of the experiments with irregular waves using the same should be checked. When using resistance wires then at least two wires should be placed on the slope and the distance between wire and slope should be minimized. However, it is best to use a different type of measuring equipment like a digital wire gauge. This measuring equipment allows the measuring ‘needles’ to be placed within a couple millimetres distance from the rough slope.
- The conclusions about the influence of the surface roughness should be checked in the case of irregular waves. No difference is expected, but this will increase the validity of the conclusion made in this study.

In this study some data is measured during the experiments, but are not used. Some recommendations can be made regarding these data.

- For a permeable core with a grading of 4 a wave gauge was placed inside the core. The measurements of this gauge may be used to determine the rise of the phreatic surface. Increase on the influence of the core permeability may be improved when this is related to the reduction of the wave run-up at the core or with computations made with the VE-model regarding the inflow volume.
- During the experiments with the irregular waves also the resistance wire on the core measured the water elevation on the slope. In this study this is not related to the surface wave run-up. When this relation is made this may be the first step to use the VE-model also for irregular waves.

- The shape of the wave run-up determines the external volume, currently, a triangular wedge run-up is used in the Volume Exchange model. With a triangular wave run-up wedge this

volume is overestimated. Regarding the wave run-up as a concave shape would probably be a better estimation of the external volume. Moreover, the shape of the volume varies with the Iribarren number, as was visible in the experiments with the smooth slope.

- The dimensionless number R_u/H in combination with only the Iribarren number is not a proper way to describe the wave run-up on rubble mound breakwaters. A beginning is made in this study by including the stone diameter in the relative wave run-up parameter. This reduced the scatter remarkably. However, it could not be proven that the stone diameter is of influence, also the layer thickness could be off influence. Further research is needed to be able to receive at a new dimensionless parameter to describe wave run-up on breakwaters.

- The type of wave breaking on a slope deviates with the permeability of the breakwater. With a permeable core the transition point between plunging and breaking occurs at a lower value of the Iribarren number. The classification of breaker type could be improved by implementing the permeability effects.

References

ALGERA, A. [2006]. Reduction of run-up through vetiver grass. Msc. Thesis, Delft University of Technology, Delft, The Netherlands.

BATTJES, J. A. AND ROOS, A. [1976]. Characteristics of flow in run-up of periodic waves, Delft University of Technology, Delft, The Netherlands.

BRUCE, T., VAN DER MEER, J.W., FRANCO, F AND PEARSON, J.M. [2006]. A comparison of overtopping performance of different rubble mound breakwater armour. ICCE 2006, San Diego.

BRUUN, P. AND GÜNBAK, A.R. [1977]. Stability of sloping structures in relation to the Iribarren number risk criteria in design. CE; The Norwegian institute of Technology, Trondheim, Norway

BURCHARTH, H. F., LIU, Z AND TROCH, P [1999]. Scaling of core material in rubble mound breakwater model tests. COPEDED V, CAPE TOWN, South Africa, p. 1518-1528.

CIRIA, CUR, CETMEF [2007]. The rock manual, The use of rock in hydraulic engineering, 2nd edition, C683, CIRIA, London, England.

DE ROUCK, J., VAN DE WALLE, B., TROCH, P., VAN DER MEER, J.W. AND VAN DAMME, L. [2007]. Wave run-up on the Zeebrugge Rubble Mound Breakwater: Full scale measurements results versus laboratory results. Journal of Coastal Research; Vol. 23, p. 584 - 591.

DE WAAL, J. P. AND VAN DER MEER, J.W. [1992]. Wave run-up and overtopping on coastal structures. ICCE 23rd, Venice, Italy, 1758-1771.

FUNKE, E. R. AND MANSARD, E.P.D. [1980]. The measurement of Incident and Reflected Spectra using least squares method. Proc. 17th ICCE volume 1 p. 154-172, Sydney, Australia.

HÖLSCHER, P., DE GROOT, M.B., VAN DER MEER, J.W. [1988]. Simulation of internal water movement in breakwaters. Proc. int. SOWAS 88, Delft, The Netherlands, p. 427-433.

HOLTHUIJSEN, L. H. [2007]. Waves in oceanic and coastal waters, Cambridge,Cambridge university press, ISBN 978-0-521-86028-4.

HUGHES, S. A. [2004]. Estimation of wave run-up on smooth, impermeable slopes using the wave momentum flux parameter. Coastal Engineering 5.1, p.1085-1104.

JUMELET, H. D. [2010]. The influence of core permeability on armour layer stability. Msc. thesis, Delft University of Technology, Delft, The Netherlands.

LOSADA, M. A. AND GIMÉNEZ CURTO, L.A. [1980]. Flow characteristics on rough permeable slopes under wave action. Coastal Engineering 4, 187-206.

MUTTRAY, M. O. [2000]. Wellenbewegung in einem geschütteten Wellenbrecher. PhD thesis, Technical University Braunschweig, Braunschweig, Germany.

OUMERACI, H., STAAL, T., PFOERTNER, S, LUDWIGS, G, AND KUDELLA, M. [2010]. Hydraulic performance, wave loading and response of Elastocoast revetments and their foundation; LWI Report 288. Braunschweig, Germany: University of Technology Braunschweig.

PULLEN, T., ALLSOP, N.W.H., BRUCE, T., KORTENHAUS, A., SCHÜTTRUMPF, H. AND VAN DER MEER, J.W. [2007]. Wave overtopping of sea defence and related structures, Evironment agency, UK, Expertise Netwerkwaterkeren, NL, Kuratorium für Forschung im Küsteningenieurwesen, DE.

SCHIERECK, G. J. [2000]. Introduction to bed, bank and shoreline protection, VSSD, Delft, Netherlands.

TAW [2002]. Technical report wave run-up and wave overtopping at dikes, Delft, The Netherlands, Technical Advisory Committee.

TROCH, P. [2000]. Experimentele studie en numerieke modellering van golfinteractie met stortsteengolfbrekers. Phd. thesis, University of Gent, Gent, Belgium.

VAN DE WALLE, B., DE ROUCK, J., TROCH, P., GEERAERTS, J. AND FRIGAARD, P. [2003[Wave run-up on breakwaters; spectral effects. Maritime Engineering I58, p. 60 - 67.

VAN DE WALLE, B. [2003]. Wave run-up on rubble mound breakwaters. Phd. thesis, University of Gent, Gent, Belgium.

VAN DER MEER, J. W. [1988]. Rock slopes and gravel beaches under wave attack. PhD thesis, Delft University of Technology, Delft, The Netherlands.

VAN DER MEER, J. W. AND STAM, C.J.M. [1992]. Wave run-up on smooth and rock slopes. Journal of WPC and OE, vol 188 No. 5, New York, p. 534-550.

VAN GENT, M. R. A. [1993]. Stationary and oscillatory flow through coarse porous media, Delft University of Technology, Delft, The Netherlands.

VAN GENT, M. R. A. [1995]. Wave interaction with permeable coastal structures. Phd. thesis, Delft University of Technology, Delft, The Netherlands.

VILAPLANA, A. M. [2010]. Evaluation of the Volume Exchange model using Van der Meer laboratory test results. additional thesis, Delft University of Technology, Delft, The Netherlands.

WIEGEL, R. L. [1959]. A presentation of cnoidal wave theory for practical application. Journal of Fluid mechanics (1960), Vol. 7, p. 273 - 286, Cambridge University press.

Appendix A

Video observations and accuracy

The run-up height is measured by using the camera recordings; the camera is in a perpendicular position above the slope. The position of the camera (or slope) and water level is not the same for each geometry or experiment sequence. Therefore, the calibration factor [mm/pixel] and water level height in pixels is different per geometry. In this appendix all the values of these parameters are given. The water level height in pixels is obtained by recording the still water level. The value of the pixel is determined by using multiple points (at least ten) over the width of the slope. For the determination of the calibration factor two methods are used.

The first method is measuring the distance between the SWL and top edge of the slope, at multiple locations (the middle sections was always the mean section). From the recording of the SWL the amount of pixels between the SWL and top edge could be obtained, leading to the calibration factor in mm/pixel. This approach is used for the smooth slopes and rough impermeable slope with an angle of 1:2. This method is not practical for rough slopes, because measuring the distance is more problematic.

The second method is placing markers every ten centimetres on the slope. From the recording in SWL situation the amount of pixels between the markers could be obtained. From the experiment with a rough impermeable slope 1:1.5 till the experiments with a permeable core this method is used.

The accuracy of this measurement depends mostly on the type of slope, in the case of a smooth slope the water line is almost always a straight line. For a rough slope the rock surface resulted in an irregular run-up. For the rough, impermeable and permeable slope multiple (pixel) points were needed, to avoid too large influences of local influences. The run-up height is determined by taking the average pixel value of the determined points. For a smooth slope and rough slope the determination of the pixels is has a precision of 5 pixels, for the smooth slopes this is a conservative approach. For the experiments with an armour layer this precision is 10 pixels. For plunging waves on an armour layer the accuracy is 15 pixels. The accuracy numbers are based on the experience during the analysis of the recordings. For every experiment three maximum wave run-up frames are analysed. The maximum run-up is the average of the three frames. For surging waves the three different values were almost always within 10 pixels of the average maximum run-up. The precision of the measurements was based on the error made by determining the SWL line and the maximum run-up. The precisions is determined as,

$$n_{tot} = \sqrt{n_{swl}^2 + n_{\max}^2}$$

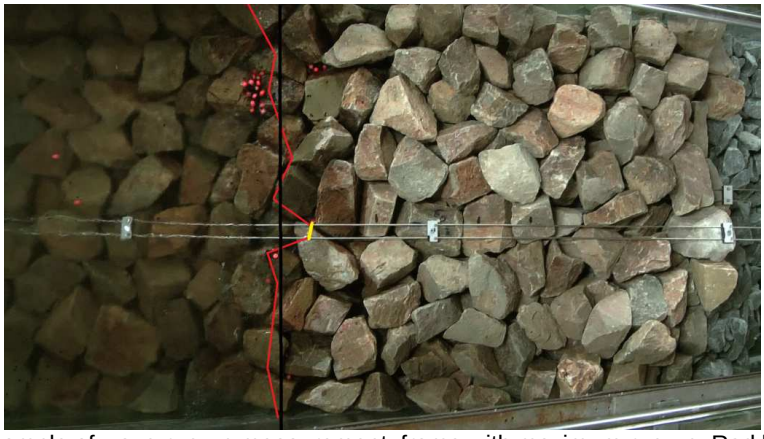

Photo 1: Example of wave run-up measurement, frame with maximum run-up. Red line: Indication of water line, Yellow: run-up level measured by resistance wire, Black line: Average wave run-up height

The accuracy P of the measurements done with the video recordings can be given in the following manner,

$P = n * \mu + x\sigma$

where,

$n =$ precision of the measurement in pixels

μ= mean calibration factor [mm/pixel]

x= distance in pixels between waterline and maximum run-up

σ= standard deviation calibration factor [mm/pixel]

eq. A.1

The standard deviation of the calibration factor is computed with,

$$\sigma = \sqrt{\frac{1}{N}\sum_{n=1}^{N}(x-\mu)^2}$$

eq. A.2

A.1 Accuracy smooth impermeable slope

The calibration factor for the smooth geometries is determined by measuring the distance between the waterline and the top edge of the slope (first method). The measurement of the distance has an accuracy of five millimetres, composed of the reading out error on both sides (1 mm on each side) and the influence of the capillary effects on the ruler. The pixel number of the waterline and the top edge of the waterline could be determined with an accuracy of 5 pixels. The values in Table A.1 are determined by computing the different variations.

Smooth slope		Distance	Pixel waterline	Pixel top edge	Mean calibration factor [mm/pixel]	Deviation, σ [mm/pixel]
1:2	Versie 1	1015 mm (+/- 5 mm)	440 (+/- 5)	1796 (+/- 2)	0.748	0.004
	Versie 2	1020 mm (+/- 5 mm)	430 (+/- 5)	1772 (+/- 2)	0.760	0.004
1:1.5	Versie 1	805 mm (+/- 5 mm)	605 (+/- 5)	1832 (+/- 2)	0.656	0.004
	Versie 2	800 mm (+/- 5 mm)	490 (+/- 5)	1746 (+/- 2)	0.647	0.004

Table A.1: Accuracy smooth slope

A.2 Accuracy rough impermeable slope

For the rough slope the same method is used as for the smooth slope, however, due to the rough character of the slope the measurement of the distance between waterline and top edge is less accurate. From the experiment with a 1:1.5 rough impermeable top layer the second method of calibration is performed. The reason for this change in calibration is that the top edge of the 1:2 slope is broken off in order to fulfil his function as a 1:1.5 slope. The top edge of the 1:1.5 slope is therefore not straight. When using the first method this would not lead to an accurate calibration factor.

Rough impermeable top layer	Distance between edge and waterline	Pixel waterline	Pixel top edge	Mean calibration factor [mm/pixel]	Deviation, σ [mm/pixel]
1:2, with $d_{n50;a}$= 0.67 m					
Versie 1	945 mm (+/- 10 mm)	580 (+/- 5)	1820 (+/- 2)	0.762	0.007
Versie 2	950 mm (+/- 10 mm)	478 (+/- 5)	1705 (+/- 2)	0.774	0.007
1:1.5 with $d_{n50;a}$= 0.067 m	-	233 (+/- 5)	-	0.584	0.009
1:1.5, with $d_{n50;c}$= 0.09 m	-	640 (+/- 5)	-	0.653	0.005
		623 (+/- 5)	-	0.643	0.008

Table A.2: Accuracy rough impermeable slope

In case of a smooth slope the still water line on the slope and the run-up line is always a (almost) straight line. Reading out the pixel of this line is therefore quite accurate. For a rough slope or a normal armour layer this line is not straight due to the different shape and height of the stones/slope. The actual run-up is in these cases given by the average maximum run-up pixel, indicated by the red line in Photo 1 and the yellow line represents the water line.

A.3 Accuracy armour layer on an impermeable core

The calibration factor [mm/pixel] is determined by placing markers on the slope at ten centimetres distance of each other. After the experiment the amount of pixel per ten cm leads to the calibration. Due to measurement errors of the distance and errors in reading the pixels, angle errors due to the rough slope a deviation of the mean calibration factor over the entire distance of the markers occurs.

Armour layer impermeable core	Mean calibration factor [mm/pixel]	Deviation, σ [mm/pixel]	Pixel waterline [-]	Variation pixel maximum run-up [-]
1:2, with $d_{n50;a}$= 0.67 m	0.734	0.009	538 (+/- 10)	+/- 10
1:1.5 with $d_{n50;a}$= 0.067 m	0.729	0.007	915 (+/- 10)	+/- 10
1:1.5, with $d_{n50;c}$= 0.09 m	0.690	0.009	859 (+/- 10)	+/- 10

Table A.3: Accuracy armour layer on an impermeable core

A.4 Accuracy armour layer on a permeable core

Armour layer impermeable core	Mean calibration factor [mm/pixel]	Deviation, σ [mm/pixel]	Pixel waterline [-]	Numbers of pixels accurate of reading out max. run-up, *n* [-]
1:2, with $d_{n50;a}$= 0.67 m, grading 1.5	0.769	0.001	563 (+/- 10)	+/- 10
Slope 1:2 with $d_{n50;a}$= 0.067 m, grading 4	0.764	0.007	576 (+/- 10)	+/- 10

Table A.4: Accuracy armour layer on an impermeable core

A single wave gauge meters has an accuracy of 2.5 mm. However, during measurements of the water elevations in a regular wave field every 0.01 s a measurement is made. Moreover, for the analysis the result of two wave gauges is used. Therefore, the mentioned accuracy does not influence the wave analysis significantly.

A.5 Influence of the slope angle

The slope angle has influence on the computation of the measured run-up parallel to the slope and the actual wave run-up (in vertical dimension). For the smooth slopes and rough impermeable 'variation' of the slope angle has a negligible influence. The vertical and horizontal distance of the slope had an accuracy of a millimetre. For the slopes with an impermeable or permeable core the construction of the slope could not be done with the accuracy of the smooth and rough impermeable slopes. After the construction of the core a measurement of the construction is made using a laser. This laser is fixed on the cart, which can travel over the length of the flume. In this way several longitudinal sections are measured by the laser. The laser measures the distance between the stones and the cart. With the help of the measurement of the core the slope angle could be adjusted. The laser measurement was an extra check for the slope angle, during construction markings on the side of the wave flume and ropes in the flume indicated the wanted slope angle. Therefore, the variation of the slope angle was not very large. The slope angle is not over the width exactly the same; however, this has no influence since the maximum run-up is chosen over the slope. In table ##, the actual slope angles are given. These slope angles are obtained by curve fitting. The 95 % confidence band leads to an error in the results of the experiments with a maximum of R_u/H= ±0.02.

Geometry	Average actual slope angle
Impermeable slope 1:1.5	1:1.49
Impermeable 1:2	1:2.04
Permeable core grading 1.5	1:1.99
Permeable	1:2.01

Table A.5: Slope angles of the slopes

A.6 Summary

Overall, the accuracy of the measurements is mostly determined by the difference in analysis of the video results. In principal every experiment has a different accuracy band width, however in appendix B only the maximum variations are given. The accuracy of each measurement can be computed with, eq. A.1 and for the final relative run-up value an extra deviation for the slope angle (±0.02) must be included.

Appendix B

Results experimental research

In this appendix the wave data and measurements of every test that is performed are given. In the table the notion “v2” stands for the second version of the experiments, this means that the same wave input parameters are used a second time. Experiment numbers with an asterisk (*) cannot be analyzed correctly due to the generation of cnoidal waves, and the analysis is based on the linear wave theory.

The experiments E045p, E046p and E047p are not mentioned in the table. After approximately half a minute a difference in wave height over the cross section of the flume occurred, which resulted in an angular wave run-up.

Above brackets placed around wave periods (E008, E039, E042), this indicates that the analysis gives a different wave period than the input in the wave generator and visually is determined. Therefore, the analysis of the wave parameters is not reliable. When in the following tables the wave periods (or on other values) is showed between brackets than the same error has occurred.

The accuracy of the measurements varies with every configuration of the slope, and also varies for every individual test. However, a different variation for every individual has no extra value and would not change the conclusions of this report. Therefore, for every experiment a single variation number is given. In this graphs shown in the report, the different variations are used.

B.1 Smooth impermeable slopes

No.	Wave height [m]	Reflection coefficient [-]	Measured run-up [m]	Relative run-up [-] (±0.07)	Wave period [s]	Wave length [m]	Wave steepness [-]	Iribarren number [-]	Breaker type
E001*	(0.067)	(0.99)	0.134	(2.00)	3.49	7.51	-	(8.42)	S
E001v2*	(0.067)	(0.99)	0.130	(1.93)	3.49	7.52	-	(8.41)	S
E002	0.063	0.92	0.134	2.12	1.60	3.08	0.020	3.98	S, concave
E002v2	0.063	0.82	0.123	1.96	1.59	3.05	0.021	3.96	S, concave
E003	0.070	0.95	0.142	2.02	1.88	3.77	0.019	4.42	S, concave
E003v2	0.071	0.95	0.133	1.88	1.88	3.77	0.019	4.42	S, concave
E004	(0.114)	(0.38)	0.203	(1.78)	~~1.60~~	~~3.08~~	-	~~2.96~~	S
E004V2	(0.100)	(0.47)	0.195	(1.95)	~~1.59~~	~~3.06~~	-	~~3.15~~	S
E005	(0.095)	(0.68)	0.194	(2.05)	~~1.56~~	~~2.98~~	-	~~3.17~~	S
E005v2	(0.100)	(0.64)	0.186	(1.86)	~~1.56~~	~~2.98~~	-	~~3.08~~	s
E006	0.094	0.90	0.205	2.19	1.70	3.33	0.028	3.47	C, concave
E006v2	0.096	0.89	0.205	2.14	1.70	3.32	0.029	3.42	C, concave
E007*	(0.108)	(0.96)	0.365	(3.37)	3.50	7.53	-	(6.64)	S

E007v2*	(0.098)	(0.97)	0.366	(3.74)	3.56	7.67	-	(7.09)	S
E008*	0.115	(0.88)	0.296	(2.58)	(1.60)	(3.07)	0.017	(2.95)	S
E008v2*	0.151	(0.49)	0.298	(1.97)	(1.59)	(3.06)	0.023	(2.56)	S
E009	0.125	0.90	0.296	2.37	1.40	2.57	0.048	2.48	p, wedge
E009v2	0.126	0.85	0.280	2.23	1.40	2.57	0.049	2.46	p, wedge
E013	0.088	0.39	0.224	2.54	1.20	2.05	0.043	2.53	P
E013v2	0.087	0.39	0.224	2.54	1.20	2.05	0.043	2.53	P
E014	0.088	0.27	0.194	2.19	0.97	1.43	0.062	2.04	P
E014v2	0.090	0.26	0.190	2.11	0.97	1.43	0.063	2.02	P
E015	0.087	0.18	0.174	2.00	0.90	1.25	0.070	1.91	P
E015v2	0.088	0.17	0.174	1.98	0.90	1.25	0.070	1.90	P

Table B.1: results smooth slope 1:2

No.	Wave height [m]	Reflection coefficient [-]	Measured run-up [m]	Relative run-up [-] (±0.07)	Wave period [s]	Wave length [m]	Wave steepness [-]	Iribarren number [-]	Breaker type
E034	0.066	0.88	0.125	1.90	1.57	3.01	0.022	5.1	-
E035	0.073	0.98	0.121	1.67	1.88	3.77	0.019	5.8	S, wedge
E035v2	0.072	0.97	0.124	1.71	1.88	3.78	0.019	5.8	S, wedge
E036	0.090	0.92	0.153	1.70	2.40	5.00	0.018	6.7	S, wedge
E036v2	0.090	0.91	0.148	1.65	2.4	5.02	0.018	6.7	S. wedge
E037	0.097	0.89	0.169	1.75	1.70	3.32	0.029	4.6	S, concave
E037v2	0.082	0.88	0.170	2.06	1.69	3.32	0.025	4.9	S, concave
E038	0.083	0.87	0.189	2.29	1.26	2.20	0.038	3.6	C, concave
E039	(0.102)	(0.04)	0.35	(3.44)	(2.33)	(4.8)	-	(6.08)	S, concave
E040	0.136	0.84	0.31	2.26	2.40	4.99	0.027	5.4	S, concave
E040v2	0.134	0.84	0.30	2.16	2.4	5.02	0.027	5.5	-
E041	0.123	0.78	0.311	2.53	1.57	3.00	0.041	3.7	s/c, concave
E042	(0.110)	(0.87)	0.31	(2.85)	(2.1)	(4.31)	-	(5.3)	-
E043	0.069	0.94	0.11	1.66	2.40	5.00	0.014	7.6	S, wedge
E044	0.091	0.83	0.18	1.97	1.20	2.04	0.045	3.3	C, concave

Table B.2: Results smooth slope 1:1.5

B.2 Rough impermeable slopes

Rough impermeable slope 1:2 with $d_{n50;a}$= 0.067 m									
No.	Wave height [m]	Reflection coefficient [-]	Measured run-up [m]	Relative run-up [-] (±0.12)	Wave period [s]	Wave length [m]	Wave steepness [-]	Iribarren number [-]	Breaker type
E016v2	(0.064)	(0.90)	0.133	(2.07)	3.49	7.48	-	(8.59)	S
E017v2	0.068	0.70	0.131	1.94	2.40	4.99	0.014	5.76	S
E018v2	0.071	0.56	0.131	1.84	1.88	3.75	0.019	4.40	S
E019v2	0.070	0.47	0.116	1.66	1.57	3.00	0.023	3.72	S
E020v2*	(0.084)	(0.80)	0.179	(2.13)	3.12	6.64	-	(6.72)	S
E021V2	0.088	0.66	0.166	1.89	2.40	4.99	0.018	5.06	S
E022v2	0.090	0.54	0.163	1.81	1.98	3.99	0.023	4.12	S
E023v2	0.088	0.52	0.154	1.75	1.70	3.31	0.027	3.57	S
E024v2*	0.106	0.89	0.370	(3.47)	3.50	7.50	-	(6.69)	S
E025v2*	0.134	0.69	0.308	(2.30)	2.83	5.98	-	(4.84)	S
E026v2	0.124	0.60	0.245	1.97	2.40	4.99	0.025	4.25	S
E027v2	0.131	0.46	0.243	1.86	2.10	4.28	0.031	3.63	S
E028v2	0.091	0.23	0.131	1.45	1.20	2.05	0.044	2.49	P/C
E029v2	0.087	0.10	0.108	1.23	0.97	1.43	0.061	2.05	P
E030v2	0.088	0.09	0.107	1.21	0.90	1.25	0.071	1.89	P
E032v2*	(0.120)	(0.89)	0.402	(3.38)	3.59	7.72	-	(6.51)	S
E033v2*	(0.118)	(0.76)	0.315	(2.65)	3.00	6.40	-	(5.44)	S
E016	0.064	0.91	0.137	2.14	3.49	7.48	0.009	8.60	S
E017	0.068	0.70	0.130	1.91	2.40	4.99	0.014	5.75	S
E018	0.072	0.56	0.133	1.86	1.88	3.75	0.019	4.39	S
E019	0.069	0.48	0.117	1.69	1.57	2.99	0.023	3.73	S
E020	(0.083)	(0.79)	0.180	(2.18)	3.11	6.61	-	(6.75)	S
E021	0.087	0.67	0.161	1.85	2.40	4.98	0.018	5.07	S
E022	0.089	0.54	0.168	1.88	1.98	3.99	0.022	4.14	S
E023	0.088	0.52	0.151	1.71	1.70	3.31	0.027	3.58	S
E024*	(0.106)	(0.91)	0.342	(3.26)	3.50	7.49	-	(6.74)	S
E025*	(0.112)	(1.35)	0.292	(2.62)	(1.41)	(2.60)	-	(2.64)	S
E026	0.123	0.62	0.255	2.08	2.40	4.98	0.025	4.27	S
E027	0.129	0.46	0.233	1.80	2.10	4.28	0.030	3.65	S
E028	0.091	0.24	0.137	1.50	1.20	2.04	0.045	2.48	P/C
E029	0.087	0.09	0.098	1.12	0.97	1.43	0.061	2.05	P
E030	0.129	0.21	0.182	1.41	1.30	2.30	0.056	2.26	P
E031	0.123	0.07	0.158	1.28	1.00	1.51	0.081	1.78	P

Table B.3: Results rough impermeable slope 1:2, d_{n50}=0.067 m

Rough impermeable slope 1:1.5 with $d_{n50;a}$= 0.067 m									
No.	Wave height [m]	Reflection coefficient [-]	Measured run-up [m]	Relative run-up [-] (±0.12)	Wave period [s]	Wave length [m]	Wave steepness [-]	Iribarren number [-]	Breaker type
E048*	(0.064)	(0.95)	0.122	(1.90)	3.49	7.52	-	(11.47)	S
E048v2*	(0.061)	(0.95)	0.121	(1.99)	3.50	7.51	-	(11.84)	S
E049	0.067	0.83	0.114	1.70	2.40	5.00	0.013	7.73	S
E050	0.070	0.72	0.130	1.86	1.88	3.77	0.019	5.92	S
E051	0.065	0.65	0.121	1.85	1.57	3.00	0.022	5.12	S
E052	0.063	0.90	0.113	1.78	2.80	5.94	0.011	9.26	S
E052v2	0.065	0.86	0.116	1.78	2.80	5.90	0.011	9.13	S
E053	0.085	0.82	0.161	1.89	2.40	5.00	0.017	6.84	S
E054	0.087	0.65	0.166	1.89	1.70	3.32	0.026	4.79	S
E055	0.083	0.55	0.142	1.71	1.38	2.52	0.033	3.98	S
E056	0.087	0.45	0.142	1.63	1.26	2.21	0.039	3.57	S
E057*	(0.054)	(0.024)	0.180	(3.38)	3.15	6.70	-	(11.35)	S
E057v2*	(0.076)	(0.034)	0.185	(2.44)	3.10	6.60	-	(9.38)	S
E058	0.090	0.66	0.170	1.89	1.98	4.01	0.023	5.49	S
E059*	(0.106)	(0.049)	0.282	(2.67)	3.50	7.50	-	8.97	S
E060	0.121	0.78	0.263	2.17	2.40	5.00	0.024	5.74	S
E061	0.121	0.63	0.251	2.07	2.10	4.29	0.028	5.02	S
E062	0.125	0.50	0.216	1.73	1.57	3.00	0.042	3.70	S
E063*	(0.134)	(0.043)	0.320	(2.40)	2.83	5.98	-	(6.45)	S
E064*	(0.116)	(0.053)	0.313	(2.69)	3.00	5.98	-	(7.32)	S
E064v2*	(0.132)	(0.056)	0.317	(2.40)	3.00	6.36	-	(6.88)	S
E065	0.096	0.42	0.151	1.58	1.20	2.05	0.047	3.23	C
E065v2	0.091	0.41	0.138	1.51	1.20	2.04	0.045	3.30	C
E066	0.086	0.26	0.129	1.50	0.97	1.43	0.060	2.76	P
E067	0.087	0.23	0.119	1.37	0.90	1.25	0.069	2.55	P

Table A.4: Rough impermeable slope 1:1.5 with d_{n50}= 0.067 m

Rough impermeable slope 1:1.5 with $d_{n50;a}$= 0.09 m									
No.	Wave height [m]	Reflection coefficient [-]	Measured run-up [m]	Relative run-up [-] (±0.12)	Wave period [s]	Wave length [m]	Wave steepness [-]	Iribarren number [-]	Breaker type
E068*	(0.067)	(0.94)	0.120	(1.79)	3.49	7.50	-	(11.25)	S
E069	0.067	0.83	0.110	1.66	2.80	5.93	0.011	9.04	S
E070	0.068	0.82	0.110	1.62	2.40	4.99	0.014	7.69	S
E071	0.071	0.70	0.120	1.67	1.88	3.76	0.019	5.86	S
E072	0.067	0.66	0.110	1.65	1.57	3.00	0.022	5.05	S
E073	0.087	0.80	0.158	1.81	2.40	4.99	0.017	6.77	S
E074	0.088	0.64	0.159	1.80	1.70	3.32	0.027	4.76	S
E075	0.084	0.57	0.141	1.67	1.38	2.51	0.034	3.96	S
E076	0.087	0.47	0.135	1.55	1.26	2.21	0.040	3.55	S/c
E077	0.090	0.67	0.163	1.80	1.98	4.00	0.023	5.49	S
E078*	(0.086)	(0.86)	0.175	(2.03)	3.12	6.66	-	(8.85)	S
E079*	(0.105)	(0.92)	0.287	(2.74)	3.50	7.52	-	(9.00)	S

E080*	(0.145)	(0.72)	0.337	(2.32)	2.83	5.99	-	(6.19)	S
E081*	(0.135)	(0.78)	0.308	(2.27)	3.00	6.38	-	(6.79)	S
E082	0.120	0.79	0.234	1.94	2.40	4.99	0.024	5.76	S
E083	0.121	0.61	0.241	2.00	2.10	4.28	0.028	5.03	S
E084	0.128	0.52	0.203	1.58	1.57	2.99	0.043	3.65	S
E071v2	0.071	0.70	0.117	1.66	1.88	3.75	0.019	5.89	S
E073v3	0.086	0.81	0.153	1.78	2.40	4.98	0.017	6.80	S
E074v2	0.089	0.64	0.161	1.80	1.70	3.31	0.027	4.74	S
E085	0.091	0.44	0.147	1.62	1.20	2.04	0.044	3.32	C
E086	0.089	0.25	0.128	1.45	0.97	1.43	0.062	2.71	P
E087	0.088	0.21	0.129	1.47	0.90	1.25	0.070	2.53	P
E088	0.126	0.44	0.200	1.59	1.30	2.31	0.055	3.05	C
E089	0.122	0.10	0.191	1.56	1.00	1.51	0.081	2.39	P
E068v2*	(0.066)	(0.95)	0.121	(1.83)	3.49	7.50	-	(11.28)	S
E072v2	0.066	0.66	0.109	1.64	1.57	3.00	0.022	5.08	S
E075v2	0.087	0.60	0.136	1.56	1.38	2.51	0.035	3.89	S
E076v2	0.086	0.52	0.134	1.56	1.26	2.21	0.039	3.58	S
E078v2*	(0.086)	(0.86)	0.173	(2.01)	3.12	6.66	-	(8.86)	s

Table B.4: results rough impermeable slope 1:1.5 with $d_{n50;a}$= 0.09 m

B.3 Armour layer on an impermeable core

Armour layer on an impermeable core, slope angle 1:1.5 with $d_{n50;a}$= 0.067 m									
No.	Wave height [m]	Reflection coefficient [-]	Measured run-up [m]	Relative run-up [-] (±0.18)	Wave period [s]	Wave length [m]	Wave steepness [-]	Iribarren number [-]	Breaker type
E094*	(0.072)	(0.73)	0.110	(1.53)	3.49	7.53	-	(10.88)	S
E095	0.071	0.61	0.094	1.34	2.80	5.95	0.012	8.82	S
E096	0.068	0.53	0.095	1.40	2.40	5.01	0.014	7.71	S
E097	0.073	0.37	0.082	1.13	2.00	4.06	0.018	6.21	S
E098	0.074	0.43	0.094	1.27	2.20	4.54	0.016	6.77	S
E099	0.069	0.34	0.074	1.08	1.88	3.77	0.018	5.99	S
E100	0.067	0.27	0.066	0.99	1.57	3.00	0.022	5.08	S
E101*	(0.086)	(0.64)	0.134	(1.59)	3.12	6.68	-	8.90	S
E102	0.102	0.58	0.146	1.44	2.60	5.48	0.019	6.82	S
E103	0.088	0.54	0.120	1.36	2.40	5.01	0.018	6.76	S
E104	0.102	0.41	0.126	1.24	2.20	4.54	0.022	5.78	S
E105	0.090	0.35	0.106	1.18	1.98	4.01	0.022	5.52	S
E106	0.090	0.3	0.106	1.18	1.70	3.33	0.027	4.75	S
E107	0.087	0.27	0.098	1.13	1.38	2.52	0.035	3.91	S
E108	0.088	0.23	0.094	1.07	1.26	2.21	0.040	3.55	S
E109	-	-	0.239	-	(1.67)	(3.25)	-	-	S
E110	0.132	0.5	0.203	1.53	2.40	5.00	0.026	5.52	S
E111	0.139	0.38	0.195	1.40	2.20	4.54	0.031	4.95	S
E112	0.136	0.33	0.166	1.22	2.00	4.06	0.033	4.54	S
E113	0.140	0.30	0.187	1.33	1.80	3.57	0.039	4.02	S

E114	0.142	0.25	0.187	1.32	1.69	3.31	0.043	3.76	S
E115	0.129	0.24	0.150	1.17	1.57	3.00	0.043	3.66	S
E116	0.106	0.17	0.118	1.11	1.20	2.05	0.052	3.09	c/p
E117	0.104	0.11	0.094	0.91	0.97	1.43	0.072	2.52	P
E118	0.098	0.12	0.090	0.92	0.85	1.12	0.087	2.28	P
E119	0.149	0.20	0.166	1.12	1.25	2.18	0.068	2.71	P
E120	0.137	0.06	0.150	1.10	1.00	1.51	0.091	2.26	P

Table B.5: results armour layer on an impermeable core, slope 1:1.5 with $d_{n50;a}$= 0.067 m

Armour layer on an impermeable core, slope angle 1:1.5 with $d_{n50;a}$= 0.09 m									
No.	Wave height [m]	Reflection coefficient [-]	Measured run-up [m]	Relative run-up [-] (±0.18)	Wave period [s]	Wave length [m]	Wave steepness [-]	Iribarren number [-]	Breaker type
E130*	(0.072)	(0.64)	0.099	(1.38)	3.20	6.85	-	(10.01)	S
E131	0.071	0.56	0.080	1.12	2.80	5.93	0.012	8.77	S
E132	0.069	0.48	0.064	0.94	2.40	5.00	0.014	7.67	S
E133	0.073	0.32	0.065	0.89	2.00	4.05	0.018	6.19	S
E134	0.074	0.39	0.069	0.94	2.20	4.53	0.016	6.78	S
E135	0.069	0.30	0.053	0.76	1.88	3.77	0.018	5.97	S
E136	0.068	0.24	0.055	0.82	1.57	3.00	0.023	5.04	S
E137*	(0.086)	(0.61)	0.133	(1.55)	3.12	6.67	-	(8.89)	S
E138	0.101	0.54	0.136	1.34	2.60	5.47	0.019	6.84	S
E139	0.088	0.50	0.101	1.14	2.40	5.00	0.018	6.76	S
E140	0.101	0.39	0.114	1.13	2.20	4.53	0.022	5.79	S
E141	0.090	0.33	0.084	0.94	1.98	4.00	0.022	5.54	S
E142	0.090	0.30	0.090	1.00	1.70	3.32	0.027	4.75	S
E143	0.088	0.27	0.084	0.95	1.38	2.52	0.035	3.89	S
E144	0.090	0.21	0.088	0.99	1.26	2.20	0.041	3.52	S
E145	0.125	0.52	0.190	1.52	2.40	5.00	0.025	5.68	S
E146	0.137	0.37	0.186	1.36	2.20	4.53	0.030	4.97	S
E147	0.134	0.32	0.167	1.25	2.00	4.05	0.033	4.58	S
E148	0.136	0.28	0.196	1.44	1.80	3.57	0.038	4.08	S
E149	0.143	0.26	0.204	1.42	1.69	3.30	0.043	3.73	S
E150	0.130	0.11	0.152	1.17	1.57	3.00	0.043	3.64	S
E151	0.108	0.22	0.116	1.07	1.20	2.05	0.053	3.05	c/p
E152	0.102	0.12	0.109	1.06	0.97	1.43	0.071	2.54	P
E153	0.130	0.60	0.152	1.17	1.30	2.31	0.080	3.02	P
E154	0.100	0.94	0.114	1.15	0.90	1.25	0.064	2.66	P
E155	0.148	0.22	0.186	1.26	1.25	2.18	0.068	2.72	p
E156	0.146	0.03	0.158	1.14	1.00	1.51	0.097	2.19	p

Table B.6: Results armour layer on an impermeable core, slope angle 1:1.5 with $d_{n50;a}$= 0.09 m

Armour layer on an impermeable core, slope angle 1:2 with $d_{n50;a}$= 0.067 m									
No.	Wave height [m]	Reflection coefficient [-]	Measured run-up [m]	Relative run-up [-] (±0.18)	Wave period [s]	Wave length [m]	Wave steepness [-]	Iribarren number [-]	Breaker type
E157*	(0.072)	(0.55)	0.109	(1.52)	3.20	6.85	-	(7.46)	S
E158	0.071	0.47	0.084	1.18	2.80	5.93	0.012	6.56	S
E159	0.068	0.41	0.074	1.09	2.40	5.00	0.014	5.75	S
E160	0.073	0.28	0.084	1.15	2.00	4.06	0.018	4.63	S
E161	0.074	0.33	0.077	1.04	2.20	4.53	0.016	5.06	S
E162	0.069	0.28	0.064	0.94	1.88	3.77	0.018	4.48	S
E163	0.068	0.23	0.063	0.93	1.57	3.00	0.023	3.77	S
E164*	(0.080)	(0.43)	0.123	1.54	(3.12)	6.64	-	(6.90)	S
E165	0.112	0.53	0.131	1.17	2.60	5.45	0.021	4.86	S
E166	0.088	0.42	0.110	1.25	2.40	4.98	0.018	5.05	S
E167	0.100	0.32	0.120	1.19	2.20	4.51	0.022	4.34	S
E168	0.089	0.27	0.095	1.06	1.98	4.00	0.022	4.14	S
E169	0.090	0.28	0.096	1.07	1.70	3.31	0.027	3.53	S
E170	0.087	0.23	0.083	0.96	1.38	2.51	0.035	2.92	c
E171	0.090	0.14	0.083	0.92	1.26	2.20	0.041	2.62	C
E172	0.132	0.44	0.182	1.38	2.40	5.00	0.026	4.13	S
E173	0.137	0.29	0.189	1.38	2.20	4.53	0.030	3.71	S
E174	0.135	0.25	0.162	1.20	2.00	4.06	0.033	3.39	S
E175	0.138	0.25	0.182	1.32	1.80	3.57	0.039	3.03	S
E176	0.143	0.23	0.189	1.32	1.69	3.30	0.043	2.79	c/p
E177	0.131	0.19	0.153	1.16	1.57	3.00	0.044	2.70	c/p
E178	0.109	0.13	0.106	0.97	1.20	2.05	0.053	2.27	P
E179	0.102	0.09	0.096	0.94	0.97	1.43	0.072	1.89	P
E180	0.101	0.12	0.092	0.91	0.90	1.25	0.081	1.77	P
E181	0.147	0.12	0.146	0.99	1.25	2.18	0.068	2.03	P
E182	0.137	0.06	0.129	0.95	1.00	1.51	0.130	1.69	P

Table B.7: Results armour layer on an impermeable core, slope angle 1:2 with $d_{n50;a}$= 0.067 m

B.4 Armour layer on permeable core

Permeable slope 1:2 with $d_{n50;a}$= 0.067 m grading 1.5									
No.	Wave height [m]	Reflection coefficient [-]	Measured run-up [m]	Relative run-up [-] (±0.17)	Wave period [s]	Wave length [m]	Wave steepness [-]	Iribarren number [-]	Breaker type
E195*	(0.074)	(0.49)	0.087	(1.17)	3.20	6.89	-	(7.33)	S
E196	0.074	0.42	0.067	0.90	2.80	5.96	0.012	6.44	S
E197	0.069	0.40	0.051	0.73	2.40	5.03	0.014	5.69	S
E198	0.073	0.26	0.051	0.70	2.00	4.06	0.018	4.62	S
E199	0.074	0.31	0.056	0.76	2.20	4.55	0.016	5.05	S
E200	0.070	0.25	0.051	0.73	1.88	3.78	0.018	4.45	S
E201	0.070	0.24	0.058	0.83	1.57	3.01	0.023	3.71	S
E202*	(0.088)	(0.47)	0.115	(1.31)	3.12	6.70	-	(6.58)	S

E203	0.102	0.39	0.124	1.22	2.60	5.50	0.019	5.09	S
E204	0.090	0.37	0.096	1.07	2.40	5.02	0.018	5.01	S
E205	0.101	0.30	0.124	1.23	2.20	4.55	0.022	4.33	S
E206	0.090	0.25	0.103	1.14	1.98	4.02	0.022	4.12	S
E207	0.090	0.25	0.112	1.24	1.70	3.34	0.027	3.54	S
E208	0.089	0.24	0.106	1.20	1.38	2.53	0.035	2.89	S
E209	0.092	0.16	0.100	1.08	1.26	2.21	0.042	2.59	S
E210	0.131	0.40	0.172	1.32	2.40	5.02	0.026	4.15	S
E211	0.136	0.28	0.183	1.34	2.20	4.55	0.030	3.73	S
E212	0.132	0.22	0.160	1.21	2.00	4.06	0.033	3.44	S
E213	0.139	0.21	0.184	1.32	1.80	3.57	0.039	3.01	S/c
E214	0.141	0.22	0.190	1.34	1.69	3.30	0.043	2.81	c/p
E215	0.133	0.18	0.155	1.16	1.57	3.00	0.044	2.69	c/p
E216	0.110	0.18	0.127	1.16	1.20	2.05	0.054	2.26	P
E217	0.105	0.11	0.100	0.95	0.97	1.43	0.073	1.87	P
E218	0.102	0.14	0.100	0.98	0.90	1.25	0.081	1.76	P
E219	0.147	0.16	0.165	1.13	1.25	2.18	0.067	2.04	P
E220	0.138	0.05	0.141	1.02	1.00	1.51	0.091	1.68	P

Table B.8: results permeable 1:2 with $d_{n50;a}$= 0.067 m, grading 1.5

Permeable slope 1:2 with $d_{n50;a}$= 0.067 m grading 4									
No.	Wave height [m]	Reflection coefficient [-]	Measured run-up [m]	Relative run-up [-] (±0.19)	Wave period [s]	Wave length [m]	Wave steepness [-]	Iribarren number [-]	Breaker type
E231*	(0.073)	(0.44)	0.087	(1.20)	3.20	6.85	-	(7.42)	S
E232	0.073	0.40	0.081	1.11	3.00	6.40	0.011	6.94	S
E233	0.075	0.39	0.084	1.12	2.90	6.16	0.012	6.63	S
E234	0.071	0.37	0.078	1.09	2.80	5.94	0.012	6.56	S
E235	0.071	0.36	0.075	1.05	2.70	5.70	0.013	6.31	S
E236	0.074	0.35	0.078	1.05	2.60	5.47	0.014	5.95	S
E237	0.071	0.33	0.077	1.08	2.50	5.24	0.014	5.85	S
E238	0.068	0.31	0.071	1.04	2.40	5.00	0.014	5.76	S
E239	0.073	0.25	0.075	1.03	2.20	4.54	0.016	5.08	S
E240	0.072	0.21	0.071	0.99	2.00	4.06	0.018	4.66	S
E241	0.069	0.21	0.068	0.99	1.88	3.77	0.018	4.48	S
E242	0.068	0.19	0.068	1.01	1.57	3.00	0.023	3.76	S
E243*	(0.086)	(0.42)	0.118	(1.38)	3.12	6.64	-	(6.66)	S
E244	0.100	0.39	0.129	1.28	2.90	6.14	0.016	5.72	S
E245	0.096	0.38	0.123	1.28	2.80	5.91	0.016	5.63	S
E246	0.100	0.36	0.122	1.22	2.60	5.45	0.018	5.13	S
E247	0.096	0.34	0.103	1.07	2.50	5.21	0.018	5.03	S
E248	0.089	0.33	0.086	0.97	2.40	4.98	0.018	5.04	S
E249	0.098	0.28	0.098	1.00	2.30	4.75	0.021	4.59	S
E250	0.099	0.24	0.112	1.13	2.20	4.51	0.022	4.37	S
E251	0.089	0.19	0.083	0.93	1.98	4.00	0.022	4.15	S
E252	0.090	0.21	0.091	1.01	1.70	3.31	0.027	3.54	S
E253	0.087	0.21	0.090	1.04	1.38	2.51	0.035	2.92	C
E254	0.135	0.35	0.190	1.41	2.50	5.22	0.026	4.25	S

E255	0.138	0.27	0.181	1.31	2.30	4.75	0.029	3.87	S
E256	0.132	0.22	0.158	1.20	2.20	4.51	0.029	3.78	S
E257	0.130	0.32	0.159	1.23	2.40	4.98	0.026	4.16	S
E258	0.130	0.16	0.150	1.15	2.00	4.04	0.032	3.47	S
E259	0.139	0.17	0.182	1.31	1.80	3.57	0.039	3.02	c/p
E260	0.142	0.18	0.173	1.22	1.69	3.28	0.043	2.80	c/p
E261	0.109	0.15	0.113	1.04	1.20	2.04	0.053	2.27	P
E262	0.101	0.11	0.100	0.99	0.90	1.25	0.081	1.77	P
E263	0.142	0.16	0.175	1.23	1.25	2.17	0.066	2.07	p

Table B.9: results rough slope 1:2 with $d_{n50;a}$= 0.067 m, grading 4

Appendix C

Wave gauges and calibration resistance wires

C.1 Introduction

In this appendix the general principle and the calibration of the wave gauges and resistance wire that measure the water elevation in the flume or on the slope are elaborated. Three wave gauges are placed behind each other with a distance of at least 3 meter from the slope. On the surface of the armour layer and between the armour layer and core, resistance wires are placed. These wires are manufactured at the Water Lab and are calibrated in the flume. The voltage output of the equipment is measured and varies with the area of the wire that is wet. The ratio between the voltage and wet area can be determined by filling the flume slowly and using the wave gauges measurements as a reference. The wave gauges are calibrated in ideal conditions and have an accuracy of 2.5 mm. In Table C.1 the calibration of the wave gauges are given.

Wave gauge	Calibration m/V
WG-1	0.0239
WG-2	0.0237
WG-3	0.0250

Table C.1: Calibration wave gauges

The ratio between voltage and water elevations (calibration factor) is depended on the slope angle, material and equipment properties. The resistance of the wire is proportional with the length and decreases with increasing cross sectional area. The diameter of the resistance wires is 3 mm (the diameter of the wave gauges wires is 4 mm). The resistance wires have an angle of approximately 1:2 or 1:1.5. The length of the resistance wires is five times larger than the length of the wave gauges and the diameter is smaller, therefore the resistance at the amplifier is placed on 20 cm instead of 50 cm. Combined with the slope angle this leads to an expected calibration factor in the order of 0.043 m/V and 0.032 m/V for a 1:2 slope, not included is the equipment properties of the pre-amplifier and connections.

C.1 General principle

The equipment that measures the water elevation in the wave flume and on the slope exists of a gauge (steel wire) with integral pre-amplifier and a separate main amplifier. The actual gauge consists of two metal electrodes that are placed in the water, at least 4 cm below the waterline. The electric resistance Rh measured between the electrodes is inverse proportional to the instantaneous depth of immersion (h) and the specific conductivity of the water, *G*. The constant of proportionality *K1* depends on the dimension of the probe.

$$R_h = \frac{K_1}{hG}$$

At the lower end of the gauge a reference electrode is placed to avoid the effect of conductivity fluctuations. The ratio of the resistance of the reference electrode and the electric resistance of the influence of the conductivity is eliminated. With this equipment this is achieved by using R_h and R_r as the input and feedback resistors of an operational amplifier, which is fed by a constant voltage source e_i. From the properties of the amplifier if follows that the output voltage,

$$e_u = e_i * \frac{R_r}{R_h}$$

$$\frac{R_r}{R_h} = \frac{K_2}{K_1} * h$$

this leads to

$$e_u \propto h$$

The accuracy of the equipment is +/- 0.5 % of the selected range. In this case a range of 50 cm is selected, thus the wave gauges have an accuracy of 0.25 cm (or 2.5 mm).

C.2 Calibration resistance wires

The resistance wires that are custom made need to be calibrated in the flume. This factor deviates with the slope angle, and varies with every change in the armour layer. The resistance wire between the armour layer and core may have some difficulties in measuring run-up at the core, because the wire may not become wet 'enough' to influence the measurement. Also, the wire has a shape that follows the irregular core which may lead to not a constant calibration factor. The standard deviation is computed by taking the difference between the measurements of the wave gauges and the measurements of the resistance wire. When the measuring results are regarded as a set of discrete random variables then the standard deviation can be computed as follows,

$$\sigma = \sqrt{\frac{1}{N}\sum_{i=1}^{N}(v-\mu)^2}$$

C.3 Impermeable slope 1:1.5 with $d_{n50;a}$= 0.067 m

Before (and after) a sequence of experiments a calibration measurement is executed. The first geometry with the resistance wires was the impermeable slope 1:1.5 with a $d_{n50;a}$= 0.067 m. Before and after the experiments conducted with regular waves a calibration measurement was performed. In the following the resistance wire at the surface of the armour layer is denoted as RW_{arm} and resistance wire between armour layer and core as RW_{core}. In total five calibration measurements are made for the resistance wires on this geometry.

Calibration	Calibration-factor [m/V]	Standard deviation with wave gauges [m]	remark
15-11-2010-A	0.038 0.040	0.005 0.003	After construction of the geometry
15-11-2010-B	0.038 0.040	0.004 0.005	
16-11-2010	0.038 0.040	0.002 0.006	Before regular wave experiments
17-11-2010	0.038 0.040	0.003 0.01	Before irregular wave experiments
18-11-2010	0.038 0.040	0.004 0.003	

Table C.2: Calibration factor RW_{arm}

In Figure C.1 an example of a calibration is shown. The oscillations in the graph are a consequence of translations wave caused by opening or closing the valve that fills the flume.

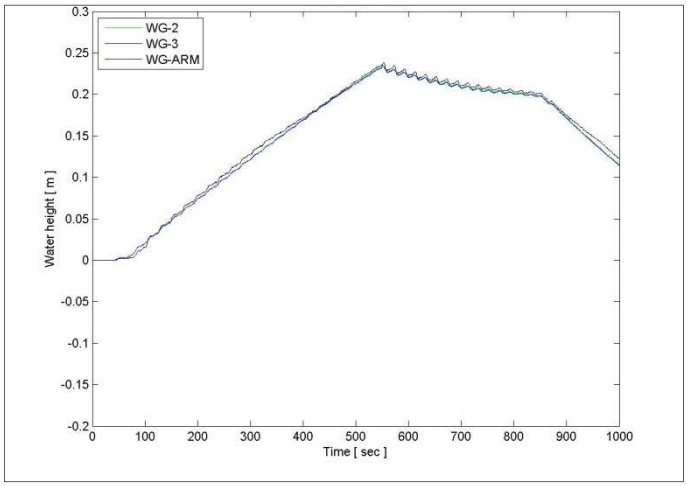

Figure C.1: Calibration of RW_{arm} before the regular wave experiments with impermeable slope 1:1.5 with $d_{n50;a}$= 0.067 m.

The resistance wire, RW_{core} was influenced by background electromagnetic radiation, see Figure C.2. This graph shows the voltage fluctuations in time, with rising water. This noise was filtered by the measuring program, which removed frequencies above 20 Hz out of the results.

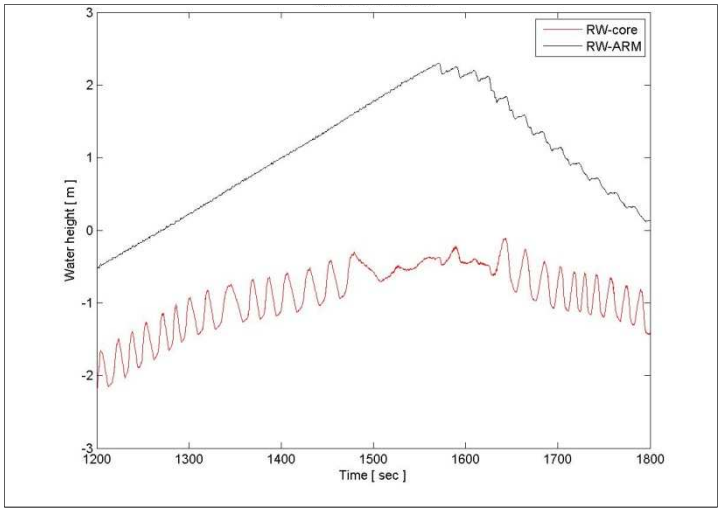

Figure C.2: Voltage fluctuations as a result of background radiations.

For the calibration of the resistance wire only two calibration measurements were useful, the first three calibrations were influenced by the background radiation. The measurements made by RW_{core} may not be reliable enough for quantitative conclusions.

Calibration	Calibration-factor [m/V]	Standard deviation [m]	remark
17-11-2010	0.054	0.06	
18-11-2010	0.054	0.07	

Table C.3: Calibration factor resistance wire core, RW_{core}

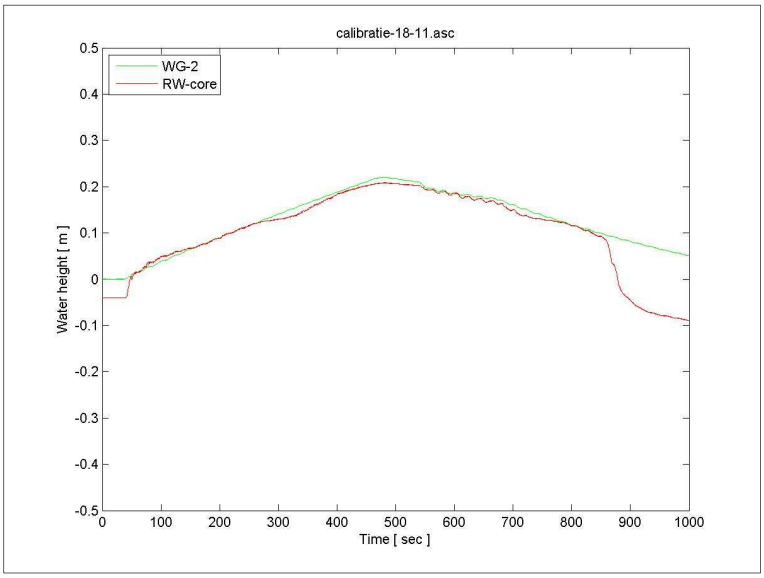

Figure C.3: Calibration measurements 18-11-2010 with factor is 0.048 m/V

In Figure C.3 the sudden drop at t= 900 s is the consequence of higher water level on the lee-side of the breakwater. The water level on the lee side pushes the plastic sheet up. This phenomenon is visible on every calibration measurement concerning the impermeable geometry.

C.4 Impermeable slope 1:2 with $d_{n50;a}$= 0.067 m

The calibration factor differs with the slope angle and also changes can occur during rebuilding of the structure. Therefore, calibration is done at the start and end of the experiments with the impermeable slope 1:2. Between the experiments with the regular waves and the irregular waves the pre-amplifier of the resistance wire broke down and was replaced. The pre-amplifier generated a direct current which leads to electrolysis at the reference electrode. Before the start of the second series with irregular waves improvement were made on the resistance wire between the core and armour layer.

Description	Calibration	Calibration factor [m/V]	Standard deviation, σ_{arm}	Calibration factor, RW_{core} [m/V]	Standard deviation, σ_{core}
Before regular wave experiments	23-11-2010	0.031	0.002	0.044	0.008
After regular wave experiments	23-11-2010	0.031	0.002	0.044	0.004
Before first series of irregular waves	24-11-2010	0.042	0.004	0.046	0.014
After first series of irregular waves	24-11-2010	0.042	0.003	0.046	0.005
Before second series of irregular waves	25-11-2010	0.042	0.003	0.049	0.005
After second series of irregular waves	25-11-2010	0.042	0.003	0.049	0.005

Table C.4: Calibration factors RW_{arm} and RW_{core} of wire on impermeable slope 1:2 with d_{n50}= 0.067 m

C.5 Permeable slope grading 1.5

After rebuilding the impermeable slope in a permeable slope the resistance wires should be calibrated. The slope angle is not changed, but the position of the resistance wires is different.

Description	Calibration	Calibration factor [m/V]	Standard deviation, σ_{arm}	Calibration factor, RW_{core} [m/V]	Standard deviation, σ_{core}
After finishing slope	26-11-2010	0.047	0.002	0.057	0.003
Before regular wave experiments	29-11-2010	0.047	0.012	0.057	0.006
After regular wave experiments	29-11-2010	0.047	0.002	0.057	0.004
Before first series of irregular waves	30-11-2010	0.047	0.002	0.057	0.004
Before second series of irregular waves	01-12-2010	0.047	0.002	0.057	0.003

Table C.5: Calibration factors RW_{arm} and RW_{core} of wire on permeable core with grading of 1.5

C.6 Permeable slope grading 4

Description	Calibration	Calibration factor [m/V]	Standard deviation, σ_{arm}	Calibration factor, RW_{core} [m/V]	Standard deviation, σ_{core}
Before regular wave experiments	09-12-2010	0.041	0.002	0.059	0.005
Before irregular wave experiments	10-12-2010	0.041	0.002	0.059	0.005
After Irregular wave experiments	10-12-2010	0.041	0.002	0.059	0.004

Table C.6: Calibration factors RW_{arm} and RW_{core} of wire on permeable core with grading of 4

C.7 Smooth slope

Description	Calibration	Calibration factor [m/V]	Standard deviation, σ_{arm}	Calibration factor, RW_{core} [m/V]	Standard deviation, σ_{core}
After irregular wave experiments	04-02-2010	0.049	0.003	-	-
After irregular wave experiments	07-02-2010	0.049	0.003	-	-

Table C.7: Calibration factors RW_{arm} of wire on smooth slope 1:2

C.8 Evaluation

The resistance wire on the surface of the armour layer has a deviation that leads to reliable results. Moreover, the deviation is almost constant with every calibration measurements when regarding the geometries separate. The resistance wire on the core has large deviations when placed on an impermeable core. Moreover, the calibration showed that the line was no a straight linear line. Only for the permeable core the resistance wire seems reliable.

Appendix D

Results resistance wire on surface

Armour layer on impermeable core slope 1:1.5 d_{n50}= 0.067 m							
No.	H [m]	T [s]	Run-up, RW-core, [m]	R_U/H, RW-core, [-]	Run-up, RW-arm, [m]	R_U/H, RW-arm, [-]	Iribarren number [-]
E095	0.071	2.80	*0.097*	*1.37*	0.100	1.42	8.82
E096	0.068	2.40	*0.075*	*1.10*	0.087	1.28	7.71
E097	0.073	2.00	*0.069*	*0.94*	0.091	1.25	6.21
E098	0.074	2.20	*0.086*	*1.16*	0.095	1.29	6.77
E099	0.069	1.88	*0.081*	*1.17*	0.085	1.23	5.99
E100	0.067	1.57	*0.060*	*0.90*	0.052	0.78	5.08
E102	0.102	2.60	*0.130*	*1.27*	0.149	1.46	6.82
E103	0.088	2.40	*0.110*	*1.25*	0.117	1.33	6.76
E104	0.102	2.20	*0.110*	*1.08*	0.123	1.21	5.78
E105	0.090	1.98	*0.097*	*1.08*	0.100	1.11	5.52
E106	0.090	1.70	*0.090*	*1.00*	0.092	1.02	4.75
E107	0.087	1.38	*0.067*	*0.77*	0.066	0.76	3.91
E108	0.088	1.26	*0.052*	*0.60*	0.056	0.64	3.55
E110	0.132	2.40	*0.159*	*1.20*	0.174	1.31	5.52
E111	0.139	2.20	*0.164*	*1.18*	0.172	1.24	4.95
E112	0.136	2.00	*0.116*	*0.85*	0.141	1.04	4.54
E113	0.140	1.80	*0.108*	*0.77*	0.140	1.00	4.02
E114	0.142	1.69	*0.099*	*0.70*	0.133	0.94	3.76
E115	0.129	1.57	*0.093*	*0.72*	0.101	0.79	3.66
E116	0.106	1.20	*0.053*	*0.50*	0.064	0.60	3.09
E117	0.104	0.97	*0.029*	*0.28*	0.050	0.48	2.52
E118	0.098	0.85	*0.017*	*0.18*	0.053	0.54	2.28
E119	0.149	1.25	*0.066*	*0.44*	0.092	0.62	2.71
E120	0.137	1.00	*0.035*	*0.26*	0.079	0.58	2.26

Table D.1: Run-up measurements on armour layer on impermeable core slope 1:1.5 d_{n50}=0.067 m

Armour layer on impermeable core slope 1:2 d_{n50}= 0.067 m							
No.	H [m]	T [s]	Run-up, RW-core, [m]	R_U/H, RW-core [-]	Run-up, RW-arm, [m]	R_U/H, RW-arm, [-]	Iribarren number [-]
E158	0.071	2.80	*0.09*	*1.21*	0.080	1.12	6.56
E159	0.068	2.40	*0.08*	*1.18*	0.069	1.02	5.75
E160	0.073	2.00	-		0.072	0.99	4.63
E161	0.074	2.20	-		0.079	1.08	5.06
E162	0.069	1.88	*0.07*	*1.02*	0.068	0.98	4.48
E163	0.068	1.57	*0.06*	*0.89*	0.057	0.84	3.77
E165	0.112	2.60	*0.13*	*1.16*	0.128	1.14	4.86
E166	0.088	2.40	*0.11*	*1.25*	0.108	1.22	5.05
E167	0.100	2.20	*0.09*	*0.90*	0.119	1.19	4.34
E168	0.089	1.98	*0.08*	*0.89*	0.095	1.07	4.14

E169	0.090	1.70	*0.08*	*0.89*	0.096	1.07	3.53
E170	0.087	1.38	*0.06*	*0.69*	0.064	0.74	2.92
E171	0.090	1.26	-	-	-	-	2.62
E172	0.132	2.40	*0.14*	*1.06*	0.173	1.31	4.13
E173	0.137	2.20	*0.14*	*1.02*	0.172	1.26	3.71
E174	0.135	2.00	*0.13*	*0.96*	0.154	1.14	3.39
E175	0.138	1.80	*0.12*	*0.87*	0.154	1.12	3.03
E176	0.143	1.69	*0.12*	*0.84*	0.141	0.99	2.79
E177	0.131	1.57	*0.07*	*0.53*	0.134	1.02	2.70
E178	0.109	1.20	*0.07*	*0.64*	0.067	0.62	2.27
E179	0.102	0.97	-		0.063	0.62	1.89
E180	0.101	0.90	*0.03*	*0.30*	0.060	0.59	1.77
E181	0.147	1.25	*0.04*	*0.27*	0.117	0.79	2.03
E182	0.137	1.00	*0.03*	*0.22*	0.073	0.53	1.69

Table D.2: Run-up measurements on armour layer on impermeable core slope 1:2 d_{n50}=0.067 m

Armour layer on permeable core 1:2 d_{n50}= 0.067 m, core grading of 1.5							
No.	H [m]	T [s]	Run-up, RW-core, [m]	R_U/H, RW-core, [-]	Run-up, RW-arm, [m]	R_U/H, RW-arm, [-]	Iribarren number [-]
E196	0.074	2.80	0.050	0.68	0.078	1.06	6.44
E197	0.069	2.40	0.039	0.56	0.072	1.04	5.69
E198	0.073	2.00	0.038	0.52	0.077	1.05	4.62
E199	0.074	2.20	0.050	0.68	0.081	1.09	5.05
E200	0.070	1.88	0.038	0.55	0.072	1.03	4.45
E201	0.070	1.57	0.035	0.51	0.066	0.95	3.71
E203	0.102	2.60	0.078	0.77	0.127	1.25	5.09
E204	0.090	2.40	0.059	0.66	0.099	1.10	5.01
E205	0.101	2.20	0.064	0.63	0.119	1.18	4.33
E206	0.090	1.98	0.047	0.52	0.092	1.02	4.12
E207	0.090	1.70	0.043	0.48	0.098	1.09	3.54
E208	0.089	1.38	0.040	0.45	0.078	0.88	2.89
E209	0.092	1.26	0.038	0.41	0.079	0.86	2.59
E210	0.131	2.40	0.092	0.70	0.161	1.23	4.15
E211	0.136	2.20	0.084	0.62	0.183	1.35	3.73
E212	0.132	2.00	0.080	0.61	0.145	1.10	3.44
E213	0.139	1.80	0.070	0.50	0.144	1.03	3.01
E214	0.141	1.69	0.065	0.46	0.140	0.99	2.81
E215	0.133	1.57	0.063	0.47	0.138	1.04	2.69
E216	0.110	1.20	0.040	0.36	0.093	0.85	2.26
E217	0.105	0.97	0.030	0.29	0.072	0.69	1.87
E218	0.102	0.90	0.027	0.27	0.065	0.64	1.76
E219	0.147	1.25	0.048	0.33	0.135	0.92	2.04
E220	0.138	1.00	0.036	0.26	0.116	0.84	1.68

Table D.3: Run-up measurements on permeable slope 1:2 d_{n50}= 0.067 m, core grading of 1.5

Armour layer on permeable core 1:2 d_{n50}= 0.067 m, core grading of 4							
No.	H [m]	T [s]	Run-up, RW-core, [m]	R_U/H, RW-core, [-]	Run-up, RW-arm, [m]	R_U/H, RW-arm, [-]	Iribarren number [-]
E232	0.073	3.00	0.062	0.85	0.086	1.18	6.94
E233	0.075	2.90	0.07	0.90	0.091	1.22	6.63
E234	0.071	2.80	0.06	0.79	0.084	1.19	6.56
E235	0.071	2.70	0.05	0.73	0.081	1.14	6.31
E236	0.074	2.60	0.06	0.74	0.087	1.17	5.95
E237	0.071	2.50	0.05	0.70	0.078	1.09	5.85
E238	0.068	2.40	0.05	0.69	0.068	1.00	5.76
E239	0.073	2.20	0.05	0.67	0.082	1.12	5.08
E240	0.072	2.00	0.05	0.65	0.072	1.00	4.66
E241	0.069	1.88	0.04	0.64	0.067	0.98	4.48
E242	0.068	1.57	0.04	0.56	0.069	1.02	3.76
E244	0.100	2.90	0.08	0.80	0.122	1.22	5.72
E245	0.096	2.80	0.08	0.80	0.114	1.18	5.63
E246	0.100	2.60	0.08	0.78	0.117	1.17	5.13
E247	0.096	2.50	0.08	0.78	0.111	1.15	5.03
E248	0.089	2.40	0.07	0.74	0.100	1.13	5.04
E249	0.098	2.30	0.07	0.72	0.110	1.12	4.59
E250	0.099	2.20	0.07	0.73	0.114	1.15	4.37
E251	0.089	1.98	0.06	0.62	0.099	1.11	4.15
E252	0.090	1.70	0.05	0.57	0.098	1.09	3.54
E253	0.087	1.38	0.04	0.48	0.090	1.03	2.92
E254	0.135	2.50	0.10	0.74	0.170	1.26	4.25
E255	0.138	2.30	0.09	0.67	0.165	1.20	3.87
E256	0.132	2.20	0.09	0.66	0.154	1.17	3.78
E257	0.130	2.40	0.09	0.69	0.151	1.16	4.16
E258	0.130	2.00	0.08	0.61	0.136	1.05	3.47
E259	0.139	1.80	0.08	0.54	0.142	1.02	3.02
E260	0.142	1.69	0.07	0.50	0.140	0.99	2.80
E261	0.109	1.20	0.04	0.41	0.097	0.89	2.27
E262	0.101	0.90	0.03	0.25	0.084	0.83	1.77
E263	0.142	1.25	0.06	0.42	0.131	0.92	2.07

Table D.4: Run-up measurements on permeable slope 1:2 d_{n50}= 0.067 m, core grading of 4

D.5 Irregular wave results

Armour layer on an impermeable core, slope angle 1:1.5 with $d_{n50;a}$= 0.067 m								
Proef	H_{m0} [m]	T_p [s]	$T_{m-1,0}$ [s]	$\xi_{m-1,0}$ [-]	$R_{u2\%}$ [m]	$R_{u2\%}/H_{m0}$ [-	$\Delta R_u/H$ [-]	ε [-]
EM121ir	0.09	1.92	1.75	4.87	0.12	1.34	0.48	0.57
EM122ir	0.09	1.82	1.65	4.59	0.11	1.21	0.43	0.56
EM123ir	0.09	1.51	1.37	3.81	0.10	1.15	0.30	0.56
EM124ir	0.09	1.45	1.32	3.68	0.10	1.07	0.29	0.56
EM125ir	0.09	2.41	2.19	6.11	0.13	1.49	0.68	0.52
EM125ir v2	0.09	2.41	2.19	6.11	-	-	0.68	0.52
EM126ir	0.09	1.92	1.75	4.87	0.11	1.25	0.48	0.56
EM127ir	0.10	1.84	1.67	4.45	0.12	1.17	0.36	0.56
EM129ir	0.09	2.54	2.31	6.44	0.14	1.70	0.73	0.61

Table D.5: Results irregular wave experiments armour layer on impermeable core, 1:1.5 and d_{n50}= 0.067 m

Armour layer on an impermeable core, slope angle 1:2 with $d_{n50;a}$= 0.067 m, d_w=0.013 m								
Proef	H_{m0}	T_p	$T_{m-1,0}$	$\xi_{m-1,0}$	$R_{u2\%}$	$R_{u2\%}/H_{m0}$	$\Delta R_u/H$	ε
EM186ir	0.090	1.43	1.30	2.71	0.08	0.93	0.21	0.56
EM187ir	0.099	1.51	1.37	2.72	0.10	1.06	0.19	0.57
EM188ir	0.091	1.82	1.65	3.43	0.10	1.15	0.34	0.58
EM188irv2	0.091	1.81	1.65	3.41	0.11	1.17	0.34	0.57
EM189ir	0.099	1.84	1.67	3.32	0.12	1.21	0.28	0.59
EM190ir	0.099	1.94	1.76	3.50	0.12	1.24	0.31	0.60
EM190irv2	0.099	1.93	1.75	3.48	0.12	1.23	0.31	0.52
EM191ir	0.090	2.35	2.14	4.45	0.12	1.35	0.53	0.59
EM192ir	0.090	2.45	2.23	4.64	0.13	1.40	0.56	0.59
EM193ir	0.091	2.72	2.47	5.12	0.15	1.60	0.64	0.59

Table D.6: Results irregular wave experiments armour layer on impermeable core, 1:2 and d_{n50}= 0.067 m

Armour layer on permeable core; 1:2 with $d_{n50;a}$= 0.067 m and grading of 1.5,								
Proef	H_{m0}	T_p	$T_{m-1,0}$	$\xi_{m-1,0}$	$R_{u2\%}$	$R_{u2\%}/H_{m0}$	$\Delta R_u/H$	ε
E194	0.088	1.77	1.61	3.39	0.10	1.13	0.35	1.57
E221	0.096	1.23	1.12	2.25	0.10	0.99	0.11	1.13
E222	0.091	1.43	1.30	2.69	0.10	1.09	0.20	1.33
E223	0.100	1.54	1.40	2.76	0.11	1.13	0.19	1.38
E224	0.090	1.78	1.62	3.37	0.11	1.18	0.34	1.61
E225	0.100	1.8	1.64	3.23	0.12	1.20	0.27	1.54
E225 v2	0.099	1.83	1.66	3.30	0.12	1.21	0.28	1.57
E226	0.100	1.89	1.72	3.39	0.13	1.26	0.29	1.63
E226 v2	0.100	1.89	1.72	3.39	0.12	1.23	0.29	1.60
E227	0.090	2.3	2.09	4.35	0.12	1.36	0.51	1.95
E228	0.091	1.92	1.75	3.61	0.12	1.30	0.37	1.78
E229	0.091	2.44	2.22	4.59	0.12	1.37	0.55	1.91
E230	0.133	1.92	1.75	2.99	0.18	1.32	0.14	1.55
E231	0.132	1.84	1.67	2.88	0.15	1.17	0.13	1.37

Table D.7: Results irregular wave experiments , permeable core, 1:2 and d_{n50}= 0.067 m

Armour layer on permeable core 1:2 with $d_{n50;a}$= 0.067 m and grading of 4, d_w= 0.014 m								
Proef	H_{m0}	T_p	$T_{m-1,0}$	ξ_m	$R_{u2\%}$	$R_{u2\%}/H_{m0}$	$\Delta R_u/H$	ε
E264ir	0.088	1.43	1.30	3.01	0.10	1.19	0.22	0.52
E265ir	0.116	1.55	1.41	2.84	0.11	0.98	0.13	-
E266ir	0.108	1.78	1.62	3.38	0.12	1.10	0.21	0.58
E267ir	0.116	1.84	1.67	3.37	0.13	1.11	0.19	0.59
E268ir	0.116	1.92	1.75	3.52	0.13	1.12	0.21	0.62
E269ir	0.116	2.34	2.13	4.29	0.14	1.22	0.29	0.63
E270ir	0.116	2.45	2.23	4.49	0.15	1.26	0.31	0.63
E271ir	0.118	2.60	2.36	4.73	0.16	1.34	0.33	0.63
E272ir	0.109	2.72	2.47	5.15	0.16	1.48	0.42	0.65
E273ir	0.115	3.26	2.96	5.46	0.18	1.57	0.48	0.69
E274ir	0.109	3.55	3.23	6.10	0.18	1.63	0.61	0.75
E275ir	0.108	3.85	3.50	6.65	0.21	1.94	0.68	0.66
E276ir	0.108	3.98	3.62	6.88	0.22	2.07	0.71	0.77

Table D.8: Results irregular wave experiments permeable core, grading 4, 1:2 and d_{n50}= 0.067 m

Smooth slope 1:2 , d_w= 0.005 m								
Proef	H_{m0}	T_p	$T_{m-1,0}$	ξ_m	$R_{u2\%}$	$R_{u2\%}/H_{m0}$	$\Delta R_u/H$	ε
E277ir	0.100	1.35	1.23	2.18	0.24	2.40	0.05	0.49
E278ir	0.092	2.10	1.91	3.54	0.25	2.70	0.15	0.54
E279ir	0.090	2.23	2.03	3.80	0.23	2.56	0.18	0.55
E280ir	0.083	2.34	2.13	4.15	0.24	2.83	0.23	0.67
E281ir	0.084	2.59	2.35	4.57	0.22	2.62	0.25	0.70
E282ir	0.075	3.30	3.00	6.16	0.21	2.80	0.44	0.76
E283ir	0.076	3.50	3.18	6.49	0.23	2.97	0.46	0.78
E284ir	0.078	3.95	3.59	7.23	0.23	2.95	0.51	0.67

Table D.9: Results irregular wave experiments smooth slope 1:2

Appendix E

Material properties

E.1 Introduction

For the experiments rubble mound material is used that is order from a supplier or that was available in the WaterLab. The armour stones were available at the Waterlab and the core stone had to be ordered. For determining the weight, grading, nominal stone diameter and porosity of the layers some measurements had to be done. The first information that was needed is the density of the material, which is important for the nominal stone diameter, grading and stability. For the armour stones the required grading is selected and the stones are handpicked to get the wanted grading. For the core material the core grading was selected based on the availability of the material at the supplier of the stones.

In total three cubic meter (≈ 3.000 kg) of core material is processed (washed, placed and removed out of the flume), and almost thousand (armour stones) are weighed. Moreover, for the experiments the armour layer is five times placed or replaced.

E.2 Armour layer properties

For the armour layer two d_{n50} with the same grading are needed. The stones used for the armour layer were present in the WaterLab in a pile of stones. First, the density of the stones is determined, by measuring the “dry” weight of the stones and the weight of the stones under water. For the armour stones this resulted in the following measurements,

No.	Dry weight [g]	Weight under water [g]	Relative density Δ [-]
1	2179	1350	1.61
2	1647	1018	1.62
3	2337	1453	1.61
4	2083	1298	1.60
5	2873	1763	1.63
6	1138	707	1.61
7	2024	1259	1.61
8	1597	972	1.64
9	1195	745	1.60
10	2036	1263	1.61
11	2286	1422	1.61
12	1691	1050	1.61
13	740	459	1.61
14	1721	1032	1.67
15	1948	1205	1.62
16	1745	1086	1.61
17	1664	1033	1.61

Table E.1: Density measurements armour stones

Next, to the measurements of the stones also the density of water is measured. For fresh water normally 1000 kg/m^3 is used. The density of the stones has a mean density, ρ_μ= 2620 kg/m^3 with a standard deviation of σ= 20 kg/m^3.

The wanted stone distribution is obtained by hand picking every stones and weighing every individual stones. The stones that are in the class range, between d_{15} - d_{50} and between d_{50} – d_{85} were placed in

the container, of course also stones smaller and larger d_{15} and d_{85} respectively were placed in the container. This led to the following stones properties, graphically presented in Figure E.1 and Figure E.2. In the figures the weight of the stones are given, with the following relation the d_n value can be computed,

$$d_n = \sqrt[3]{\frac{W}{\rho_s}} \qquad \text{eq. E.1}$$

$$d_n = 0.84d \qquad \text{eq. E.2}$$

With the help of the graphs it can be determined that the wanted stone distribution is also achieved. For the armour stones of d_{n50}= 0.067 m the actual is also d_{n50}= 0.067 m, d_{15}= 0.060 m and d_{85}= 0.074 m. This leads to a grading d_{85}/d_{15}= 1.23. For the second armour stones (of d_{n50}= 0.09 m) the actual stones size is also d_{n50}= 0.090 m, d_{15}= 0.081 and d_{85}= 0.097. Thus, d_{85}/d_{15}= 1.2 (1.98).

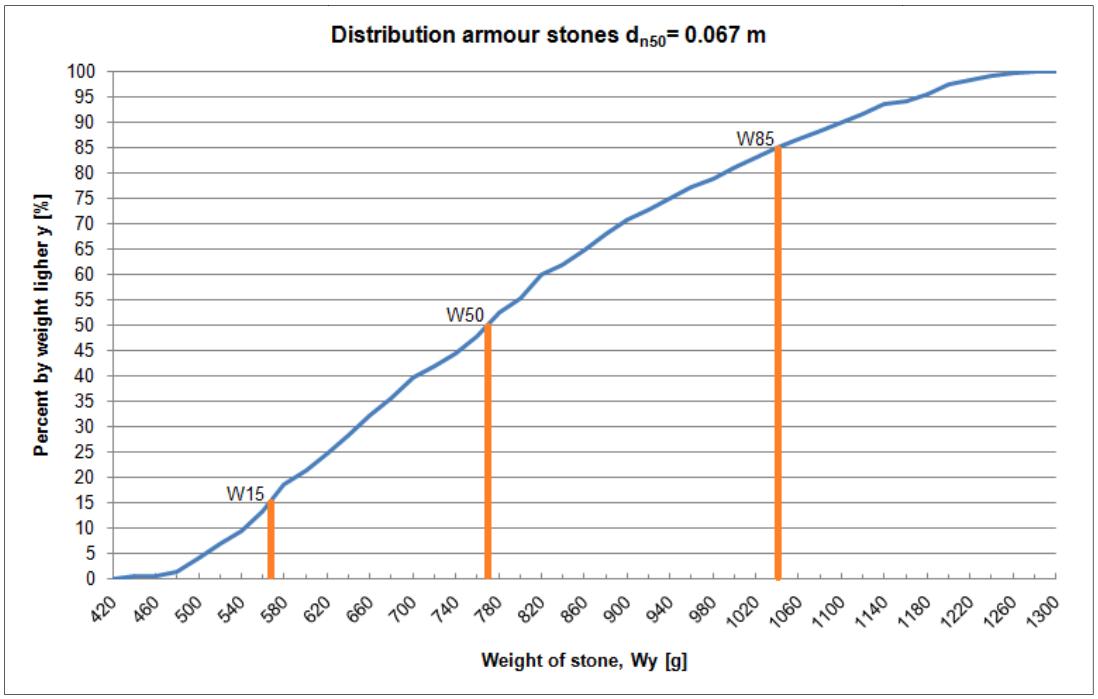

Figure E.1: Distribution armour stones d_{n50}= 0.067 m with grading of 1.2

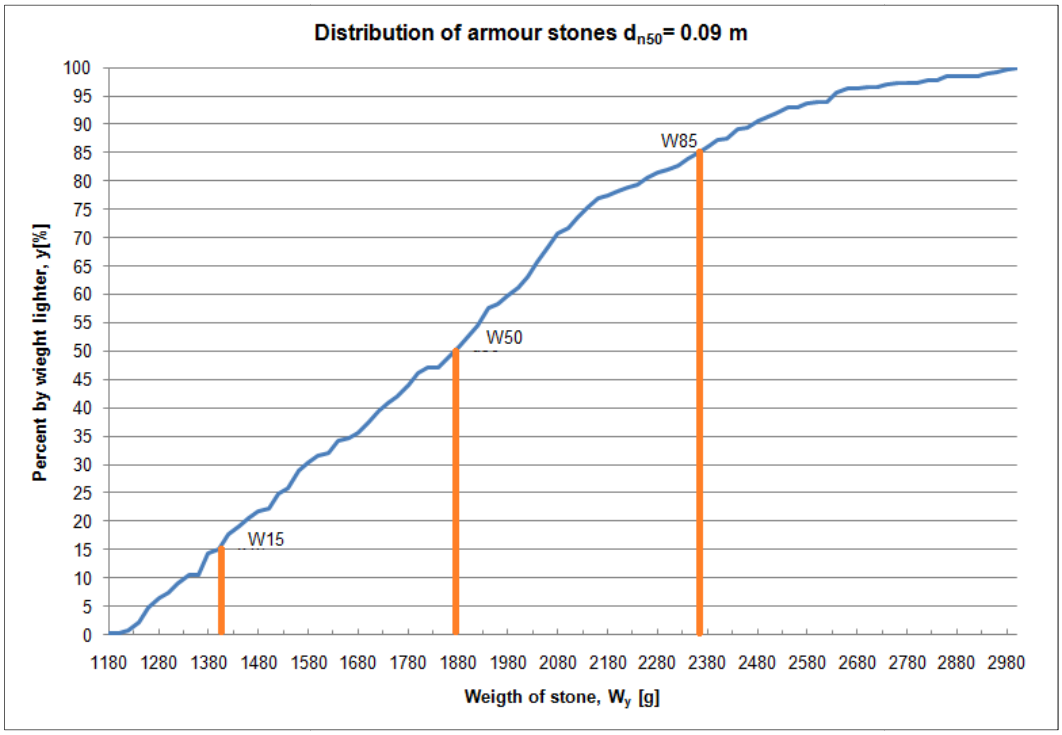

Figure E.2: Distribution of the armour stones d_{n50}= 0.09 m with grading of 1.2

The porosity of the armour material is determined by filling a large bucket with stones and filling the bucket with water. Volume of water needed to fill the bucket is determined by using a measuring cup. Before the test the volume of the empty bucket is determined, filled with only water the bucket had a weight of 10980 gram, 11.1 L. During the test, the weight of the bucket filled with stones and filled with water and stones are determined. Next, to this the volume of water was needed to fill the bucket is measured. In total six test were done, which lead to a mean n= 0.41 for the stone mixture with d_{n50}= 0.067 m.

For the stone mixture of d_{n50}= 0.09 m a larger bucket of 90 L is used. The dimensions of the container are measured, in order to know the volume of the bucket. After the container is filled with stones, and the stones are compacted, the container is filled with water till the top edge. The final step, is removing the stones and measuring the water level inside the container. This method is performed three times which lead to an average of porosity n= 0.40.

The standard deviation of both measurements is quite small (respectively 0.002 and 0.003), however, only a limited amount of measurements are made and also the edge of the bucket/ container have an influence that is not in correspondence with a real stone layer in a breakwater. When the stones are placed in the bucket/container the influence of the edges is as much reduced by placing the stones first at the edges and then in the middle. At the edge a porosity of 100 % occurs were in reality a porosity of around 40 % is expected. The volume influenced by the flat edges of the bucket/ container can be determined by taking the surface area multiplied by a half of the stone diameter d_{50}, and also the expected porosity is taken into account. Over this area that is “influenced” the inaccuracy of the measurements has its effect. This area, indicated with the dashed line in Figure E.3, leads to a variation in porosity dependent on the ratio of this area on the total volume.

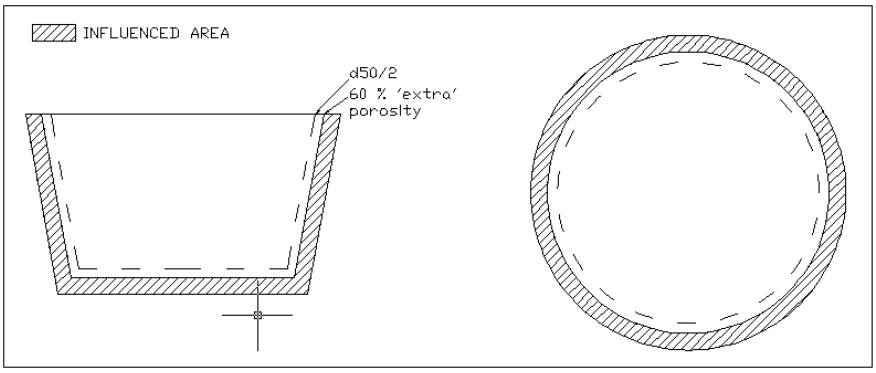

Figure E.3: Sketch of the container with the area influenced by the edge indicated by the dashed lines

For the porosity measurements done for the large stone diameters (d_{n50}= 0.09 m) this leads to a variation of 8 %. This leads to a porosity of n= 0.40 ± 0.03. For the small stone diameters two type of buckets are used, 11 L and 44 L. For the small bucket six measurements are done and with the above variation this leads to a porosity n=0.41 ±0.04. With bucket of 44 L three measurements are done, which leads to the following porosity n= 0.42 ±0.03.

Volume	Inner height [cm]	Diameter bottom	Diameter top	Volume [cm^3]	d_{50} [m]	Area of influence [cm^3]	Variation [%]
11 L	23	23	26	11090*	0.079	1097	10
44 L	30	37.5	47.3	43700*	0.079	3003	7
90 L	35.5	63	50	90180	0.107	7460	8

Table E.2

* Volume determined by filling the bucket with water and measuring the weight.

The above method of determining the accuracy of the measurements of the porosity is conservative. In reality the accuracy is larger when the actual material is placed as bulk material. However, in this situation the stone are placed as an armour layer, and this leads to a different porosity. So, the method that is used to determine the porosity is not a good method to determine the porosity of a layer that has of a thickness of two stones. Unfortunately, no better method was available. Nevertheless, it indicates that the porosity of the two types of armour layers is almost the same.

E. 3 Core material properties

Two different core properties are used in the experiments with both d_{n50}= 0.033 m (d_{50}= 0.40 m) and with a grading of 1.5 and 4. Both materials originate from a stone quarry in Norway, the rock is called “Norwegian sandstone”. Based on 14 measurements the density is determined, ρ= 2590 kg/m^3 with a variation of 3 kg/m^3. This leads to the following, W_{50}= 90 g (d_{n50}= 0.033 m), W_{15}= 40 g (d_{n15}= 0.026 m) and W_{85}= 160 g (d_{n85}= 0.040). This leads to a grading of 1.54. The material that should have been delivered was d_{15}/d_{85}= 31/50 mm with eq. E.2 it is checked that this corresponds with the measurements on the sample. From the second core material no sample is taken to determine the distribution, the requirements of the supplier are d_{15}/d_{85}= 20/80 mm.

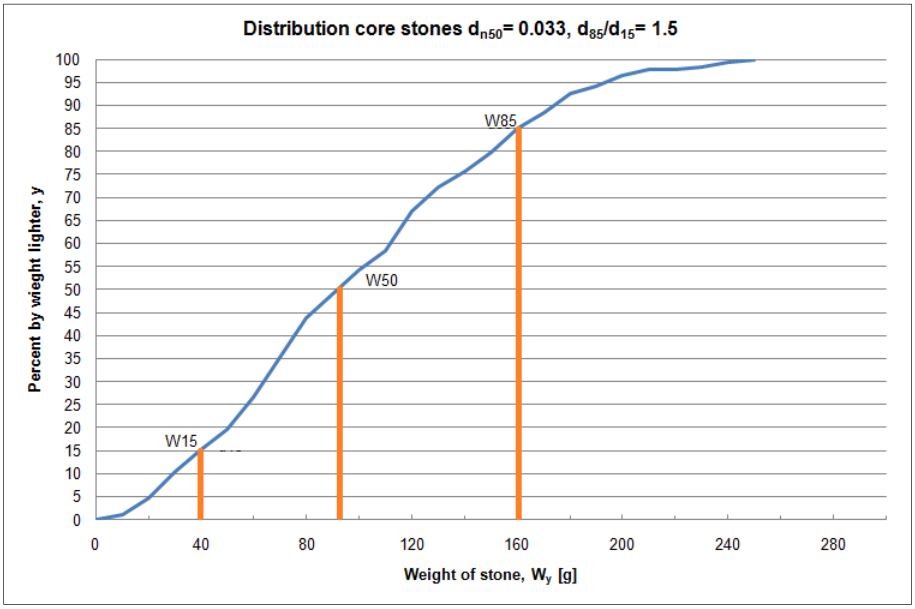

Figure E.4: Distribution of core material, d_{n50}= 0.033 m, d_{85}/d_{15}= 1.5

E.4 Porosity measurements

For this material the porosity is determined using the 11L bucket, see Table E.2. Three measurements are done whereby the stones are compacted. The sample that is used to determine the grading is also used for determining the porosity. Also, three measurements are done without compaction of the stones, but this is not comparable with the experiment set-up in the flume. In the flume the core is compacted during construction and due to the waves. The bucket is placed on a weighing scale and the following weights are recorded, filled with water, filled with only stones and filled with water and stones. In table ## the average results of the measurements are given,

	Core stones, grading 1.5
Porosity, compacted	0.43 [-]
Porosity, loose	0.48 [-]
Area of influence	570
Volume bucket	10990
Variation	5 [%]
Range porosity compacted.	0.41 - 0.45

Table E.3: Porosity core material

For the grading of 4 the porosity is determined with the same method only due to the range of the stones a bucket (“mortar shell”) of approximately 63 L is used. The weight of the bucket filled with stones, water and stones and only with water is known. With this method five measurements are done, in which the core stones were compacted. Next, to these measurements two measurements were done without compacting the stones. When regarding the size of the mortar shell, core stone diameter and wide grading the influence of the edge is small enough to be negligible.

	Core stones, grading 4
Porosity, compacted	0.36 [-]
Porosity, loose	0.40 [-]
Variation of measurements	0.01 [%]
Range porosity compacted.	0.35 - 0.37

Table E.4: Porosity core material, Norwegian sand stone

Appendix F

Core scaling

In scale model test of breakwaters the Froude scaling laws are almost always used. From Froude scaling it follows that the material diameters are linear geometrically scaled. For armour layers this does not give problems when using normal scales. For the core, however, this can give problems. When scaling the core the flow in the core can become more laminar than in prototype occurs. A reduction in flow velocities leads to lower Reynolds numbers. In the case of low Reynolds numbers viscous forces may not be negligible anymore. When this is the case a different flow type in the scaled core than in prototype core will occur, and therefore the model does not represent the real situation. In BURCHARTH ET AL. [1999] a method is suggested to avoid this problem by scaling the core in a different manner. The basis of this method is a prototype scale breakwater, which is scaled for test in laboratories. In this case no prototype breakwater is considered. But the method can be used to predict a characteristic velocity in the core. With this velocity a Reynolds number can be computed.
The method suggest in BURCHARTH et al. [1999] is stated below. In the method at six points in the breakwater and at different wave stages the velocity is computed. The damping coefficient of the core is computed according to the following,

$$\delta = 0.0141\frac{n^{1/2}L_p^2}{H_s b} \qquad \text{eq. F.1}$$

The horizontal pressure gradient are computed by eq. F.2

$$I_x = -\frac{\pi H_s}{L'}e^{-\delta\frac{2\pi}{L'}x}\left[\delta\cos\left(\frac{2\pi}{L'}x+\frac{2\pi}{T_p}t\right)+\sin\left(\frac{2\pi}{L'}x+\frac{2\pi}{T_p}t\right)\right] \qquad \text{eq. F.2}$$

Where x is the horizontal distance in the core, L' is the effective wave length given by $L/D^{1/2}$ and t is the regarded moment of the wave period. When the horizontal pressure gradient is known, the pore velocity can be calculated by the Forchheimer equation,

$$I_x = \alpha\left(\frac{1-n}{n}\right)^2\frac{\nu}{gd_{50}^2}\left(\frac{U}{n}\right)+\beta\frac{1-n}{n}\frac{1}{gd_{50}}\left(\frac{U}{n}\right)^2 \qquad \text{eq. F.3}$$

In this study only nominal diameters are used. The relation $d_{n50}=0.84d_{50}$ is used for the conversion, see CUR/CIRIA [2007].The values α and β are depended on the Reynolds number, shape and the grading of the stones. An estimate of these values should be done in the first place, which should be checked afterwards. The velocity in the core is calculated for 0.1T till 0.5T and at six different locations. At SWL at the surface, at quarter of the width B and at the half of the width of the core B. Also, at the three cross sections at a level of H_{m0} below SWL.

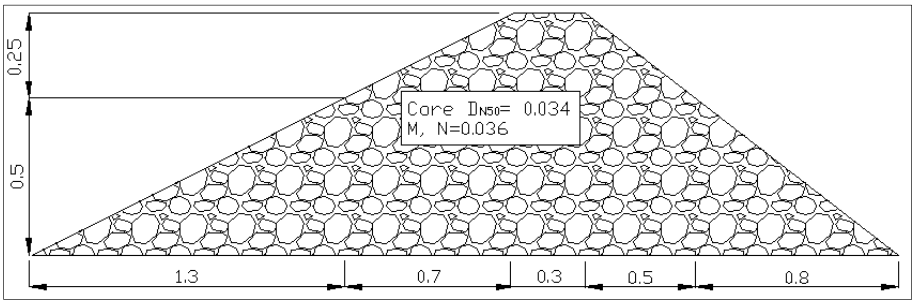

Figure F.1: Core of the physical scale model

This method is developed to have a scaling law for a prototype core that is in accordance with the Froude law, but provide a solution to the problem of too small Reynolds numbers. The Reynolds number should be large enough to avoid influence of viscous forces. When the Re> 300 in the core the flow regime is of the same classification as it were a prototype breakwater and it can be said that the viscous forces are negligible.

For the values of α an β constant values are used, which in fact are not constant over the wave period. The values are dependent on the Reynolds and Keulegan carpenter values. Normally, and also in this method constant values are used. In appendix G the values of α and β in the Forchheimer flow and for the fully turbulent flow are given. In Table F.1 the values which are used are given.

The governing situation is the characteristic velocity in the case of low wave steepness and with the lowest core permeability. For a permeable core with a grading of 4 the porosity is 0.36. In the experiments with an permeable core the smallest significant wave height H_{m0}=0 .11 m. Long waves give the lowest Reynolds number in the core, and still these values must give a fully turbulent flow. The values of α and β vary between different research and type of flow, therefore, different shape coefficient values are used.

H_{m0}	T_p	δ (SWL/-y)	α (or α')	β (or β')	Re
0.11	4.0	4.47/ 4.0	360	3.6	690
			1007	0.63	>690
			0	3.6	620
			0	2.7	720

Table F.1: Computed Reynolds numbers with the method of BURCHARTH [1999]

In Table F.1 the results of the computation with different shape coefficient are given. The flow in the core has a characteristic velocity that leads to a fully turbulent flow in the core. So, the core in the physical scale model is correctly scaled.

Appendix G

Shape coefficients *α* and *β*

In this appendix various shape coefficients determined by various researchers are given for the Forchheimer or fully turbulent type of flow as stated in Troch [2000] original authors of research can be found in the tables. For Reynolds smaller than approximately 300-400 the α and β values or valid for higher Reynolds numbers α' and β' can best be used.

Research	Shape	Porosity [-]	d_{50} [mm]	Re [-]	α [-]	β [-]
Burcharth and Christensen [1991]	Uniform, spherical particles				~190	~1.8
	Uniform rounded sand grains				~240	~2.8
	Irregular, angular grains				To 360 or more	To 3.6 or more
Dudgeon [1966]**	Angular rock	0.455 0.515 0.438 0.483	16 14 25 37	<400 <200 <400 <500	622 479 425 92	5.4 4.0 5.3 10.8

Table F.2: Values of α and β for the Forchheimer equation.
** Data calculated from Dudgeon [1966] graphs, not from data points

Material	Packing	d_{85}/d_{15}	α'	β'	Re	Source
Round rock	Random	1.4 1.7 - 1.3	~10,000 1,400 – 15,000 160 – 9,800 -	2.2 2.2 – 2.9 1.7 – 2.2 1.9	< 2,100 – 8,050 500 – 3,600 - 750 – 7,500	B D H W
Semi-round rock	Random	1.9 1.3	~3,000 -	2.7 2.4	800 - 2,100 750 – 7,500	B W
Irregular rock	Random	1.4 – 1.8 1.6 - 1.3 – 1.4 1.3	1,400 – 13,000 270 – 1,400 90 – 540 980 – 2,100 -	2.4 - 3.0 4.1 – 11 3.0 – 3.7 2.5 – 2.9 3.7	600 – 10,300 400 – 8,200 - 300 – 5,700 750 – 7,500	B D H Sh W
Equant rock	Random	1.2	-	3.6	750 – 7,500	W
Tabular rock	Random	1.4 1.2	3,000 -	1.5 3.7	1,500 – 18,000 750 – 7,500	Sm W

Table F.3: List of α' and β' coefficient for fully turbulent flow, gathered by Burcharth and Andersen [1995]. B: Burcharth and Christensen [1991]; D: Dudgeon [1966]; H: Hannoura and McCorquodale [1978]; Sh: Shih [1990]; Sm: Smith [1991] and W: Williams [1992].

Material	d_{50} [m]	n [-]	α'	β'
Irregular rock	0.061	0.44	1791	0.55
Semi round rock	0.049	0.45	0	0.88
Round rock	0.049	0.39	1066	0.29
Irregular rock	0.020	0.45	1662	1.07
Irregular rock	0.031	0.39	1007	0.63
Spheres	0.046	0.48	2070	0.69

Table F.4: Values for α' and β' for fully turbulent flow, from Van Gent [1995].

Appendix H

Shape of the wave run-up

In Jumelet [2010] the following statements are made regarding the shape of the wave run-up. The maximum run-up and shape of the wave on the slope is modelled according to the theory of Hughes [2004], see Figure F.2.

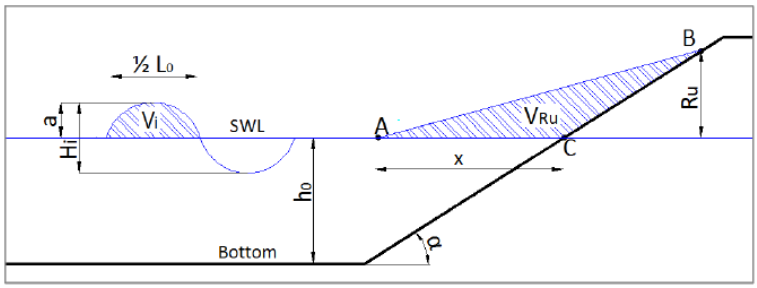

Figure F.2: Triangular run-up wedge on a smooth impermeable slope, JUMELET [2010]

The incoming sinusoidal wave crest has the same volume as the run-up wedge. The incoming volume can be determined as follows (with half the wave length),

$$V_i = \frac{H_s L_0}{2\pi} \qquad \text{eq. F.4}$$

The volume of the wedge can be determined by,

$$V_{ru} = \frac{1}{2} x R_u \qquad \text{eq. F.5}$$

The run-up height can be described by the incoming energy of the wave, and by the potential energy of the wave at maximum run-up. At maximum run-up it is assumed that the water has a negligible velocity. The energy of the wave run-up triangle can be described as,

$$E_{pot} = E_{tot} = E_{ru} = \frac{1}{6} \rho g R_u^{\,2} x \qquad \text{eq. F.6}$$

In case of a smooth impermeable slope it is assumed that the incoming volume is equal to the run-up volume ($V_i = V_{ru}$) and no energy dissipation ($E_i = E_{pot}$) will occur, this leads to the following equations for R_u and d, see

$$R_u = \frac{3}{4}\pi H \qquad \text{eq. F.7}$$

$$x = \frac{4L_0}{3\pi^2} \qquad \text{eq. F.8}$$

The volume of the wave run-up can now be determined from substituting the above equations in V_{ru}.

$$V_{ru} = \frac{2}{3}\frac{L_0}{\pi^2} R_u \qquad \text{eq. F.9}$$

When regarding the relative wave run-up then according to eq. F.7 this is $R_u/H = 2.36$. In the results of the experiment this run-up height is not reached, and also not in the results of BRUUN and GÜNBAK [1977]. Of course, in reality some dissipation will occur. Appendix B shows that the reflection coefficient is ±0.90 for surging waves. Large part of the dissipation is caused by the run-down motion. Moreover, the incoming wave volume is not matching the real situation for long waves. In this latter case the wave shape is not sinusoidal. Assuming a sinusoidal wave shape leads to an overestimation.

Appendix I

Results Irregular waves

In section 4.2 the results of the irregular waves are presented, and a large difference with the expectations is found. In this appendix the possible causes are considered.
In the study of VAN DE WALLE [2003] also a large variation was found, especially for a spectral width range between 0.55 – 0.62, see Figure F.4. In the same study more experiments on wave run-up on rubble mound breakwater are considered, and between the results a large scatter is visible. In the experiments at the GWK step run-up gauges are used to measure the wave run-up.

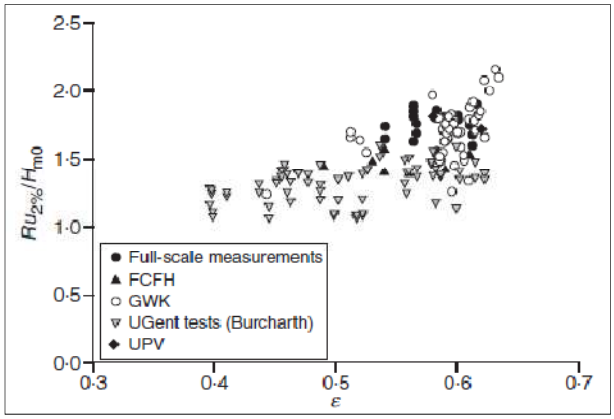

Figure F.3: Relative wave run-up values for experiments conducted laboratories. VAN DE WALLE [2004]

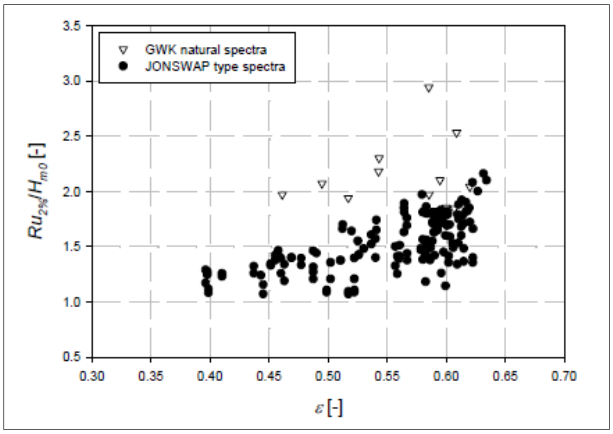

Figure F.4: Relative wave run-up values for experiments conducted in laboratories compared with natural spectra test performed in the GWK.

In this thesis the spectral width parameter varied between ε= 0.55 – 0.64. The same range as were the large scatter is found in Figure F.4. In the above figures it is clearer that with small scale tests the values of the relative run-up are mostly lower than with large scale tests.

The difference between the results and the expectations is a structural phenomenon, so the local stone configuration can be left out of considerations (also a difference was found on a smooth slope). Also, in case of regular waves the local stone configurations is more important since the same type of wave runs up the slope. The calibration factor cannot be the problem, since for regular waves the results matches the results of the video analysis. The remaining causes are:

- Shape of the spectrum
- Measuring method
- Analysis of $R_{u2\%}$
- Wave analysis

The wave analysis is performed with the standard wave analysis programs of the WaterLab. Moreover, the significant wave heights and peak period requested from the wave are also measured. The analysis of $R_{u2\%}$ is done by deriving the local maxima with a threshold of 0.02 m of the measurements. This results in the value and the number of run-up events *N.* The thresholds avoids that local maxima below SWL and run-up as a cause of the moving water (not actual incoming waves) are not included in the results. When increasing the thresholds this will also lead to an increase of the value $R_{u2\%}$. However, the analysis will not be the (main) problem, since in some measurements even the maximum wave run-up value will not lead to the expected values. An example of the measurements on a smooth slope is given in Figure F.5.

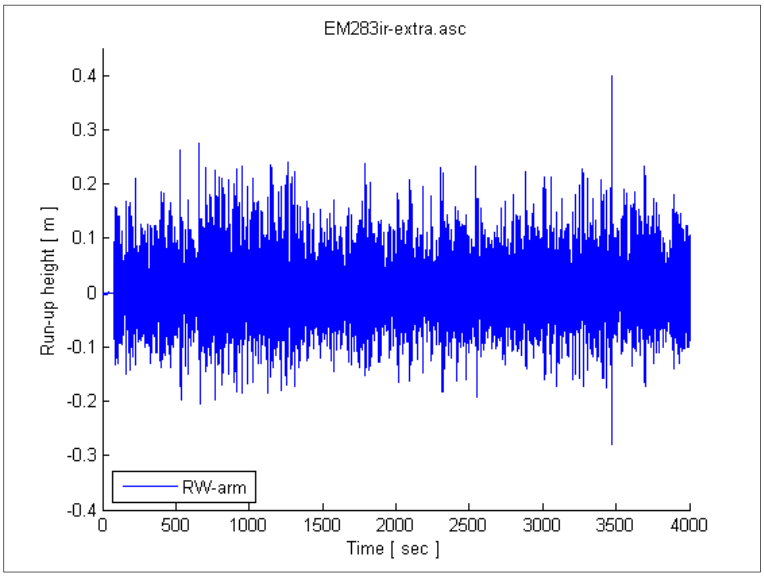

Figure F.5: Measurements of wave run-up of experiment E283ir

In section 3.4.2 an equation for determining the theoretical error caused by the distance between the wire and the slope is given. In VAN DE WALLE [2003] the results of a resistance wire is compared with the results of digital wire gauge. The wires have a distance of less than 2 mm to the slope. According to this study for values of s< 0.02 the error ΔR_u made is at least five times the distance between the wire and the slope. In appendix D the values for ΔR_u are given, which are used to adjust the measurements. As mentioned in section 4.2 the error made is not only caused by ΔR_u, but also by model effects.

Appendix J

Wave analysis

In this appendix the principle of the wave analysis of the regular and irregular waves are given. The matlab files used for the analysis are not given, because the method has already be used and proven by in a lot of previous studies performed in the WaterLab. Also, in this appendix the difference between linear, cnoidal waves and why the method of analysing the waves is only applicable for the linear waves. The water elevation data is acquired by placing three wave gauges in the wave flume.

J.1 Regular waves analysis

For the wave analysis for the regular waves a program called *Refreg* is used to determine amplitude of the incoming wave, reflected wave and the phases of the incoming and reflected wave. Also the wave period and wave length are determined. The program *Refreg* only uses the data of two wave gauges for the computation. The optimum distance between the gauges is one fourth of the wave length. For a reliable result at least twenty wave periods should be used for the computations. To compute the wave properties of regular waves the basic wave equation are used. For the reflecting wave only first harmonics are used.

$$\eta(x_1,t) = a_i\cos(kx_1 - \omega t + \phi_i) + a_r\cos(kx_1 + \omega t + \phi_r)$$
$$\eta(x_2,t) = a_i\cos(kx_2 - \omega t + \phi_i) + a_r\cos(kx_2 + \omega t + \phi_r) \quad \text{eq. J.1}$$

Where,

η	Water-surface elevation relative to the mean water level [m]
t	Time [s]
$a_{i,n}$, $a_{r,n}$	Amplitude of the incoming and the reflected wave [m]
k_n	Wave number [-]
ω_n	Angular wave frequency [s^{-1}]
$\varphi_{i,n}$,$\varphi_{r,n}$	Phase of the incoming and the reflected wave [°]

By rewriting the equation eventually they can be written as matrices, see eq. J.4.

$$\eta(x_1,t) = A_1\cos(\omega t) + B_1\sin(\omega t) \quad \text{eq. J.2}$$

$$\eta(x_2,t) = A_2\cos(\omega t) + B_2\sin(\omega t) \quad \text{eq. J.3}$$

$$\begin{pmatrix} e^{ikx_1} & e^{-ikx_1} \\ e^{ikx_2} & e^{-ikx_2} \end{pmatrix} \begin{pmatrix} a_i\, e^{i\phi_i} \\ a_r\, e^{-i\phi_r} \end{pmatrix} = \begin{pmatrix} A_1 + iB_1 \\ A_2 + iB_2 \end{pmatrix} \quad \text{eq. J.4}$$

The values of A and B can be found by using a fast Fourier transform with eq. J.2 and eq. J.3. The wave period is determined by the program by finding in the measurements two zero down crossings at the beginning and at the end of the measurements from one wave gauge. This will results in multiple wave periods, but the wave period used is the value with the highest fast Fourier transform coefficient value.

J.2 Irregular wave analysis

For irregular waves the wave analysis is performed by the program *Decom*p that is based on the method of ZELT and SKJELBREIA [1992] (Manual Waterlab) determines the variance spectrum, computes the peak period and the significant wave height. For irregular waves the results of the three wave gauges are used to determine the incoming and reflective wave. The measured values can be given as a sum of incident and reflected waves, see Manual Waterlab

$$\eta\left(x_p,t\right)=\sum_{j=1}^{N-1}\left(a_{i,j}e^{i\omega t x_p}+a_{r,j}e^{i\omega t x_p}\right)e^{i\omega_j t} \qquad \text{eq. J.5}$$

From the measurements a variance density spectrum is made from the water elevations, see HOLTHUIJSSEN [2007]. This leads to a variance density spectrum of the results of the separate wave gauges. From the average spectrum the peak period and the spectral moments are determined. From the spectral moments the mean period (eq. J.6), spectral width (
eq. J.7) and significant wave height (eq. J.8) can be determined. In Figure J.1 an example of a variance density spectrum is given.

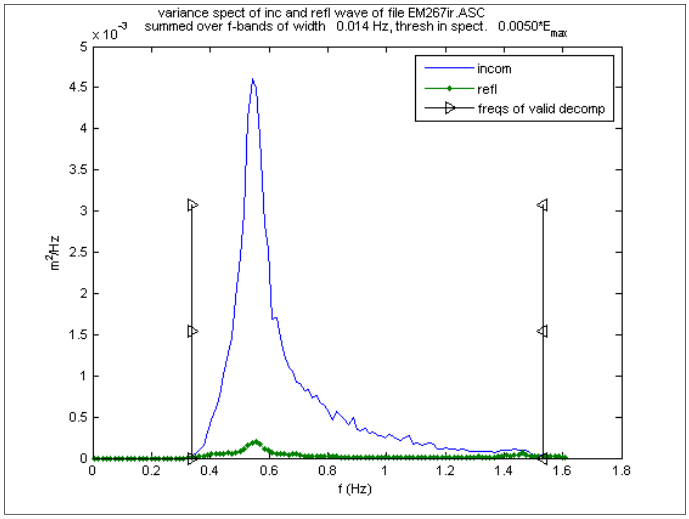

Figure J.1: Example of a variance density spectrum

$$T_{0,1}=m_0/m_1 \qquad \text{eq. J.6}$$

$$\varepsilon=\sqrt{1-\frac{m_2^2}{(m_0 m_4)}} \qquad \text{eq. J.7}$$

$$H_{m0}=4\sqrt{m_0} \qquad \text{eq. J.8}$$

J.3 Cnoidal wave theory

In the experimental results, see appendix B, a couple of times a measured value is not used in the analysis by referring to that the analysis must be done according to the cnoidal wave theory. In this appendix the cnoidal wave theory is considered as stated in WIEGEL [1959].

The applicability of the linear wave theory has its limits, see Figure J.2. When considering wave periods longer than 3 s with a water depth of 0.5 m one can see that with almost any wave height the cnoidal wave theory is applicable.

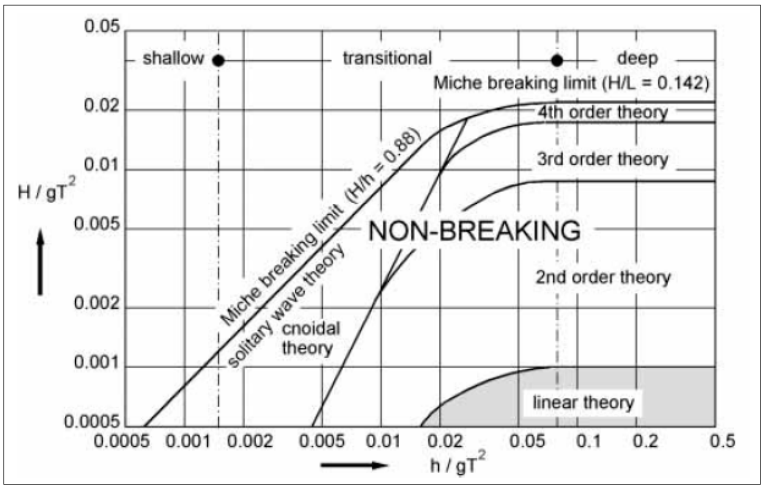

Figure J.2: Validity of wave theories, LEMÉHAUTÉ [1976] (SCHIERECK [2000])

The program that computes the wave properties (incoming wave, reflected wave, etcetera) uses the basic linear wave theory equations, see eq. J.1. When determining the wave height and period with this program it resulted in wave heights that are in the order of 1.5 times smaller than was demanded from the wave generator. Normally, the wave height deviates only ±10% from the demanded and analysed wave height. So, using the program leads to a not correct analysis of the wave height. In Figure J.3 the wave profiles of a sinusoidal wave and a cnoidal wave are depicted. With a sinusoidal wave the amplitude is the distance between SWL and crest/ trough. For a cnoidal wave this is not the case, the part below SWL is distinctive lower. When analysing according to the linear wave equations the amplitude (and wave height) are misinterpreted.

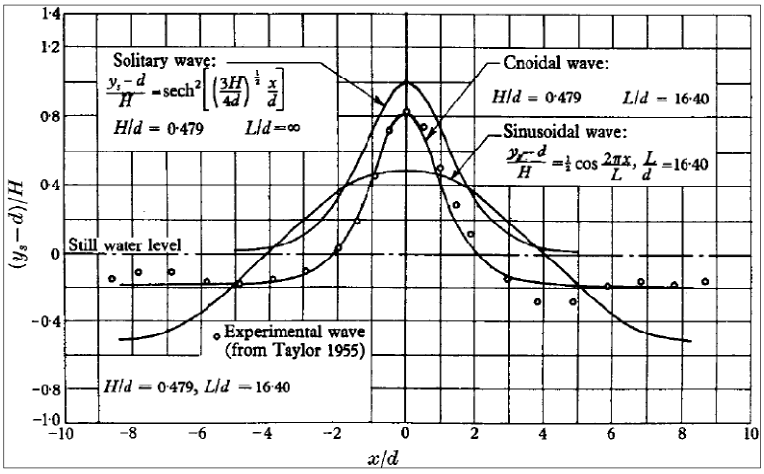

Figure J.3: Comparison wave profiles

Moreover, with a cnoidal wave water elevations is mostly situated above SWL. This leads to a larger potential energy. From the side view video recordings the following is visible, after maximum run-up the rushed up volume rushes back and creates a wake below SWL. At that moment the incoming water elevation is not present yet. First the water line returns till a couple of centimetres below SWL, then the peak of the wave arrives at the slope and the wave will run-up. The shape of the wave is the same as in Figure J.3. Moreover, the return flow during run-down does not have any dissipating effect on the coming wave that runs up the slope.

Appendix K

Derivation P-factor with the volume exchange model

K.1 Adjustments Volume Exchange model

In chapter six a number of adjustments are suggested regarding the VE-model. In this appendix the adjusted VE-model is elaborated and the derivation for a formula for the permeability coefficient *P* is given.

The volume exchange is given by the volume on the (core) slope without inflow and the volume of inflow,

$$V_{ru;c} - V_{b;N} \qquad \text{eq. K.1}$$

The volume of the wave run-up at the core $V_{ru;c}$ is given as a triangle wedge shape that has a base *d* and with core run-up height $R_{u;c}$, see eq. K.4. The base of the triangle is related to the wave length limited by the water depth, because no deep water situation was created during the experiments.

$$V_{ru,c} = \frac{1}{2} d R_{u;c} \qquad \text{eq. K.2}$$

$$d = \frac{4L}{3\pi^2} \qquad \text{eq. K.3}$$

$$R_{u;c} = 1.63 * \tanh(0.14\xi) * H \qquad \text{eq. K.4}$$

For the turbulent term a constant shape coefficient of β= 3.6 is used. The laminar term and inertial term are not included. The porous flow equation is given by,

$$I = bu^2 \qquad \text{eq. K.5}$$

$$b = \beta \frac{1-n}{n^3} \frac{1}{gd} \qquad \text{eq. K.6}$$

The imposed core run-up for the first iteration is given by eq. K.4. By taking the *sin α* of this the inflow length is obtained. For the determination of the gradient only the inflow period is changed when comparing it with the VE-model as derived in JUMELET [2010]. For the computations a value of one sixth of the wave period is assumed. The notion *N* indicates that a number of iterations must be performed to receive at the final inflow volume. A hydraulic gradient equal or smaller than one is only justified when no disconnection of the phreatic water line occurs, see section 2.2.1

$$\frac{1}{2} * n * \left(\frac{1}{I}\right) * R_{u;c;N}^2 = \frac{1}{\varpi} \sqrt{I/b} * \frac{R_{u;c;N}}{\sin\alpha} \left(1 - \cos\left(\varpi \frac{T_0}{6}\right)\right) \qquad \text{eq. K.7}$$

$$V_{b;N} = \frac{1}{\omega} \sqrt{\frac{I}{b}} \frac{R_{u;c}}{\sin\alpha} \left(1 - \cos\left(\omega * \frac{T_0}{6}\right)\right) \quad \leq 1 \qquad \text{eq. K.8}$$

The reduction factor of wave run-up at the core can then be computed by,

$$R_{u;c;r} = \frac{V_{ru;c} - V_{b;N}}{V_{ru;c}} * R_{u;c;imp} \qquad \text{eq. K.9}$$

K.2 Computations with the tested structures

The adjusted VE-model is used to compute the reduction factor for the tested structure with a permeable core. For the core with a grading of 1.5 a porosity of n= 0.43 and for a grading of 4.0 a porosity of n= 0.36 was found, see appendix E. For all the experiments performed with $\xi > 3.0$ the reduction factor are computed. In appendix D (or B) the hydraulic properties are given. In Figure K.1 and Figure K.2 the results are given, and compared with the measured reduction factors.

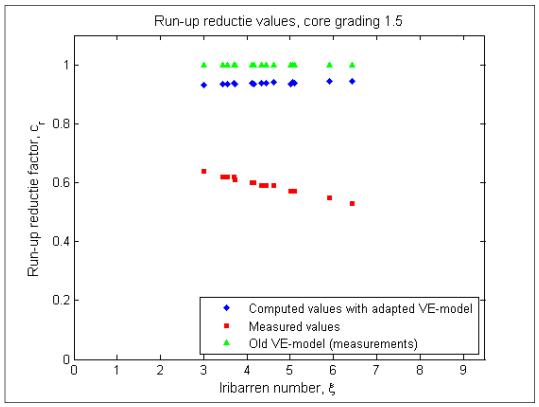

Figure K.1: Comparison between measured and computed c_r values, core grading 1.5

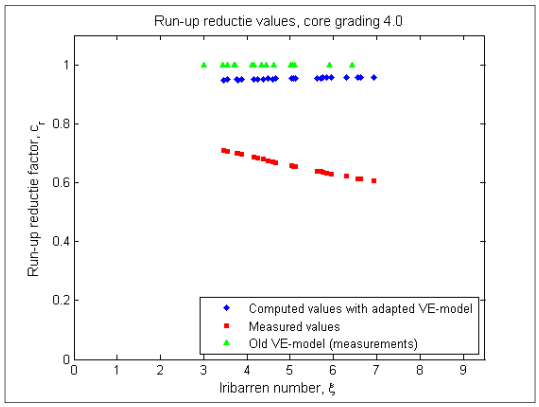

Figure K.2: Comparison between measured and computed c_r values, core grading 4.0

The figures show that a large difference exists between the computed and the measured values. A probable cause of this is the shape of the wave run-up as was assumed in the VE-model, see appendix H. In reality the volume of the wave run-up is lower. Probably it has a more concave shape run-up and this gives a lower volume than a triangle wedge shape. When regarding eq. K.9, one can see that with a smaller external volume the inflow volume has relatively more influence on the reduction factor. The difference in trend can be caused, by the base length of the triangle. The base length is dependent on the wave length, so with increasing Iribarren number also the volume increases. When the increase of the external volume is larger than the increase of inflow volume then the c_r factor increases. But, as showed in the graphs this occurred not in the experiments, a distinctive larger reduction is found.

In this study no quantitative investigation is done to the shape of the wave run-up. To adjust the error made by the volume exchange model a reduction factor γ_{cr} is derived. The reduction factor is derived by determining the quotient between the computed and measured values.

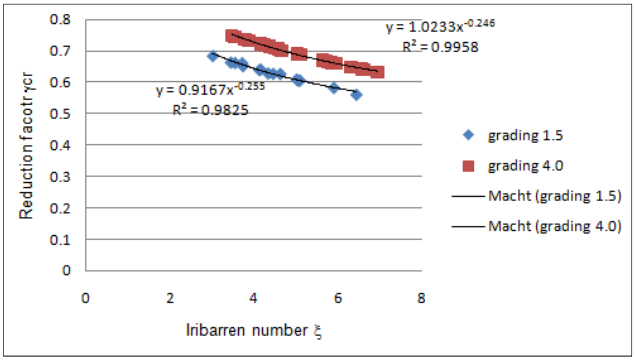

Figure K.3: Curve fitting line for the derivation of γ_{cr}

In Figure K.3 the curve fitting line for the reduction factor is given. It showed that this is not only dependent on the Iribarren number. The only other varied parameter between the two structures is the porosity of the core. The final equation factor γ_{cr} is as follows,

$$\gamma_{cr} = 1.60 * (1 - n_c)\xi^{-0.25} \qquad \text{eq. K.10}$$

K.3 Derivation of a formula for the permeability coefficient

In this section computations with the adjusted volume exchange model are made with the structures tested by VAN DER MEER [1988]. Those structures represented a P-factor of 0.1, 0.5 or 0.6. In Table K.1the structural properties of the tested structures in VAN DER MEER [1988] and the tested structures in this study are given. The porosity values of the VAN DER MEER [1988] structures are assumed values based on the considerations described in JUMELET [2010].

		P=0.6	P=0.5	P=0.1	Core grading 1.5	Core grading 4.0
Armour layer	d_{85}/d_{15} [-]	1.25	1.25	1.25	1.2	1.2
	d_{n50a} [m]	0.036	0.036	0.036	0.067	0.067
	Porosity *n* [-]	0.4	0.4	0.4	(0.41)	(0.41)
Filter layer	d_{n50a}/d_{n50f} [-]	-	-	4.5	-	-
	d_{85}/d_{15} [-]	-	-	2.25	-	-
	Porosity *n* [-]	-	-	0.38	-	-
Core	d_{n50a}/d_{n50c} [-]	-	3.2	-	2.0	2.0
	d_{85}/d_{15} [-]	-	1.5	-	1.5	4.0
	Porosity *n* [-]	-	0.4	-	0.43	0.36

Table K.1: Values of the VAN DER MEER [1988] tested structures, and structural properties of the structures tested in this study.

The reduced run-up values are determined by including eq. K.10.

$$R_{u;cr;\gamma} = \gamma_{cr} * \frac{V_{ru;c} - V_{b;N}}{V_{ru;c}} * R_{u;c;imp}$$

When regarding the run-up reduction factor ,

$$c_{r;\gamma} = \gamma_{cr} \frac{R_{u;c;r}}{R_{u;c;imp}} \qquad \text{eq. K.11}$$

In Table K.2 the results of the computations with the different structures are given. It shows that for Iribarren numbers lower than 5.0 the reduction factor is larger than 1.0 for cases with a P=0.1. Of course this is in reality not possible. However, in the curve fitting procedure for the derivation of the P-formula these values are used.

Iribarren number	$c_{r;\gamma}$ P=0.1	$c_{r;\gamma}$ P=0.5	$c_{r;\gamma}$ P=0.6	Fit line
6.4	0.955	0.579	0.573	$a1*c_{r;\gamma}^{-3.36}$
5.9	0.967	0.592	0.585	$a2*c_{r;\gamma}^{-3.42}$
5.0	0.999	0.615	0.607	$a3*c_{r;\gamma}^{-3.46}$
5.1	1.009	0.613	0.605	$a4*c_{r;\gamma}^{-3.36}$
4.9	1.020	0.634	0.626	$a5*c_{r;\gamma}^{-3.42}$
4.3	1.050	0.638	0.629	$a6*c_{r;\gamma}^{-3.37}$
3.5	1.067	0.669	0.660	$a7*c_{r;\gamma}^{-3.59}$

Table K.2: Results of computations with the adjusted VE-model

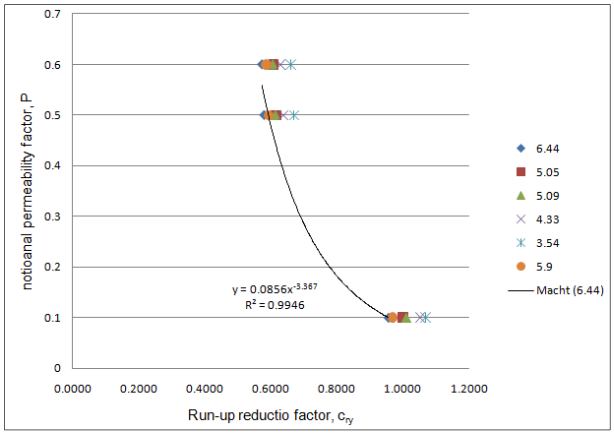

Figure K.4: Curve fit line for run-up reduction factor $c_{r;y}$

For the P-formula this leads to the following equation, see also Figure K.4.

$$P = a_n * c_{r;y}^{-3.4} \qquad \text{eq. K.12}$$

The value of a_n can be determined by relating the Iribarren number with eq. K.12. The Iribarren number is of influence, as it is also of influence for the core run-up and see Table K.2. With the help of *Matlab* the following trend line were found,

Structure type	Fit line
P=0.1	$0.36\xi^{-0.8}$ with $R^2 = 0.90$
P=0.5	$0.35\xi^{-0.8}$ with $R^2 = 0.99$
P=0.6	$0.40\xi^{-0.8}$ with $R^2 = 0.99$

Table K.3: Curve fit lines for the influence of the Iribarren number

The general curve fitting relation with a correlation of 0.92 becomes,

$$P = 0.37\xi^{-0.8} c_{r;y}^{-3.4} \qquad \text{eq. K.13}$$

Appendix L

Images of the experimental program

Photo 2: Overview of the wave flumes at the WaterLab. The wave flume is used for this study

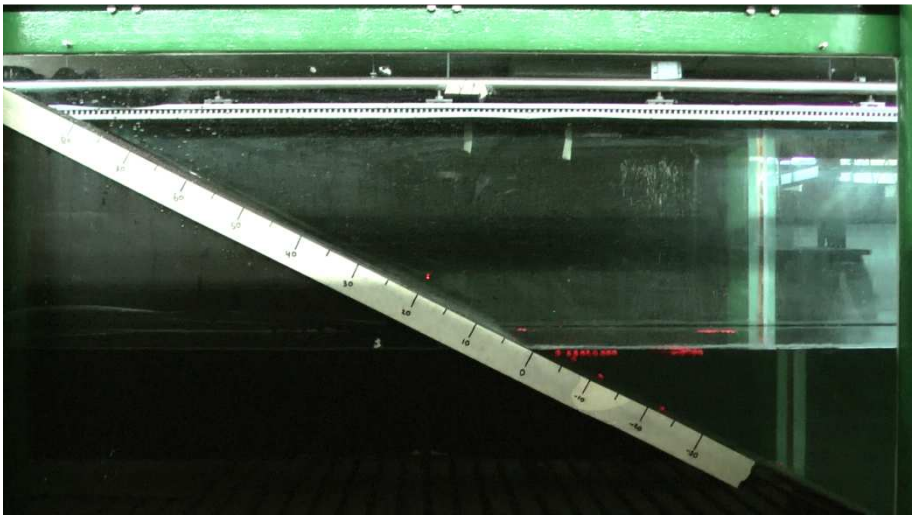

Photo 3: Side view image of the smooth slope 1:1.5

Photo 4: Side view of the rough impermeable slope 1:1.5

Photo 5: Side view of the armour layer on impermeable core

Photo 6: Side view of an armour layer on permeable core

Photo 7: Wave gauges

Photo 8: Armour layer with resistance wire on the slope

Photo 9

Photo 10

Photo 11

Photo 12

Photo 9 till Photo 12: Example of side view wave recording under irregular waves

Photo 13: Building the core (grading 4)

Photo 14: Finished breakwater